الجمهوريــة الجزائريــة الديمقراطيــة الشعبيــة
People's Democratic Republic of Algeria
وزارة التعلـيـم العـالي والبـحـث العلـمـي
Ministry of Higher Education and Scientific Research

MUSTAPHA Stambouli University
Of Mascara

جامعة مصطفى اسطمبولي
معسكر

Faculty of Science and Technology
Electrotechnical Department
Water Sciences and Techniques Laboratory (LSTE)

DOCTORAL THESIS

In Telecommunications Systems

Entitled

Contribution to the Realization of Miniature DGS Hybrid Microwave Components based on SIW Technology for Telecommunications Systems

***Presented by*: CHERIF Nabil**

June 16, 2022

The jury committee:

BERKA Mohammed	Associate Pr (A)	Mascara Univ	President
ABRI Mehadji	Full Professor	Tlemcen Univ	Supervisor
FELLAH Benzerga	Associate Pr (A)	Mascara Univ	Co-Supervisor
MAHDJOUB Zoubir	Full Professor	Sidi Belabbes Univ	Examiner
BENDAOUDI Amina	Associate Pr (A)	Sidi Belabbes Univ	Examiner
GHOUALI Samir	Associate Pr (A)	Mascara Univ	Examiner

Academic year: 2021/2022

الجمهوريــة الجزائريــة الديمقراطيــة الشعبيــة
République Algérienne Démocratique et Populaire
وزارة التعلـيـم العـالي والبـحـث العـلمـي
Ministère de l'Enseignement Supérieur et de la Recherche Scientifique

Université MUSTAPHA Stambouli
Mascara

جامعة مصطفى اسطمبولي
معسكر

Faculté Des Sciences Et De La Technologie
Département D'Electrotechnique
Laboratoire Des Sciences Et Techniques De l'Eau (LSTE)

THÈSE DE DOCTORAT

Spécialité : Systèmes De Télécommunications

Filière : Télécommunications

Intitulée :

Contribution à la Réalisation des Composants Hyperfréquences en Technologie SIW Miniature DGS Hybride pour les Systèmes de Télécommunications

Présentée par **: CHERIF Nabil**

Le 16/06/2022

Devant le jury :

BERKA Mohammed	MCA	Univ. Mascara	Président
ABRI Mehadji	Professeur	Univ. Tlemcen	Directeur
FELLAH Benzerga	MCA	Univ. Mascara	Co-Directeur
MAHDJOUB Zoubir	Professeur	Univ. Sidi Belabbes	Examinateur
BENDAOUDI Amina	MCA	Univ. Sidi Belabbes	Examinatrice
GHOUALI Samir	MCA	Univ. Mascara	Examinateur

Année Universitaire : 2021/2022

Acknowledgment

Foremost, we would like to thanks ALLAH who has given us the power and patience to complete this research project.

This thesis was prepared within the LSTE laboratory of Mascara University under the guidance of Mr. ABRI Mehadji, professor at the University of Tlemcen; I would like to express my deep gratitude to him for agreeing to guide this research work during three years of the thesis preparation. I thank him for his support and advices both on the research and humanitarian front. Mr. ABRI Mehadji is awesome supervisor.

Special thanks to our Co-Supervisor Mr. FELLAH Benzerga, lecturer researcher at Mascara University for his valuable help in mastering HFSS and CST software, his tips and for sharing his expertise in SIW technology with us.

We want to thank the president of jury Mr. BERKA Mohammed Associate professor at the Mascara University for agreeing to chair the jury of my thesis, and the examiners: Mr. MAHDJOUB Zoubir professor at the Sidi Belabbes University, Mme. BENDAOUDI Amina associate professor at the Sidi Belabbes University and Mr. GHOUALI Samir associate professor at the Mascara University; who were generous in sharing their expertise and their valuable time through their valuable comments and great efforts to improve my manuscript.

With gratitude and sincere thanks to Mr. MERABET Boualem, professor at Mascara University, for his keenness on good progress for the telecommunications doctoral training.

Finally, I extend my most sincere thanks to all those who have contributed directly or indirectly to the realization of this work.

Summary

The trend for the development of communication systems is moving towards minimized weight, reduced size, multiple functions, increased reliability and low cost. Microwave components such as waveguides, filters, etc. represent a very important part of modern telecommunications systems: satellite embedded systems, telecommunication systems in general, etc. To address this problem and for a smaller footprint, scientists have opted for the development of planar structures. A new technology that represents a very promising solution has emerged, namely substrate integrated waveguides (SIW). SIW technology has developed mainly because it shows several advantages such as low production cost, good quality factor and ease of integration into telecommunication circuits. This thesis work is part of the proposal of novel miniature DGS hybrid microwave components based on SIW technology for telecommunications systems that meet all of these required specifications. The simulation will be completed using powerful simulation software such as CST Microwave studio and HFSS, and the simulated models will be manufactured and measured in order to compare the simulated results with those of measurement.

Keywords: microwave components, DGS, SIW technology, design, realization, measurement.

Résumé

La tendance pour le développement des systèmes de communication se dirige vers un poids minimisé, une taille réduite, de multiples fonctions, une fiabilité accrue et un faible coût. Les composants microonde tels que les guides d'ondes, les filtres, ...etc représentent une partie très importante des systèmes de télécommunications modernes : systèmes embarqués sur satellite, systèmes de télécommunication en générale,...etc. Pour répondre à ce problème et pour un encombrement moindre, les scientifiques ont optés au développement des structures planaires. Une nouvelle technologie qui représente une solution très prometteuse a vu le jour à savoir les guides d'ondes intégrés au substrat (ou SIW en anglais : Substrat Integrated Waveguide). La technologie SIW s'est développée principalement parce qu'elle montre plusieurs avantages tels qu'un faible coût de production, un bon facteur de qualité et une facilité d'intégration aux circuits de télécommunication. Ce travail de thèse s'inscrit dans le cadre de proposition des nouvelles composants hyperfréquences en technologie SIW miniature DGS Hybride pour les systèmes de télécommunications répondant à l'ensemble de ces spécifications exigées. La simulation sera achevée en utilisant des logiciels de simulation performants tels que CST Microwave studio et HFSS, et les modèles simulés seront fabriqués et mesurés afin de confronter les résultats simulées avec ceux de mesure.

Mots clés : composants hyperfréquences, DGS, technologie SIW, conception, réalisation, mesure.

الملخص

الميول في تطوير أنظمة الاتصالات يتجه نحو تقليل الوزن وتقليل الحجم والوظائف المتعددة والموثوقية المتزايدة والتكلفة المنخفضة. تمثل مكونات الميكروويف مثل الأدلة الموجية والمرشحات وما إلى ذلك جزءًا مهمًا جدًا من أنظمة الاتصالات الحديثة: أنظمة الأقمار الصناعية المدمجة و أنظمة الاتصالات بشكل عام ... إلخ. لمعالجة هذه المشكلة ولتقليل الحجم، اختار العلماء تطوير الهياكل المستوية. ظهرت تقنية جديدة تمثل حلاً واعدًا للغاية، و هي الدليل الموجي المدمج في الركيزة (Substrate Integrated Waveguide بالإنجليزية) تطورت تقنية الدليل الموجي المدمج في الركيزة لأنها أظهرت : العديد من المزايا مثل انخفاض تكلفة الإنتاج, عامل جودة جيد وسهولة الاندماج في دوائر الاتصالات السلكية و اللاسلكية في هذه الأطروحة سنقوم باقتراح مكونات ميكروويف جديدة مصغرة و هجينة تعتمد على تقنيات الدليل الموجي المدمج في الركيزة و DGS لأنظمة الاتصالات التي تلبي جميع هذه المواصفات المطلوبة. ستتم المحاكاة باستخدام برامج قوية مثل HFSS و CST Microwave studio ، وسيتم تصنيع نماذج المحاكاة وقياسها من أجل المقارنة بينها.

الكلمات المفتاحية : مكونات الميكروويف، .تكنولوجيا SIW، DGS، التصميم، التصنيع، القياس.

Contents

CHAPTER II: SIW Filters Design, Fabrication and Measurement

CHAPTER III: SIW Traveling Wave Antennas Array Design

List of figures

List of tables

List of acronyms

SIW	Substrate integrated waveguide
HMSIW	Half Mode Substrate integrated waveguide
DGS	Defected Ground Structure
VPDGS	Vertically Periodic Defected Ground Structure
HPDGS	Horizontally Periodic Defected Ground Structure
HPF	High Pass Filter
LPF	Low Pass Filter
CPW	Coplanar Waveguides
TWA	Travelling Wave Antenna
PCB	Printed Circuit Board
GHz	Giga Hertz
THz	Tera Hertz
TE	Transverse Electrique
TM	Transverse Magnetic
TEM	Transverse Electric and Magnetic
DFW	Dielectric Filled Waveguide
FIT	finite integration technique
FDTD	Finite Difference Time Domain.
HFSS	High Frequency Structure Simulator
CST	Computer Simulation Technology
LTSA	Linearly Tapered Slot Antenna
SICs	Substrate Integrated Circuits
TX	Transmitter
RX	Receiver

General Introduction

Recently, development of the communication systems has focused on minimizing the weight, reducing the size, and increasing reliability at lower cost. Microwave components such as power dividers, antennas, filters and diplexers that are a very important part of modern telecommunications systems: embedded satellite systems, telecommunication systems in general [1]. Among the most widely used microwave components is the rectangular waveguide, but because of its big structure, it is difficult to manufacture it cheaply and integrate it into planar structures. To solve this problem, scientists have turned to the study and development of a new planar structure, which is the substrate integrated waveguide (SIW) [2].

The SIW technology is used for the design and manufacture of various components serving microwave systems with low cost, compact size and high quality factor Q such as antipodal antenna [3], leaky wave antenna [4], filter [5] and power divider [6]. The half mode substrate integrated waveguide HMSIW based on modified of the SIW structure by reducing the waveguide width and the surface area of the metallic plans nearly half compared with the SIW, it shows similar propagation characteristic compared to the SIW and smaller size. Several SIW filter based on half mode have proposed since its introduction [7].

Defected Ground Structure (DGS) is another promising technology based on a geometrical periodic and/or aperiodic slots engraved on the ground plane of microwave circuits. The defects on the ground plane disturb the current distribution of the ground plane; this disturbance changes the structure characteristics by including some parameters (slot resistance, slot capacitance and slot inductance) to the structure parameters [2].

In this work, we have proposed a novel configuration of many Hyperfrequency components based on SIW, HMSIW and DGS for solving the problems of the size, the performance and the cost. The work of this thesis is divided as follows:

The first chapter describe the planar, SIW and DGS components, first we started by introduce the theory of classical waveguide, than we passed to the characterization of the planar and SIW technologies, after that we presented the DGS filters, Shuntinductive SIW filters, SIW diplexers and SIW traveling wave antenna and planar antenna array.

The second chapter is dedicated to the presentation of novel configuration of the planar filters based on SIW, HMSIW and DGS cells by using CST and HFSS simulators. Many empirical parameters were calculated such as SIW Width and via diameter, also the taper transition is used between the structures. In order to validate the proposed filters, they were fabricated and measured.

The third chapter is dedicated to the design of novel configuration of the traveling wave antennas elements based on SIW for mm-waves and sub terahertz using CST and HFSS simulators, those antennas were used for construct the antennas array. The return loss, gain and radiation pattern of the proposed antennas and antennas array were analysed and optimized.

We ended our thesis by a general conclusion and perspective

CHAPTER I

SIW and DGS Microwave Components Characteristics

I. 1. Introduction

The recent development of communication systems requiring minimized weight, reduced size, and increased reliability with low cost. Waveguide is considered an effective transmission line and it is among the most used components in microwave systems, so it has taken a large share in academic and industrial research. It exist many waveguide types according to the functional frequency band (metallic waveguide, planar waveguide….). In this chapter, we will be interested for introducing some notions on planar, substrate integrated waveguide and DGS technologies. In addition, SIW Filters and SIW antennas will be discussed and characterized.

I. 2. Rectangular Waveguide

A waveguide is a physical system that is used to guide acoustic waves or electromagnetic waves to keep them confined in a particular environment, over a certain distance. The rectangular waveguide is one of the most used microwave components and the wave propagation in it is governed by the Maxwell equations. The internal guide geometry allows defining a cut-off frequency, which is the minimum frequency that must have the wave to propagate [8].

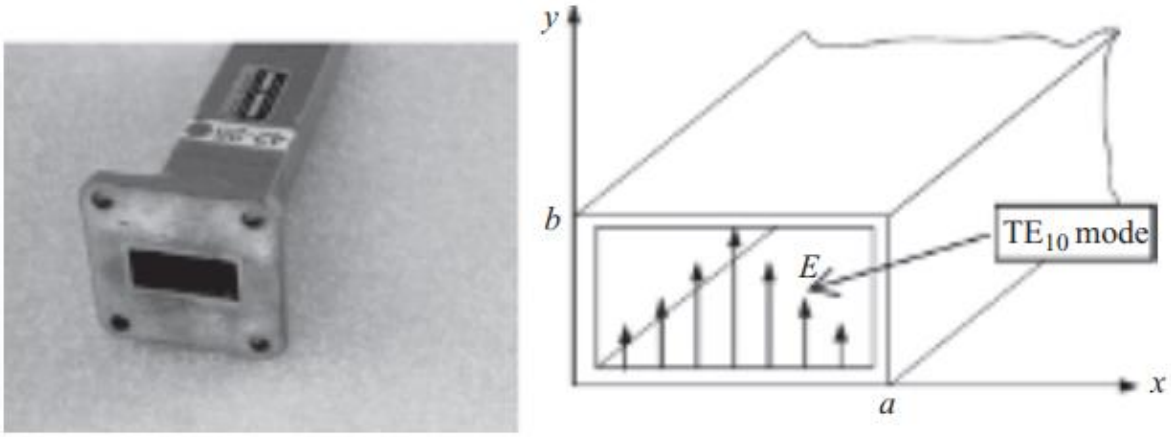

Figure I. 1. Rectangular waveguide [58].

We are going to study the propagation waves in lossless metal guides, with rectangular section, filled with a dielectric of relative permittivity ε_r and permeability μ_r, linear, homogeneous, isotropic [9].

I. 2. 1. Equations of the Electromagnetic Field Components in Rectangular Waveguide

The Maxwell equations that govern the electromagnetic field in the rectangular waveguide are written as follow [10].

Maxwell-Faraday law: $$\overrightarrow{rot}\vec{E} = -\frac{\partial \vec{\beta}}{\partial t} \quad \text{(I.1)}$$

Ampere-Maxwell law: $$\overrightarrow{rot}\vec{H} = \vec{J} + \frac{\partial \vec{D}}{\partial t} \quad \text{(I.2)}$$

Maxwell-Gauss electric law: $$\overrightarrow{div}\vec{E} = \frac{\rho}{\varepsilon_0} \quad \text{(I.3)}$$

Maxwell-Gauss magnetic law: $$\overrightarrow{div}\vec{B} = 0 \quad \text{(I.4)}$$

To deduce the propagation equations of E and H filed we have to use the vector identity: $\overrightarrow{rot}(\overrightarrow{rot}) = \overrightarrow{grad}(div) - laplacien$

$$\Delta^2 \vec{E} = -\omega^2 \varepsilon \mu \vec{E} \quad \text{(I.5)}$$

$$\Delta^2 \vec{H} = -\omega^2 \varepsilon \mu \vec{H} \quad \text{(I.6)}$$

We research the solution of the equations 5 and 6 on the Oz axis as a function of the transverse component along the Ox axis in the following form:

$$\vec{E}(x, y, z, t) = \vec{E}(x, y) e^{jwt - \gamma z} \quad \text{(I.7)}$$

$$\vec{H}(x, y, z, t) = \vec{H}(x, y) e^{jwt - \gamma z} \quad \text{(I.8)}$$

$$\gamma = \alpha + j\beta_g \quad \text{(I.9)}$$

$$\beta_g = \sqrt{k^2 - \left(\left(\frac{m}{a}\right)^2 - \left(\frac{n}{b}\right)^2\right)} \quad \text{(I.10)}$$

γ ,α, β represent respectively the coefficient of propagation, attenuation and the longitudinal propagation constant and by injected (7) and (8) in (5) and (6), respectively we obtained the following equations:

$$\Delta^2_t \vec{E} + (k^2 + \gamma^2)\vec{E} = 0 \tag{I.11}$$

$$\Delta^2_t \vec{H} + (k^2 + \gamma^2)\vec{H} = 0 \tag{I.12}$$

Δ^2_t Is the transverse laplacian and it is given by $\Delta^2_t = \frac{\partial^2}{\partial^2 x} + \frac{\partial^2}{\partial^2 y}$

$$K^2 c = k^2 + \gamma^2 \tag{I.13}$$

In waveguide theory, an electromagnetic wave can propagate within the waveguide in a many formats. These different types of waves correspond to the different elements within an electromagnetic wave.

TE mode: based on transverse electric waves, and it features by $E_z = 0$, $H_z \neq 0$

TM mode: based on transverse magnetic waves, and it features by $H_z = 0$, $E_z \neq 0$

TEM mode: based on transverse electric and magnetic waves and it features by $E_z \neq 0$, $H_z \neq 0$.

The components of the fields depend on both x and y, the modes are denoted by TMnm or TEnm, where n and m are integers that relate to variations of the fields in the x and y direction.

I. 2. 2. Analysis of TE Mode

The Wave equation of Hz component is given by equation 14.

$$\frac{\partial^2 H_z}{\partial x^2} + \frac{\partial^2 H_z}{\partial y^2} + \frac{\partial^2 H_z}{\partial z^2} = -\omega^2 \varepsilon \mu H_z \text{, with } \frac{\partial^2 H_z}{\partial z^2} = 0 \tag{I.14}$$

The solution of Hz is given by equation 15

$$Hz(x, y) = Ho \cos(\frac{n\pi}{a} x) \cos(\frac{m\pi}{b} y) \exp\left[j(\omega t - \beta z) \right] \tag{I.15}$$

For a plane waveguide, the relation of dispersion is given by $k^2 = (n\pi / a)^2$ and for rectangular waveguide is additionally includes the b term; therefore, the dispersion relation is given by the following equation:

$$k^2 = (\frac{n\pi}{a})^2 + (\frac{m\pi}{b})^2 = \omega^2 \varepsilon_0 \varepsilon_r \mu_0 - \beta^2 \tag{I.16}$$

By developing the first and second Maxwell's equations and substitute the equation 15 in the transverse component equations, we obtained the expression of the electromagnetic field:

$$Ex(x,y) = H_0 \frac{j\omega\mu}{k^2} \frac{n\pi}{b} \cos(\frac{m\pi}{a}x) \sin(\frac{n\pi}{b}y) \quad \text{(I.17)}$$

$$Ey(x,y) = -H_0 \frac{j\omega\mu}{k^2} \frac{m\pi}{a} \sin(\frac{m\pi}{a}x) \cos(\frac{n\pi}{b}y) \quad \text{(I.18)}$$

$$Hx(x,y) = H_0 \frac{\gamma}{k^2} \frac{m\pi}{a} \sin(\frac{m\pi}{a}x) \cos(\frac{n\pi}{b}y) \quad \text{(I.19)}$$

$$Hy(x,y) = H_0 \frac{\gamma}{k^2} \frac{n\pi}{b} \cos(\frac{m\pi}{a}x) \sin(\frac{n\pi}{b}y) \quad \text{(I.20)}$$

I. 2. 3. Analysis of TM Mode

The magnetic field is purely transverse (Hz = 0, Ez ≠ 0). By following the same approach, we find the expression of Ez that becomes equal zero on the guide walls.

$$Ez(x,y) = Eo \sin(\frac{n\pi}{a}x) \sin(\frac{m\pi}{b}y) \exp\left[j(\omega t - \beta z)\right] \quad \text{(I.21)}$$

The mode with the lowest cut-off frequency is the TM_{11} mode, which has the same cut-off frequency as the TE_{11}.

I. 3. Planar Technology

Planar technologies are complementary to voluminous technologies because of the size, the important weight and the bad connectivity of the voluminous technologies, the scientists opted for the development of the planar structures. They are also suitable for mass production, and therefore cost reduction. The principle is based on the use of a dielectric substrate in the form of plates, metalized on one or two sides. Several designs are possible for example the coplanar and microstrip line [11].

I. 3. 1. Microstrip Line

It is used for the manufacture of microwave circuits; the microstrip structure consists of a metallic conductor deposited on the upper face of a dielectric substrate and a ground plane on

the bottom face. In a microstrip line, the field lines are mostly concentrated in the dielectric between the metallized line and the ground plane, although a small portion is also found in the air above the substrate. This implies that a microstrip line cannot support pure TEM mode, since the phase velocity of TEM fields in the dielectric differs from that in air.

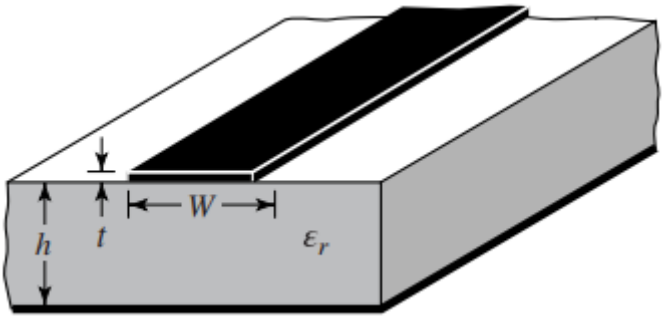

Figure I. 2. Microstrip line structure [58].

The wave propagation in this inhomogeneous structure takes place partly in the dielectric, partly in air, the proportion depends on the dielectric constant value of the substrate. The propagation constant, phase velocity and characteristic impedance can be approximated using static and quasi-static solutions. The phase velocity and the propagation constant are given by:

$$v_p = \frac{c}{\sqrt{\varepsilon_e}} \tag{I.22}$$

$$\beta = \beta_0 \sqrt{\varepsilon_e} \tag{I.23}$$

With: $\beta_o = \frac{2\pi . f}{c} = \frac{2\pi}{\lambda_o}$

The effective dielectric constant takes an intermediate value between 1 and the dielectric constant of the substrate: $1 < \varepsilon_e < \varepsilon_r$

The effective dielectric constant depends on the thickness of the substrate h and the width of the metallization W. It can be approximated by the equation 20:

$$\varepsilon_e = \frac{\varepsilon_r + 1}{2} + \frac{\varepsilon_r - 1}{2} . \frac{1}{\sqrt{1 + 12\frac{h}{W}}} \tag{I.24}$$

The characteristic impedance of the microstrip line is given by the following equations:

$$Z_o = \begin{cases} \dfrac{60}{\sqrt{\varepsilon_e}} \ln\left(\dfrac{8h}{W} + \dfrac{W}{4h}\right) & W/h \le 1 \\ \dfrac{120\pi}{\sqrt{\varepsilon_e}\left[\dfrac{W}{h} + 1.393 + 0.667.\ln\left(\dfrac{W}{h} + 1.444\right)\right]} & W/h \ge 1 \end{cases} \quad \text{(I.25)}$$

If we want to calculate the ratio W/h for a characteristic impedance Z_0 of the microstrip line, the following equation can be used:

$$\frac{W}{h} = \begin{cases} \dfrac{8.e^A}{e^{2A} - 2} & W/h < 2 \\ \dfrac{2}{\pi}.\left[B - 1 - \ln(2B-1) + \dfrac{\varepsilon_r - 1}{2.\varepsilon_r}.\left\{\ln(B-1) + 0.39 - \dfrac{0.61}{\varepsilon_r}\right\}\right] & W/h > 2 \end{cases} \quad \text{(I.26)}$$

Where:

$$A = \frac{Z_o}{60}.\sqrt{\frac{\varepsilon_r + 1}{2}} + \frac{\varepsilon_r - 1}{\varepsilon_r + 1}.\left(0.23 + \frac{0.11}{\varepsilon_r}\right) \quad \text{(I.27)}$$

$$B = \frac{377\pi}{2.Z_o.\sqrt{\varepsilon_r}} \quad \text{(I.28)}$$

The attenuation in the microstrip line due to dielectric losses is given by following equation:

$$\alpha_d = \frac{k_o \varepsilon_r (\varepsilon_e - 1)\tan(\delta)}{2\sqrt{\varepsilon_e(\varepsilon_r - 1)}} \quad \text{(I.29)}$$

$\tan(\delta)$ is the dielectric loss tangent

The attenuation due to losses in the conductor is approximated by the following equation:

$$\alpha_c = \frac{R_s}{Z_o.W}. \quad \text{(I.30)}$$

Where

$$R_s = \sqrt{\frac{\omega \mu_o}{2\sigma}} \quad \text{(I.31)}$$

I. 4. SIW Technology

A novel technology of the integrated circuits called "substrate integrated circuits (SICs) was presented in [12]. This idée has unified the monolithic and hybrid integrations of many planar and non-planar circuits that are fabricated in single substrate or multilayer platforms. The concept is the made or synthesized, any nonplanar structures in planar form, which presents the foundation of SICs. Hybrid design strategy is an easy-to-use method with low cost, which is of critical importance for the development of systems and high-volume millimeter-wave Integrated circuits. The transmission line is an important technology for developing high frequency electromagnetic hardware. The choice of the transmission lines is depend on mass-production scheme, density integration and the cost. Among the most used components as transmission line is the rectangular waveguide with their salient features such as high quality factor and low insertion loss etc. However, due to its voluminous structure and non-planar geometry, it is impossible to use it for to design and develop microwave integrated circuits. Strip lines and coplanar waveguides (CPW) are presently the principal choices of integration for the development of microwave circuits because they characterised by low profile and easy manufacturing. Unfortunately, the performances of microstrip-like circuits are limited by physical properties such as field or current singularities occurring at the stripline [13]. SIW structure keeps the majority of the advantages of the classical waveguides. The most important feature of SIW technology is its capacity of enabling a possible complete integration of all the components on the same substrate, including passive components, active elements, and even antennas as presented in [14] [15] [16] [17]. SIW techniques can be used to solve many problems. A problem arising at high frequency is the appearance (trapping) of surface waves that generally reduces the efficiency of antenna. The SIW can effectively control this phenomenon. As SIW components are bounded by conducting surfaces on both sides of the substrate, they exhibit the merits of very low leakage loss / radiation and insensitive to outer interferences. This development of SIW allows the demonstration and applications of innovative passive and active circuits, antennas, and systems at microwave and millimeter wave frequencies covering a very broad frequency including sub-gigahertz and sub-terahertz.

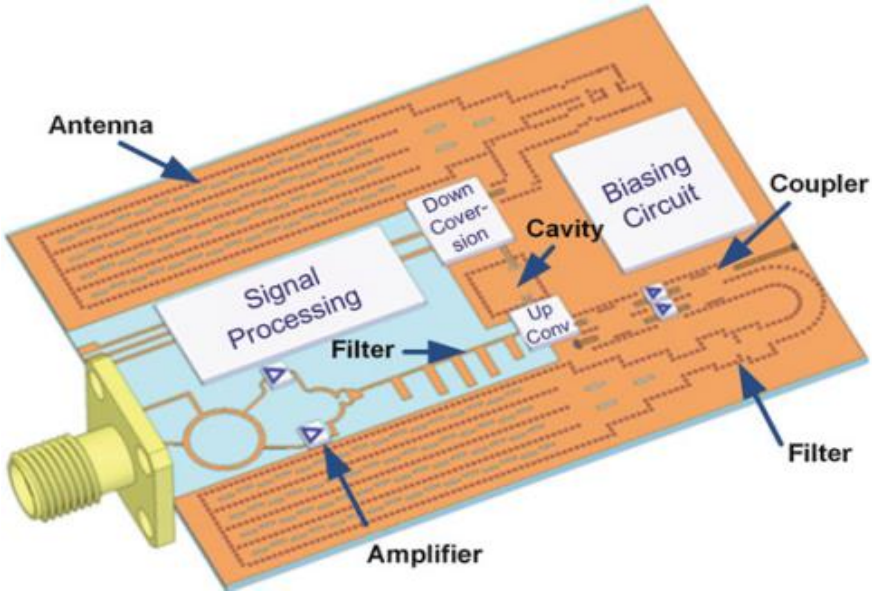

Figure I. 3. Combined SIW components, with active and DSP circuits on the same substrate [13]

I. 4. 1. SIW Line Configurations

The SIW structures can be arranged in different configurations. Depending on applications in term of allowed space, integrability, task and performance, one of them can specially be preferred. The Table I. 1 shown a collection of some important configurations. The H to E plane interconnection shown in Table I.1 is very useful in the design of multipolarization antenna feeding. A 2-layered T-type structure was proposed for the first time in 2005, for the miniaturization of an SIW in multi-layered substrates. L-FSIW was proposed for the first time in 2013 to build a series of couplers.

Table I. 1 SIW line configurations [13].

Type	H-plane SIW line	Two plane SIW line	C-type SIW line	L-type SIW line
Structure	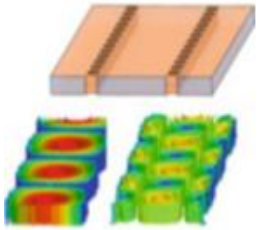	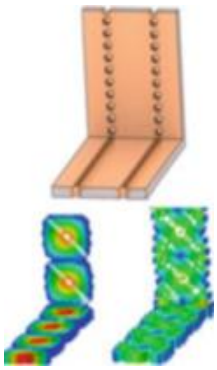	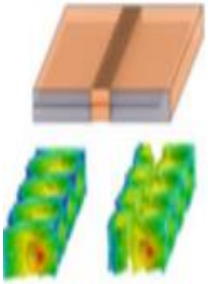	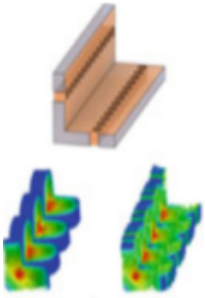

I. 4. 2. SIW Design Basics and Techniques

The SIW is a rectangular waveguide-like structure in an integrated planar form, which can be design and fabricated by using two rows of conducting cylinders, vias or slots embedded in a substrate that is electrically sandwiched by two parallel metal plates as shown in Figure I.4 [13].

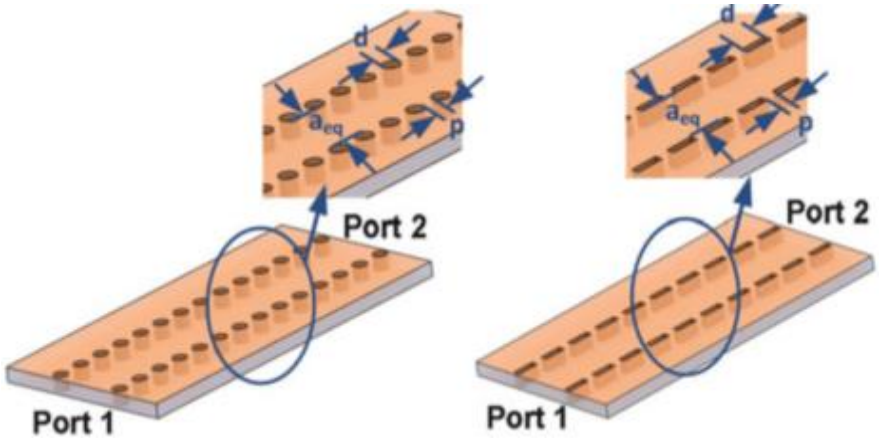

Figure I. 4. SIW geometry [13].

The operating band is delimited by the monomode propagation of quasi-TE_{10} wave as its cut-off frequency is only related to equivalent width a_{eq} of the synthesized waveguide as long as the waveguide height or substrate thickness is smaller than this width. The main empirical SIW design equation is related to its width "Wsiw" and it is given by equation 32

$$Wsiw = a_{eq} + \frac{d^2}{0.95p} \tag{I.32}$$

Highlighted more precise formulas are proposed by Ya in [23] by giving the normalised width of the SIW equivalent waveguide, which is convenient and handy for design.

$$a_{eq} = Wsiw\left\{\xi_1 + \frac{\xi_2}{\frac{p}{d} + \frac{\xi_1 + \xi_2 - \xi_3}{\xi_3 - \xi_1}}\right\} \tag{I.33}$$

Where:

$$\xi_1 = 1.0198 + \frac{0.3465}{\frac{Wsiw}{p} - 1.0684} \tag{I.34}$$

$$\xi_2 = -0.1183 - \frac{1.2729}{\frac{Wsiw}{p} - 1.2010} \tag{I.35}$$

$$\xi_3 = -0.1183 - \frac{1.2729}{\frac{Wsiw}{p} - 1.2010} \tag{I.36}$$

To minimize the radiation and return loss due to the field leakage from the gaps between vias two conditions are required: $d < 0.2 \times \lambda g$ and $p \leq 2 \times d$ where λg is the guided wavelength [1].

$$\lambda g = \frac{2\pi}{\sqrt{\frac{(2\pi f)^2 \varepsilon_r}{c^2} - \left(\frac{\pi}{a}\right)^2}} \tag{I.37}$$

In a conventional rectangular waveguide, the width of the guide is calculated from the desired cut-off frequency

$$f_c = \frac{c}{2\pi}\sqrt{\left(\frac{m\pi}{a}\right)^2 + \left(\frac{n\pi}{b}\right)^2} \tag{I.38}$$

With:
a, b: are the waveguide dimensions.
m, n: are the mode numbers.

For dielectric filled waveguide DFW, with the same cut-off frequency the dimension "a_{eq}" of the waveguide is calculated by Equation 38 where ε_r is the relative dielectric constant of the dielectric that fills the waveguide.

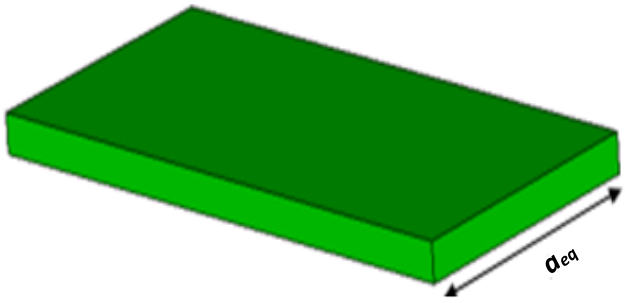

Figure I. 5. Dielectric filled waveguide geometry.

$$a_{eq} = \frac{a}{\sqrt{\varepsilon_r}} \tag{I.39}$$

I. 4. 3. Transition From Microstrip Lines to SIW

Once the SW is designed, it must be have a transition to a transmission line, which is connected to a network analyzer in practice. Different waveguide-to-SIW transitions are detailed in the literature. Most of these transitions are based on waveguide-to-microstrip or to-CPW. A transition from SIW to a microstrip line has been presented by Deslandes in [21].

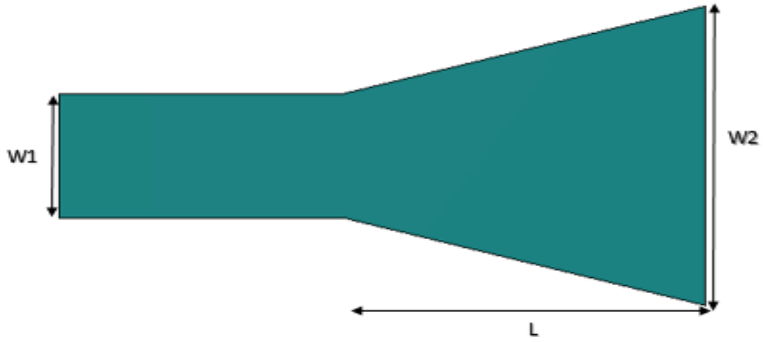

Figure I. 6. Taper transition geometry.

This transition contains three main parameters, namely the initial width W1, the final width W2 and the length L of the profiled line. The initial width of the microstrip line W1 must be calculated to obtain the desired characteristic impedance. This width is generally chosen to obtain a characteristic impedance of 50 ohms and the final width W2 is calculated for an impedance defined by the following relation:

$$Z_{pi} = Z_{TE}\frac{\pi^2 h}{8Wsiw} \tag{I.40}$$

Z_{TE}: represent the wave impedance for the TE_{10} mode and it is given by equation 41.

$$Z_{TE} = j\omega\frac{\mu'}{\beta} = \sqrt{\frac{\mu}{\varepsilon_r}}\times\frac{\lambda_g}{\lambda} \tag{I.41}$$

I. 5. Defected Ground Structure

Defected Ground Structure (DGS) is a geometrical slot etched on the ground plane of microwave components. A single defect or a number of periodic and/or aperiodic defects configurations may be comprised in DGS. Consequently, defects embedded on the ground plane of microwave components are mention to as DGS. This ground plane defects disturb the distribution of current in the ground plane; this disturbance changes the structure characteristics [22].

I. 5. 1. DGS Unit

In the literature, many geometries cells engraved in the ground plane have been presented [23] [24] [25] [26]. In Figure I.7 it is shown different shapes including spiral head, arrowhead-slot and H shape slots, a square open-loop with a slot in middle section, open-loop dumbbell andinterdigital DGS. The new DGS unit could control the two transmission zeros near the passband edges and easily control the frequency of the slot by changing the length of the metal fingers [27-28].

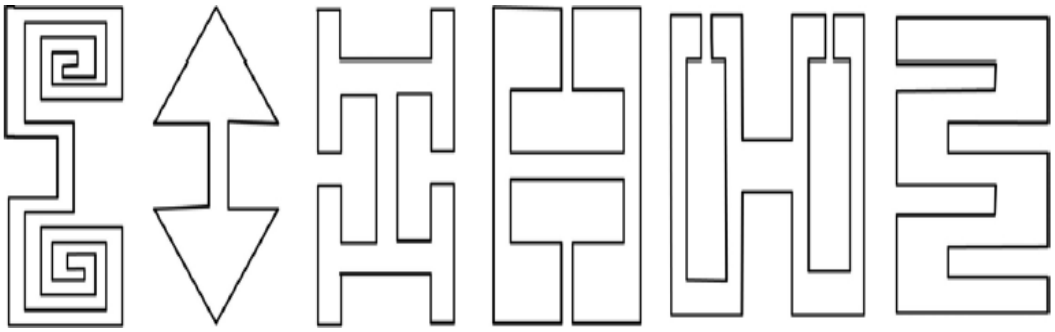

Figure I. 7. Various DGSs: (a) spiral head, (b) arrowhead-slot, (c) Shape slots, (d) a square open loop with a slot in middle section, (e) open-loop dumbbell and (f) interdigital DGS [29].

I. 5. 2. Periodic DGS

Periodic DGS structures have extensively used in microwave circuits applications. In periodic structure, there are two important properties: the additional equivalent components and the slow-wave effect and by using these properties, higher level of miniaturization is achieved. By cascading the resonant cells in the ground plane, the level of return loss, stopband and bandwidth are improved according to the number of DGS cells. There are two types of periodicity. They are named VPDGS and HPDGS as shown in the Figure I.8 [29]. The main parameters that affecting the performance of microwave components based on DGS are DGS shape, distance between two DGS cells and the distribution of the DGSs cells in the ground plan.

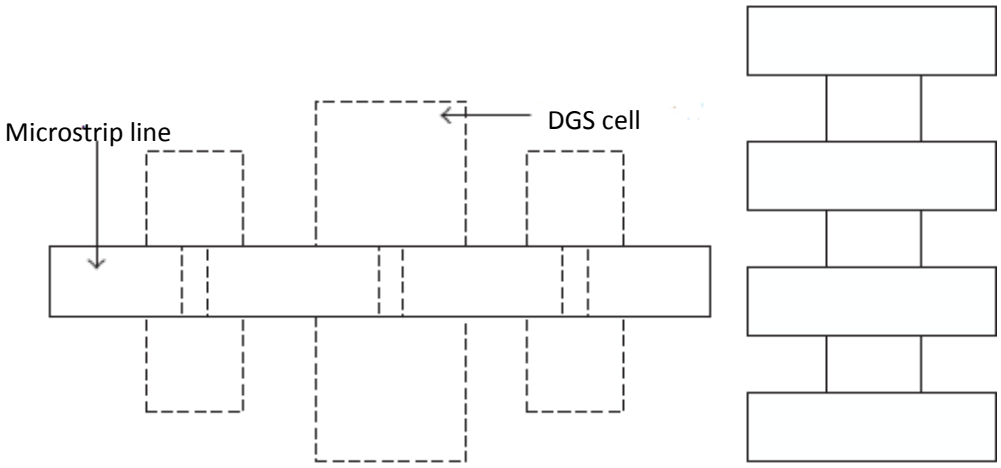

(a) (b)

Figure I. 8. Periodic DGS: (a) HPDGS, (b) VPDGS [29].

I. 5. 3. Equivalent Circuit of DGS

Among the most efficient modelling of the DGS unit is a parallel resonant circuit R, L and C connected to transmission lines on its sides, as show in Figure I.9.

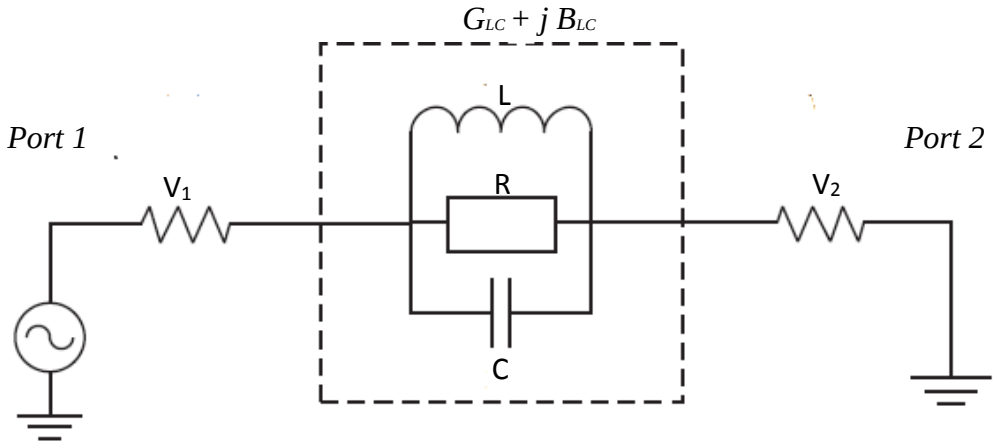

Figure I. 9. DGS Unit equivalent RLC circuit [29].

$$C = \frac{\omega_c}{2Z_0(\omega_0^{\,2} - \omega_c^{\,2})} \tag{I.42}$$

$$L = \frac{1}{4\pi^2 f_0^{\,2} C} \tag{I.43}$$

$$R(\omega) = \frac{2Z_0}{\sqrt{\dfrac{1}{|S11(\omega)|^2 - (2Z_0(\omega C - \dfrac{1}{\omega L}))^2 - 1}}} \tag{I.44}$$

I. 5. 4. DGS Applications for Microwave Circuits

DGS technique is extensively used for the design of compact active and passive devices. According on the DGS geometries, each shape provides its own distinctive characteristics such circuit functions as unwanted signal filtering, antenna and diplexer can be designed by setting the required DGS patterns, which correspond to the desired circuit operations.

I. 5. 4. 1. Bandpass Effects

DGS has been used for bandpass filter (BPF) response, many work has been done related to bandpass filter to overcome the abovementioned problems. In [30] a microstrip bandpass filter was presented, operating in the range from 2.9 GHz to 3.1 GHz (200 MHz), the substrate material used for the filter was Roger 4350B with size of 53.7 × 17.6 mm^2. The stop band rejection was available from 3.1 GHz to 4 GHz. In [31] new compact S-Band Bandpass Filter (BPF) With Wideband Passband was proposed with high rejection. Another, HMSIW-based bandpass filter with step impedance resonators operating in the range from 3.4 GHz to 3.6 GHz (200 MHz); sized at 21 × 12 mm2 was proposed in [32]. Next, a SIW based Koch fractal electromagnetic Bandgap (KFEBG) bandpass filter was presented in [33]; the filter operated in the frequency range from 3.2 GHz to 3.6 GHz (400 MHz) and the substrate material used for the filter was Arlon AD1000 with complete area of about 106 × 12 mm2. In [34] a compact dual-plane resonant cell (DP-RC) SIW BPF with two U-shape slots on the top metal plate and two H-shape fractal DGS etched on the bottom metal plate of a SIW cavity is proposed, the filter can produce two transmission zeros on the upper band that can extend the upper stopband. In [35] a dual-mode SIW bandpass filter is presented with a good stop band performance but the filter size is large. In [36] a BPF is proposed using CSRR with a good analysis of the parameter effect over the filter output characteristics. However, the filter is poorly adapted.

I. 5. 4. 2. Stopband Effects

For reject, a certain band of frequency it must be engraved a defect on the metallic ground plane. We notice that The DGS allow us to realize a planar band-stop filter; at this stopband, a Surface wave and other leakage transmission are suppressed. Inside the conventional dumbbell shaped DGS a square patch has been inserted to modify its frequency response and to allow the control of the rejected frequency. Now we can rejected high, Low or even multiple frequencies by the choice of the good positions of the short circuits that can be placed along the

circumference of the square patch. The varactor diode was placed between the square patch and CPW ground to make it tuneable as illustrated in Figure I. 10. Substrate Integrated Waveguide (SIW) has been used with DGS for realising a band-stop filter [37-38]. It has been found that the proposed DGS SIW cavity filters present very promising performances with low insertion loss and high stopband rejection. SIW DGS filters are valuable in the realization of low cost microwave and millimeter-wave systems. Compactness has been achieved using a SIW filter with DGS resonators with better frequency selectivity and wide stopband.

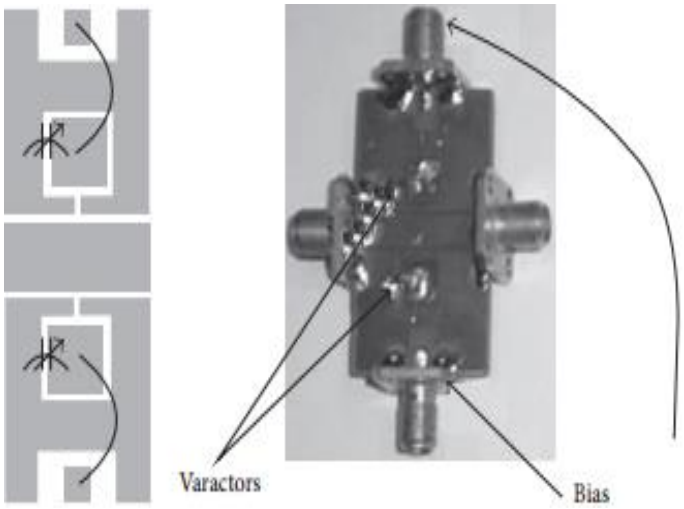

(a) (b)

Figure I. 10. (a) Schematic of the tunable band-stop filter (b) Fabricated M-DGS with the capacitors.

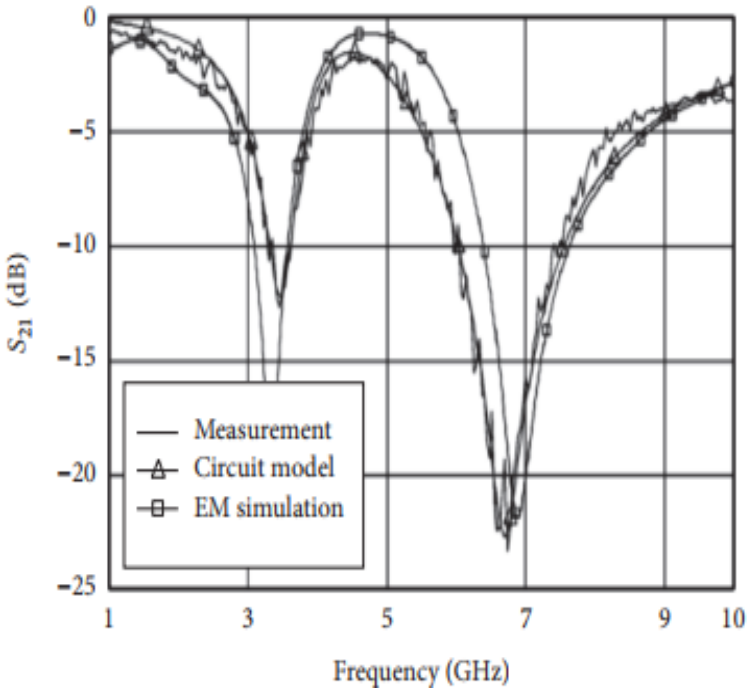

Figure I. 11. Simulation and measurement results for the HCR DGS low pass filter.

I. 5. 4. 3. LowPass Effects

In [39] a new technique is proposed to design an N –pole DGS LPF. The microstrip line used in the proposed DGS-LPF was wider than conventional microstrip, and the proposed DGS-LPF neither has open stubs, nor high-impedance lines, which have been essentially required in conventional design. The shunt capacitances are realized by the widely transmission line and the series inductances are realized by the DGSs.

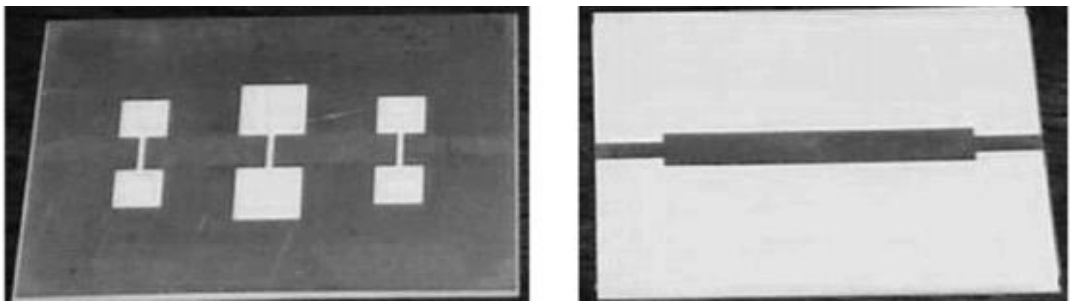

Figure I. 12. Five-pole DGS-LPF (a) Bottom side (b) Top side [39].

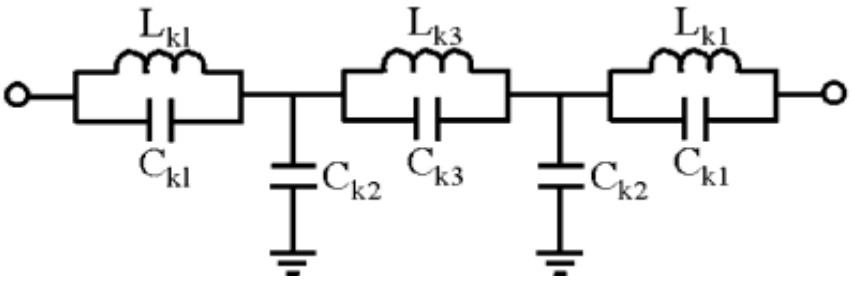

Figure I. 13. Modified five-pole prototype LPF using an L–C resonator [39].

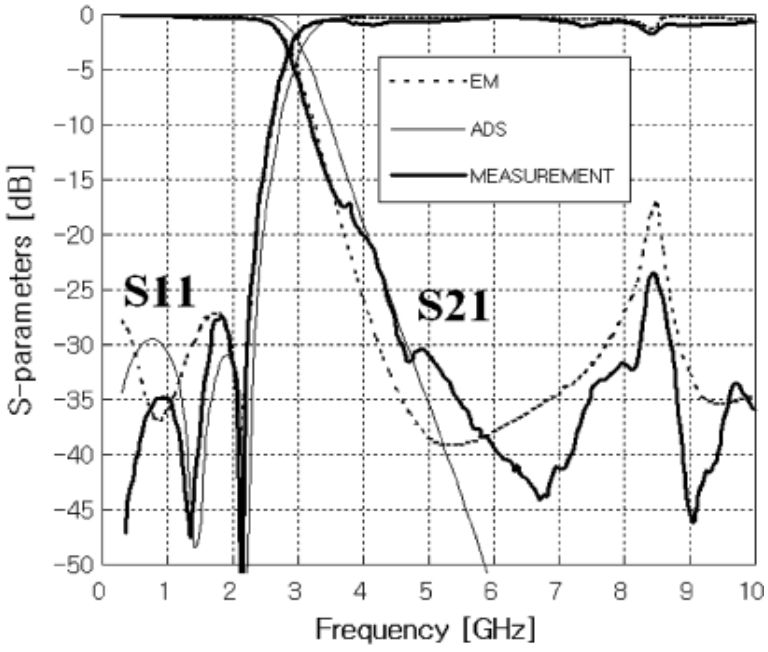

Figure I. 14. Performances of the five-pole DGS-LPF [39].

In [27] a novel low-pass filter with an ultra-wide stopband is presented, the filter is comprised of a new cross-shape defected ground structure (CSDGS).

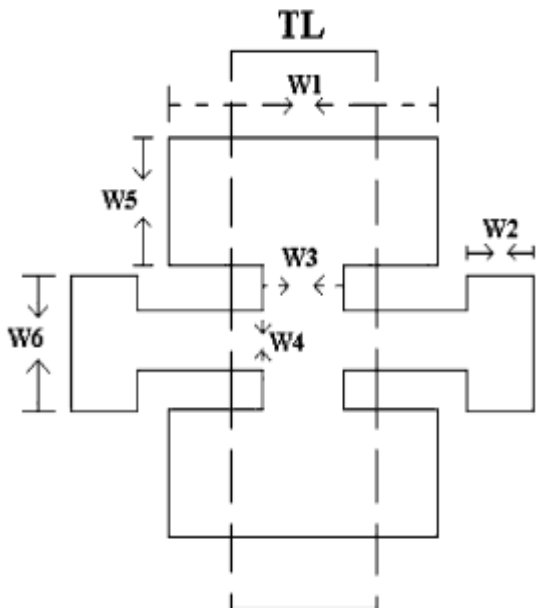

Figure I. 15. Configuration of cross-shape DGS cell [27].

The proposed filter is modelled by an equivalent circuit using H shape DGS model and I shape DGS model.

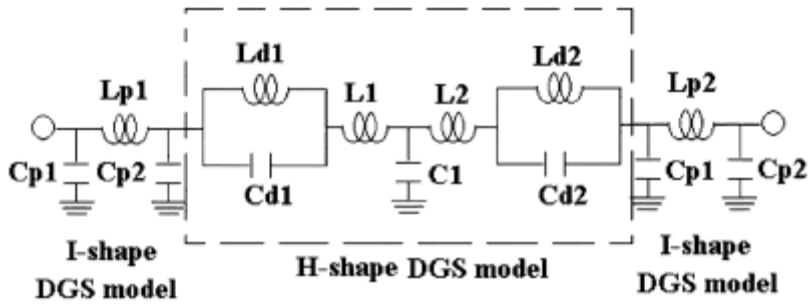

Figure I. 16. Equivalent circuit using H shape DGS model and I shape DGS model [27].

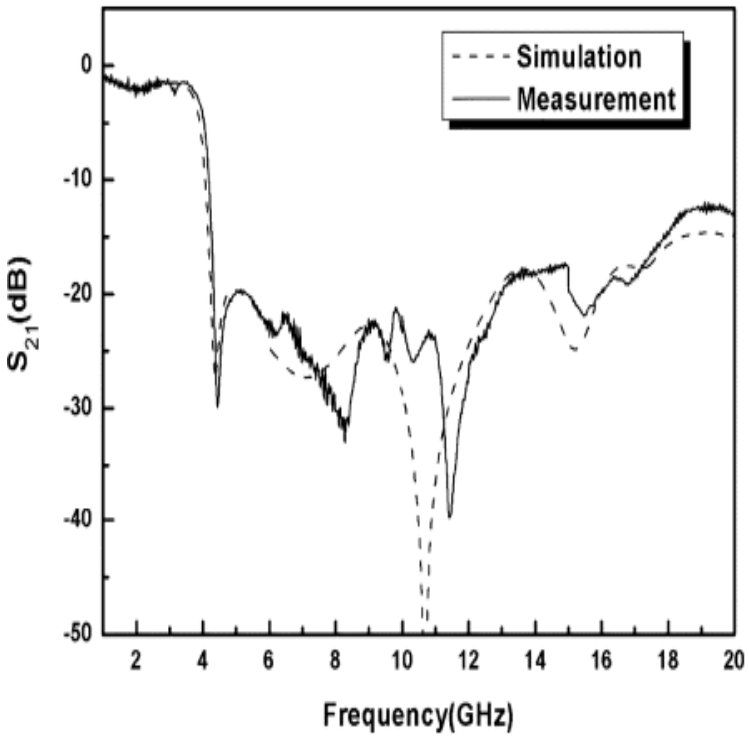

Figure I. 17. S_{21} of the DGS filter [27].

I. 5. 4. 4. HighPass Effects

In [40] a highPass filter based on SCSRR is presented. The proposed HPF filter is fabricated on Arlon 5880 with the relative dielectric constant εr = 2.2 and with a loss tangent of δ = 0.0023 with a thickness of 0.8mm as shown in Figure I.18. The SCSRR is etched exactly beneath of parallel-coupled inter-digital transmission line configuration. The simulated and measured frequency responses are shown in Figure I.19.

(a) (b)

Figure I. 18. The proposed HPF (a) Top view (b) Bottom view [40].

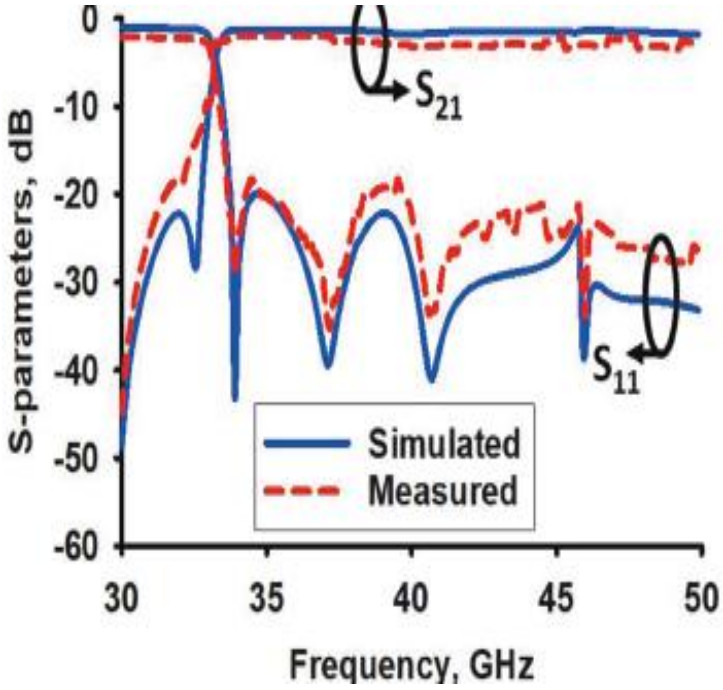

Figure I. 19. Comparison between simulated and measured results [40].

From Figure I. 19 it is observed that measured and simulated responses are in good agreement. However, some minor deviation is observed due to fabrication precision error and connector losses. Further, Figure I. 19 shows the proposed HPF filter has measured maximum insertion loss of 1.45 dB from 34.1 GHz to 50 GHz. The fabricated filter has a better Passband measured return loss of 19 dB and measured 3 dB cut-off frequency (fc) of 34.1GHz.

I. 5. 4. 5. Slow-Wave Effect

Among the advantages of DGS is the slow-wave effect, which is caused by the equivalent LC components. The transmission lines with DGS have much higher impedance and increased slow-wave factor than conventional lines so the circuit size can be reduced with these properties, such as microwave Rat-race hybrid couplers and amplifiers. In Figure I.20 DGS Doherty power amplifier (DDA) could reduce the circuit size by the trivial insertion loss, slow-wave effect and excellent harmonic termination characteristic effect compared with the conventional Doherty power amplifier (CDA), the radios of the reduced lengths to CDA are 62% at the peaking amplifier output and 71% at the carrier amplifier output [29].

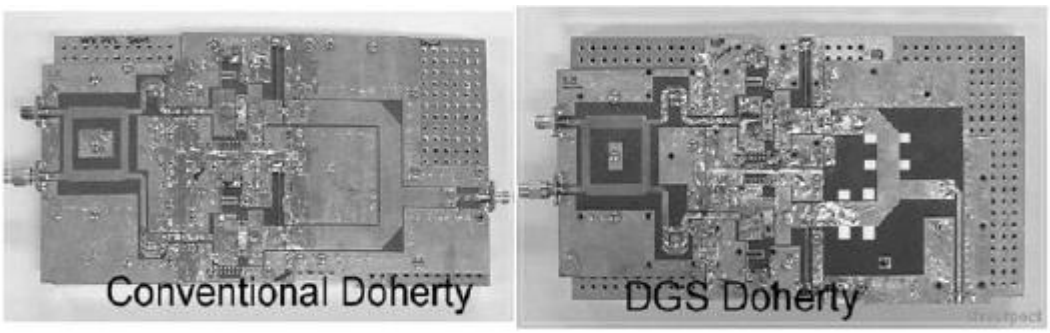

Figure I. 20. Comparison between CDA and DDA size [29].

I. 6. Substrate Integrated Waveguide Filters

I. 6. 1. Shuntinductive SIW Filters

Shuntinductive coupling is easily and efficiently technique can be used to design a SIW filters, resembling that in an air-filled rectangular waveguide filter. There are two types of the ShuntInductive coupling either an iris or a shuntinductive post. The Figure I.21 represent a three-pole SIW bandpass filter configuration using shuntinductive posts. The SIW filter consists of two microstrip-to-SIW transitions and four coupling posts in the middle of the guide. The two large posts are used for the inter-resonator couplings and the two small posts are used to facilitate the input and output couplings. The relative dielectric constant of the used substrate is 2.2 and its loss tangent is tan δ = 0.001 and its thickness is 0.25 mm. The simulations results of the filter is plotted in the Figure I.22. For control the couplings, the posts used in an inductive-post filter may have different diameters, all centered in the middle of the guide. Where it produces a larger coupling for the smaller diameter. For reducing the fabrication complexity and cost, a new filter design is presented in [41] by using an offset post arrangement with the same post diameter [42].

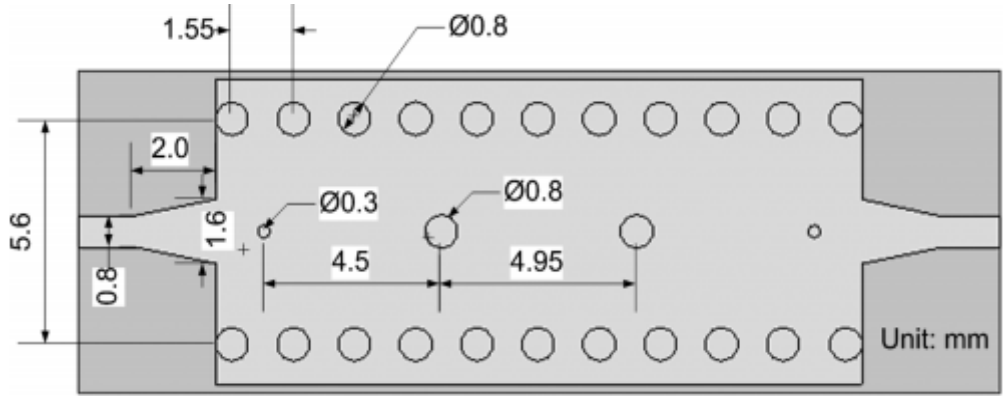

Figure I. 21. SIW filter shunt-inductive posts configuration [42].

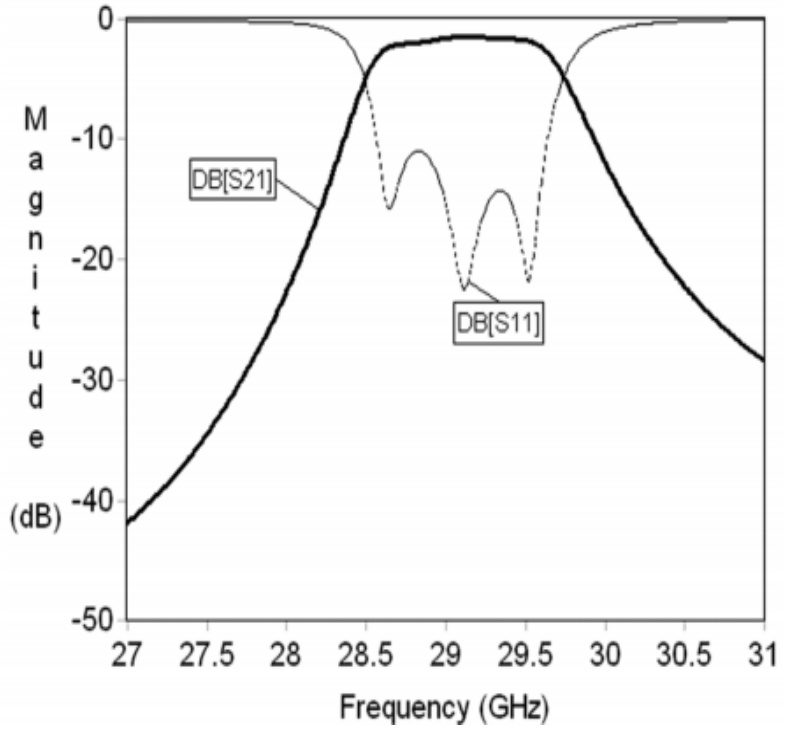

Figure I. 22. S parameters of SIW filter [42].

To design a filter based on posts of the same diameter, first it must be modelled a post in rectangular waveguide by a Pi network. For calculate Xa and Xb it must be used the theory developed by Marcuvitz in [43] for posts in a waveguide. This Pi network is then transformed into a -k inverter using equation 44. With this model, we determine the offset posts position of the filter on the basis of the synthesis techniques for inductive posts in the rectangular waveguide, as presented in [44].

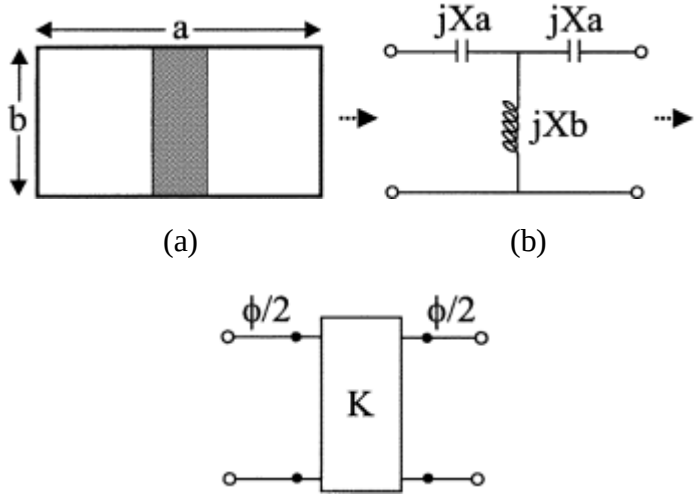

Figure I. 23. The inductive post filter design process. (a) Post in waveguide. (b) Equivalent Pi network. (c) Equivalent K-inverter network [41].

$$k = Z_0 \left| \tan\left(\frac{\phi}{2} + \tan^{-1} \frac{Xa}{Z_0} \right) \right| \tag{I.45}$$

$$\phi = \tan^{-1}\left(\frac{2Xb}{Z_0} + \frac{Xa}{Z_0} \right) - \tan^{-1} \frac{Xa}{Z_0} \tag{I.46}$$

I. 6. 2. SIW Folded-Waveguide Resonator Filters

Substrate integrated waveguide filters using folded-waveguide resonators have been presented and demonstrated in [45] [46] [47]. The Figure I.24 demonstrate a two-pole substrate integrated folded-waveguide resonator filter configuration. It composed of two substrate integrated folded waveguide resonators, which are coupled to each other by coupling aperture and they are separated by a metallic vias common cavity wall. A microstrip-stripline transition is required at the input or output to ensure that the filter can be easily integrated with other microwave circuits. The used dielectric substrate has a relative permittivity of 3.2 and a thickness of h = 0.762 mm for each layer. The results of the filter simulation are presented in the Figure I.25. The proposed filter has good rejection, good selectivity and low losses.

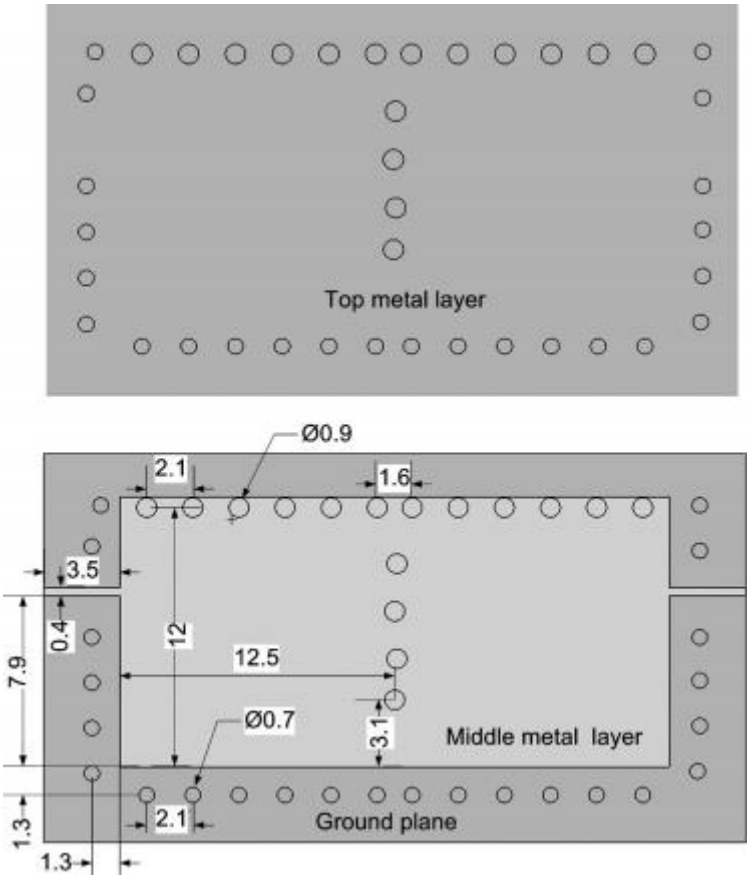

Figure I. 24. Configuration of the designed substrate integrated folded-waveguide filter [42].

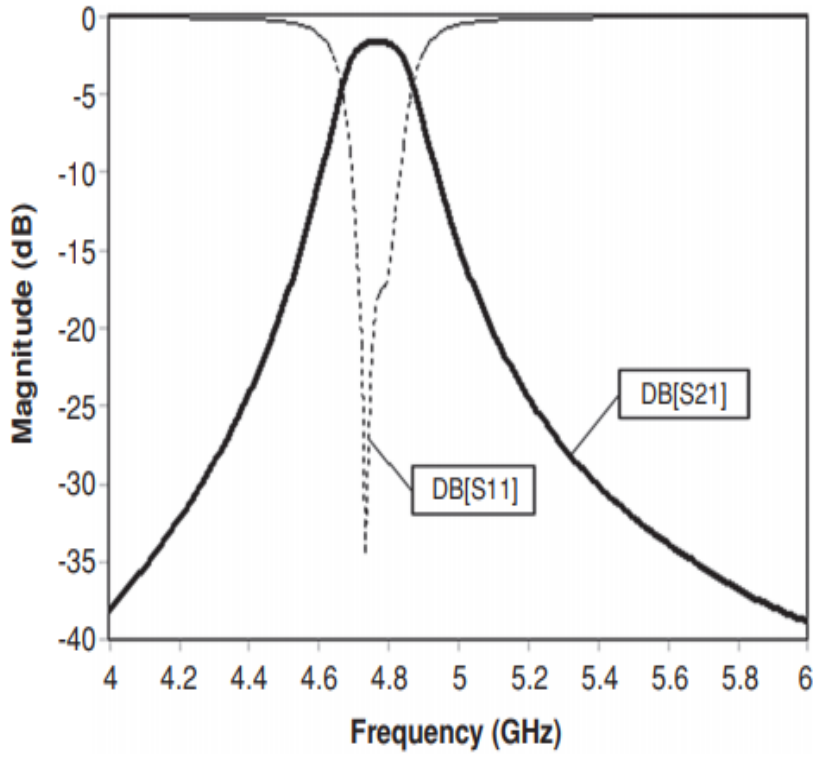

Figure I. 25. S parameter of the substrate integrated folded-waveguide filter [42].

I. 6. 3. SIW Diplexers

Diplexers are very important components that are used in microwave systems its role is to permit the transmission and reception by the antenna at the same time. Figure I.26 represent a generalized diplexer diagram where two filters is matched to a T-junction power divider. The diplexer uses two filters, where one filter provides Tx signal path and the other provides Rx signal path separately. Diplexers have require a strict bandwidth and stopband, to avoid the interaction between the TX with RX channels [48]. The best chose to construct the diplexer is half wavelength bandpass filters as they provide the best trade-off between channel performance and filter size. The insertion loss of the diplexer affects on the overall noise figure of the receiver system since the diplexer is connected directly to the antenna, also it can affect the antenna sensitivity. In order to minimise the insertion losses, it is preferred to use a diplexers, which have high Q filters. One more type of diplexer configuration made up of two identical channel filters and two identical hybrid couplers as can be shown in Figure I. 27. In its current form, if ports 1 and 3 are selected to construct the TX channel, a second filter could be added to port 2 to construct the RX channel. Among the advantages of the diplexer based on hybrid couplers is the increased power handling ability as a consequence of the hybrid couplers that supplying only half the input power to one of the diplexing channels.

this type of diplexer is suitable for the future satellite ground stations where the required power handling of Q/V band waveguide diplexers is in excess of 500 W [49] . The disadvantage of the diplexers based on hybrid coupler compared with diplexer based on T-junction is that they have larger size and have a higher insertion loss [48].

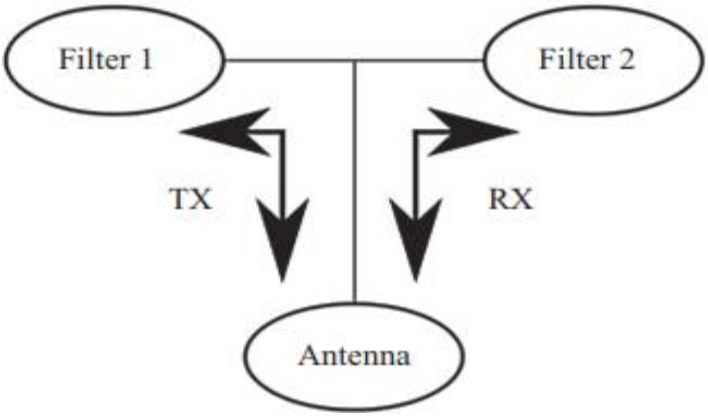

Figure I. 26. A generalised T-junction diplexer block diagram [50].

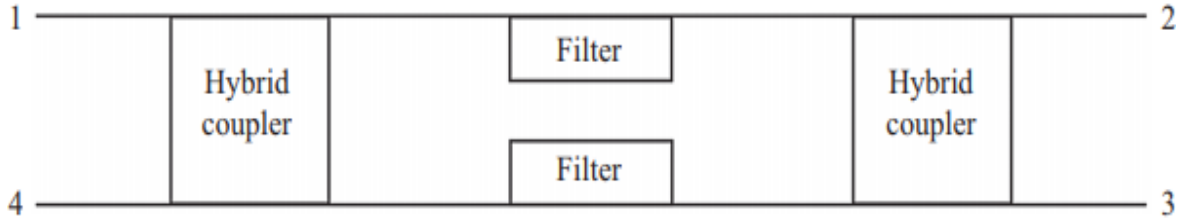

Figure I. 27. Hybrid Couplers based diplexer block diagram [50].

I .6. 3. 1. Hybrid Coupler Type Diplexer Operation

In this section, the author demonstrates the operation of the diplexer based on hybrid couplers. The RX filter has been removed from the analysis to simplify the demonstration. Consider the schematic in Figure I.28 [50].

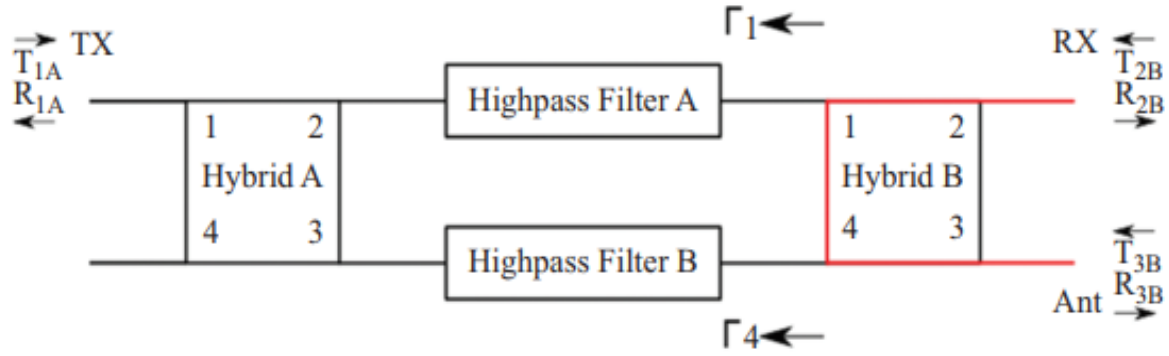

Figure I. 28. Schematic diagram showing a signal being routed to the RX port from the antenna port [50].

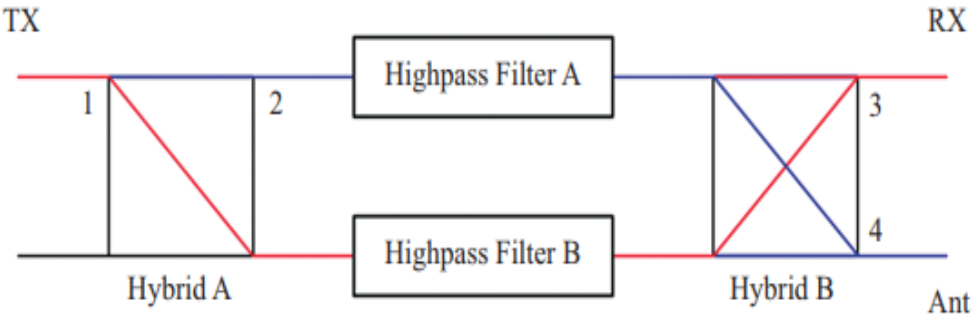

Figure I. 29. Schematic diagram showing the TX–Antenna path of the diplexer [50].

For a signal passed from the antenna to the RX port, the following scattering matrix is valid for identical highpass filters and hybrid couplers.

$$\begin{bmatrix} R_{2B} \\ R_{3B} \end{bmatrix} = \begin{pmatrix} \frac{1}{2}(\Gamma 4 - \Gamma 1) & \frac{j}{2}(\Gamma 1 + \Gamma 4) \\ \frac{j}{2}(\Gamma 1 + \Gamma 4) & \frac{1}{2}(\Gamma 1 - \Gamma 4) \end{pmatrix} \begin{bmatrix} T_{2B} \\ T_{3B} \end{bmatrix} \tag{I.47}$$

Where *T* and *R* represent the transmitted and reflected waves, respectively. Looking from the antenna port, the high-pass filters act like a load with a reflection coefficient $\Gamma = \Gamma_1 = \Gamma_4$. In this case, the matrix 46 can be reduced to equation 48.

$$S_{Ant-RX} = \frac{R_{2B}}{T_{3B}} = j\Gamma \tag{I.48}$$

If $\Gamma = 1$, a signal detected at the antenna will be redirected completely to the RX port without any additional loss. This requires the high-pass filters to have enough rejection below the cut-off frequency to ensure there is a significant reflection in the RX frequency band. In Figure I.29, we consider a signal incident at the TX port. At point 1, the signal is split into two components after passing through Hybrid A that has a 90 phase difference when viewed from point 2. The signals pass through the identical high-pass filters, which act as phase shifters, and then are combined in Hybrid B. At point 3, the signals meet with a 180° phase difference and cancel due to destructive interference. Nevertheless, at point 4 the signals meet in phase and are passed to the antenna. For lossless, ideal components, the isolation between the RX and antenna port is ideal [50].

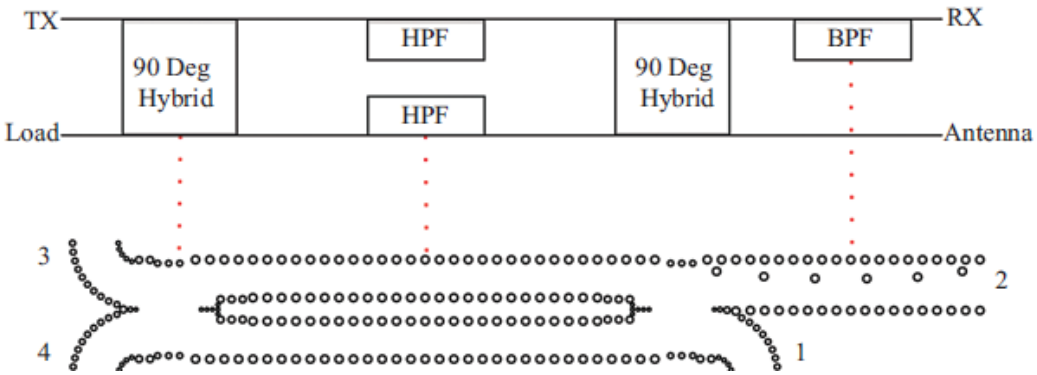

(a)

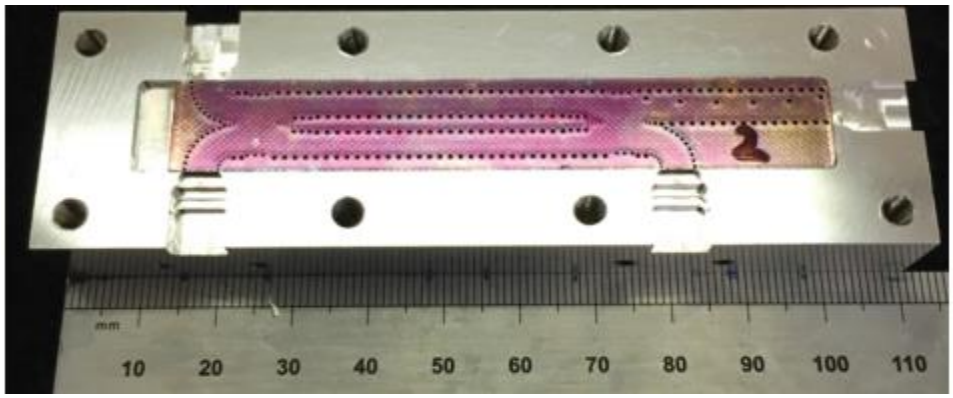

(b)

Figure I. 30. (a) SIW diplexer Schematic diagram (b) The fabricated SIW diplexer [50].

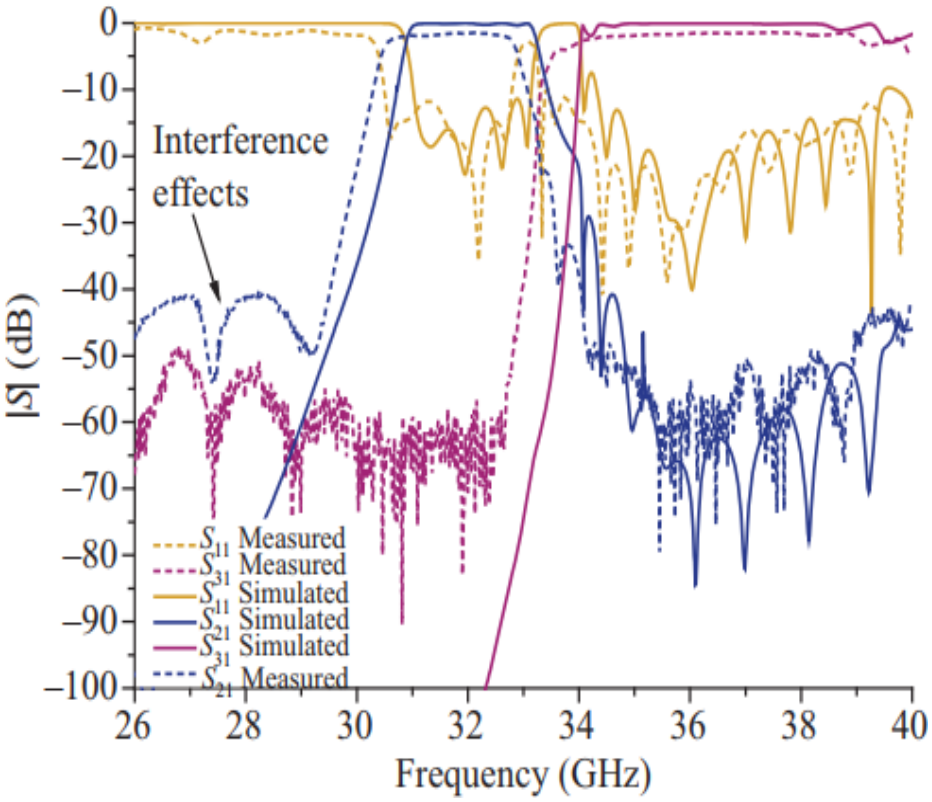

Figure I. 31. The S parameters of the proposed diplexer [50].

The measured transmitted bandwidth of the bandpass channel is ranging from 30.62 to 32.72 GHz, while the measured cut-off frequency of the high-pass channel is about of 33.63 GHz. This corresponds to a shift of 350 MHz and 430 MHz, respectively. It should be noted that the measured bandwidth of the bandpass filter is 6.63 %, which is marginally larger than the desired 6.25 %. In this case, more energy is passing through the filter which can only be attributed to a positive error in the via *x* position or a reduction in via diameter. Assuming that these errors are systematic during the diplexer's fabrication, the shift in cut-off frequency of the high-pass filter can also be attributed to these errors.

I. 6. 4. Substrate Integrated Traveling-Wave Antennas

Traveling-wave antenna or nonresonant antenna based on traveling wave on a transmission line as the main radiating mechanism. In Traveling-wave antenna, the current travels in one direction to generate the electromagnetic waves. The traveling-wave antenna often has a wider bandwidth compared with the resonant antenna. The main advantage of the non-resonant antenna for high frequency is the easier for the energy to radiate out from the discontinuities of open transmission lines so it is very suitable for millimeter-wave applications. Also By enclosed guided-wave structures with properly designed slots or open apertures, the leakage can be generated. According to different operating principles, traveling-wave antennas fall into two general categories: surface-wave antennas (will be studier in our work) and leaky-wave antennas. The radiation of surface wave is only at discontinuities. That means the total radiation pattern of a basic surface-wave antenna is formed by interferences at the beginning and the end of the structure. The discontinuities can be placed along the whole surface-wave structure. In this section, some substrate integrated surface-wave antennas are presented, including substrate-integrated waveguide (SIW)-fed tapered slot antenna (TSA), SIW Vivaldi Antenna, SIW-fed Yagi-Uda antenna and SIW-fed log-periodic dipole array [51].

I. 6. 4. 1. SIW Fed Linear Tapered Slot Antenna

The TSAs were presented in the late 1950s. They based on a traveling wave propagating along the surface of the antenna taper with a phase velocity less than the speed of light in free space [52]. Under this condition the endfire radiation occurs. For a typical TSA, the performance of a moderate gain, wide bandwidth, and a pair of symmetric beams in both the H- and E-planes could be anticipate. Therefore, this structure is a suitable element for millimeter-wave, and the

stand-alone antennas. There are many feeding types for TSA such as slotline, stripline, finline or SIW. By nature, the current of a typical TSA is planar, etched on a thin substrate with low permittivity dielectric. A balun is often necessary to drive the antenna. As a result, it is important to consider the possibility that the feedline may radiate or couple with the antenna element, which degrade the antenna performance. The antipodal TSA consists of two gradually flaring conductor claddings on opposite sides of a dielectric substrate. The bandwidth limitation caused by balun can be eliminate, When the SIW waveguide is used to feed the antipodal TSA, therefore, wideband characteristics are indeed obtainable. The features of SIW TSAs are: low profile, low weight, wideband characteristics, and they are easy to integrate with other planar circuits [51]. An SIW-based structure is able to avoid the power radiated from the feedline. Figure I.32 presents the configuration of an SIW-fed TSA. The feeding SIW is designed to only support the TE_{10} mode, and the electric field direction is gradually changed from the vertical to the horizontal, as shown in Figure I.32.

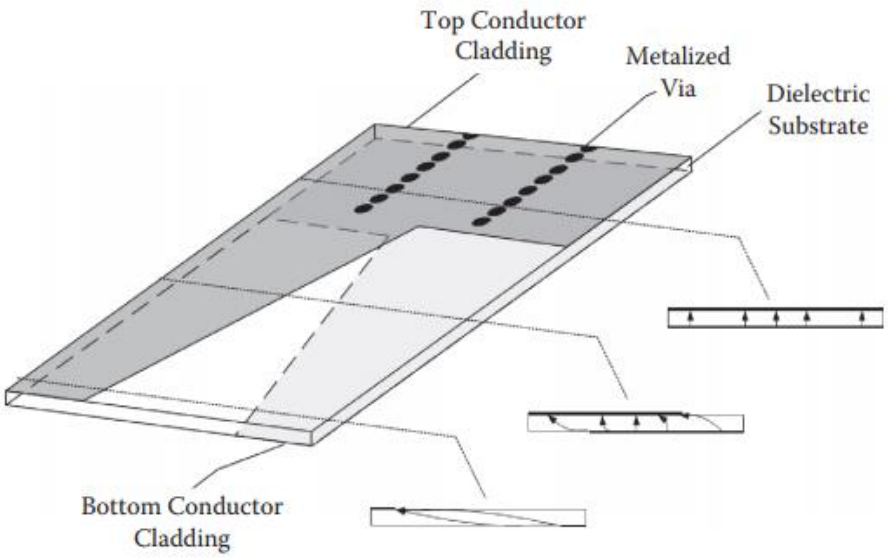

Figure I. 32. SIW-fed TSA Configuration and the electric field distribution within the antenna [51].

I. 6. 4. 2. SIW Vivaldi Antenna

Many works have been presented about Vivaldi antenna and it undergoes many upgraded, including adding the corrugated edges for a better radiation pattern and other improvements by changing the shape, length, dielectric constant, and dielectric thickness for controlling beam width. The Vivaldi Antenna has a profile defined as an exponential curve in the xOy plane, which can be defined by the following function:

$$y(x) = Ae^{Rx} \tag{I.49}$$

Where R defines how the slot is widening and the parameter A is determined by the equation 49 the profile of the antenna is calculated by the two points $p1$ $(x1,\ y1)$ and $p2$ $(x2,\ y2)$. p1 and p2 are two start and end points, respectively.

$$A = \frac{y2-y1}{e^{RX2}-e^{RX1}} \tag{I.50}$$

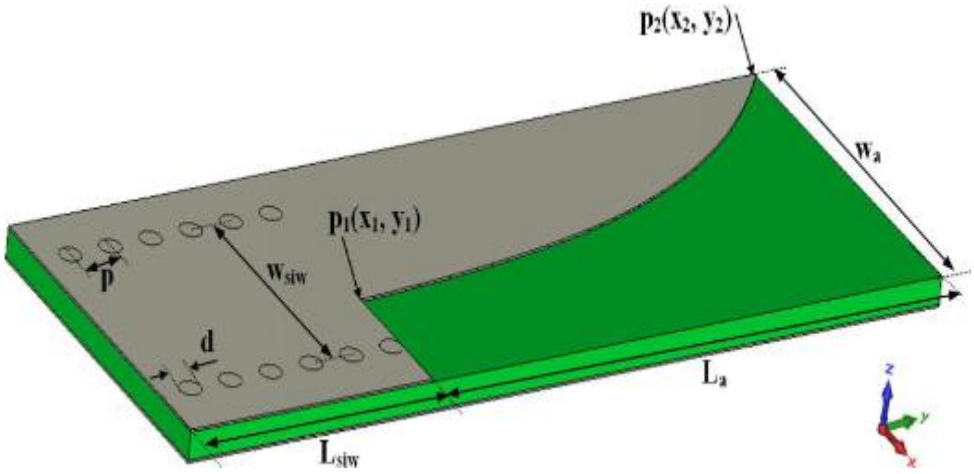

Figure I. 33. SIW Vivaldi antenna configuration [57].

I. 6. 4. 3. SIW Fed Yagi Uda Antenna

Among the most recognized surface wave antennas is the printed Yagi-Uda antenna, its features are low cost, low profile, and easy integration with other planar circuits. The feeding technique of the Yagi-Uda antenna mainly determines its performance. For drive this type of antenna a baluns must be integrated.

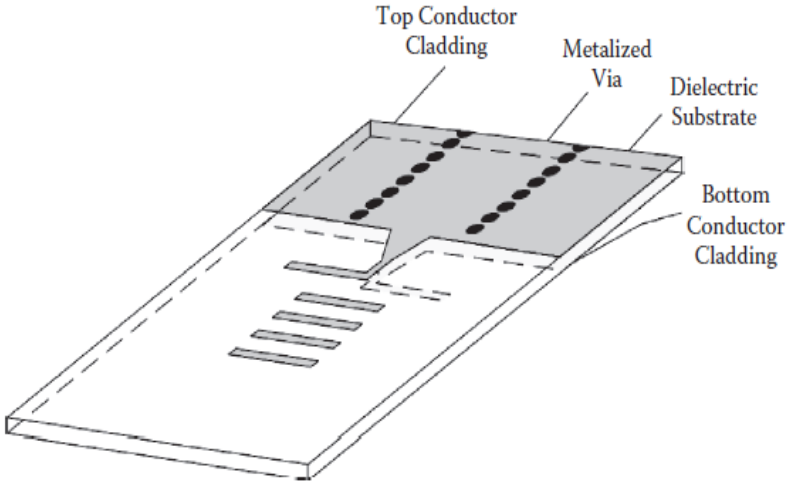

Figure I. 34. SIW Yagi-Uda antenna Configuration [51].

The Figure I.34 represent a Yagi-Uda antenna fed by SIW technology that was proposed in [53]. The design in Figure I.34 has four director elements and if we want to improve the antenna gain, we must add more director elements. Meanwhile, the design parameters and the complexity of the design will be increased. To match the SIW feedline and the printed Yagi-Uda antenna the design needs a tapered coupled line, which complicates the design of the antenna. The SIW feedline is still a little larger than its micro strip counterparts to overcome these weaknesses, an HMSIW-fed Yagi-Uda antenna was presented in [54]. The Figure I.35 represent the proposed configuration, the HMSIW feedline is directly connected to the Yagi-Uda antenna through a coupled line without tapering.

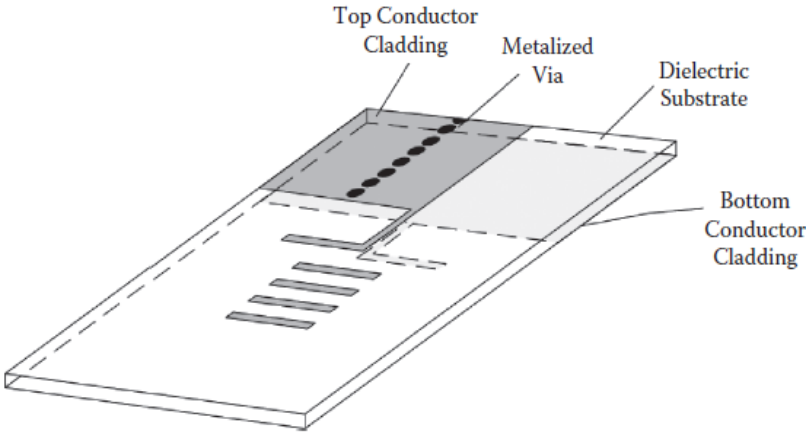

Figure I. 35. HMSIW Yagi-Uda antenna Configuration [51].

I. 6. 4. 4. SIW Fed Log-Periodic Dipole Array Antenna

The printed log-periodic dipole array antenna fed by an SIW or an HMSIW was developed in [55]. The printed log-periodic dipole array antenna is a development of the printed dipole antenna. This antenna will achieve very wide impedance bandwidth when the number of dipole elements are increased.

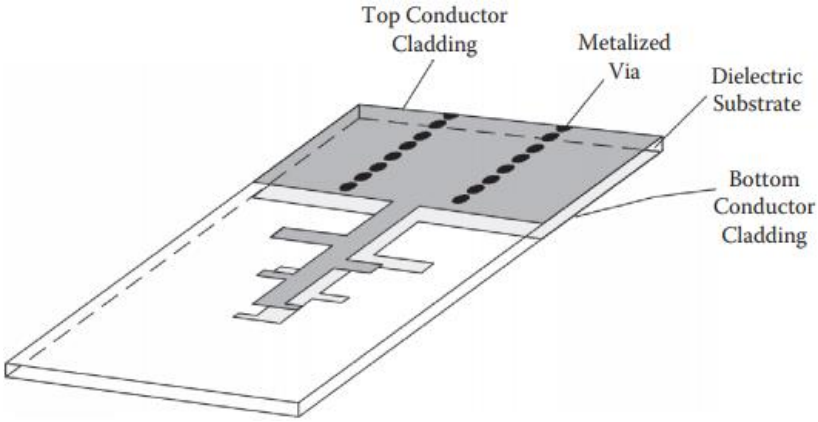

Figure I. 36. SIW log periodic dipole antenna Configuration [51].

I. 7. Planar Array

For form a rectangular or planar array it is necessary to placing elements along a line (to form a linear array), or positioned individual radiators along a rectangular grid. Many variables are provided in planar array for shape and control the pattern of the array. Planar arrays are more versatile and can provide more symmetrical patterns with lower side lobes. In addition, they can be used to scan the main beam of the antenna toward any point in space. They are used for much application such as search radar, tracking radar, communications, and others [56].

I. 7. 1. Array Factor

In a planar array, if M elements are initially placed along the x-axis, the array factor of it is given by equation 51:

$$AF = \sum_{m=1} \mathrm{I}_{\mathrm{m1}} e^{j(m-1)(kdx\sin\theta\cos\phi+\beta x)} \tag{I.51}$$

Where I_{m1} represents the excitation coefficient of each element of the array. dx and β_x represent respectively, the spacing and progressive phase shift between the elements along the x-axis. If N such arrays are placed next to each other in the y-direction, a distance d_y apart and with a progressive phase β_y.

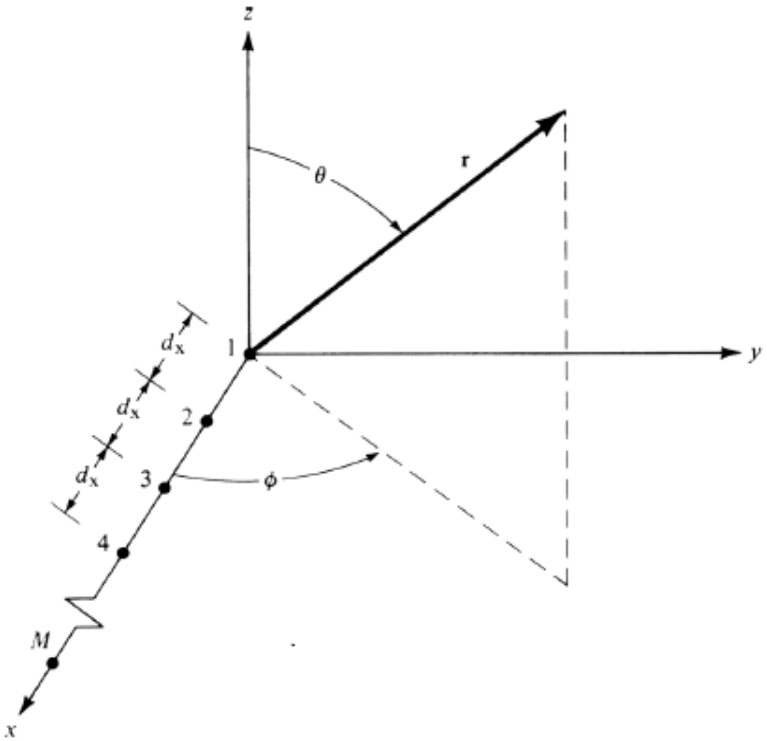

Figure I. 37. Linear array geometry[56].

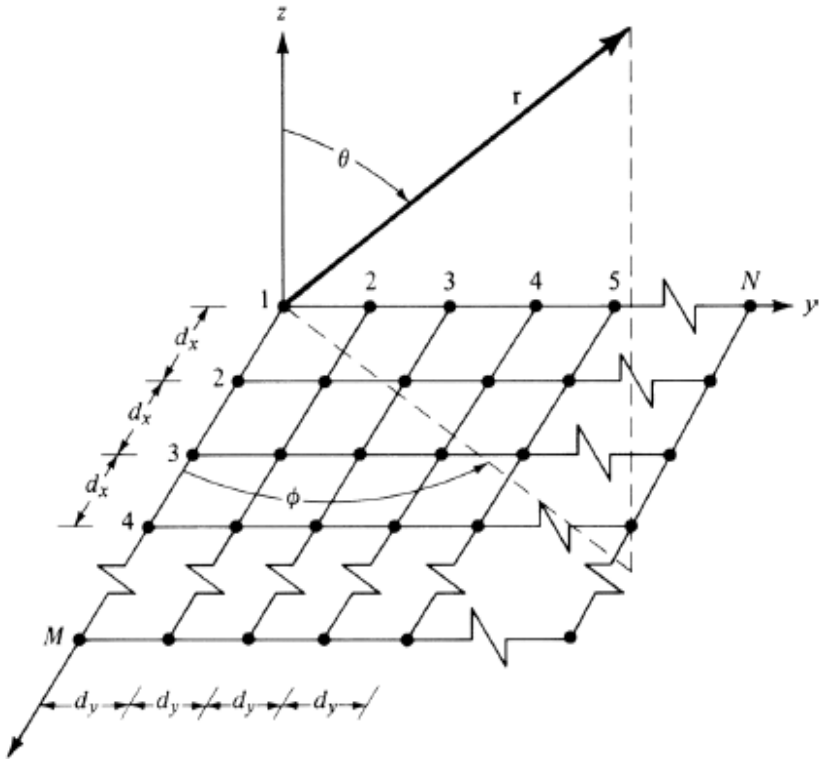

Figure I. 38. Planar array geometry [56].

The entire planar array factor is given by the following equation:

$$AF = \sum_{n=1}^{N} I_{1n} \left[\sum_{m=1}^{M} I_{m1} e^{j(m-1)(kdx \sin\theta \cos\phi + \beta x)} \right] e^{j(n-1)(kdy \sin\theta \sin\phi + \beta y)} \quad \text{(I.52)}$$

Or

$$AF = S_{xm} S_{yn} \quad \text{(I.53)}$$

Where

$$S_{xm} = \sum_{m=1}^{M} I_{m1} e^{j(m-1)(kdx \sin\theta \cos\phi + \beta x)} \quad \text{(I.54)}$$

$$S_{yn} = \sum_{n=1}^{N} I_{1n} e^{j(n-1)(kdy \sin\theta \cos\phi + \beta y)} \quad \text{(I.55)}$$

We notice that the rectangular array pattern is the product of the array factors of the arrays in the *x* and *y* directions. The normalized form of equation 52 is written as:

$$AF(\theta,\phi)=\left[\frac{1}{M}\frac{\sin\left(\frac{M}{2}\psi_x\right)}{\sin\left(\frac{\psi_x}{2}\right)}\right]\left[\frac{1}{N}\frac{\sin\left(\frac{N}{2}\psi_y\right)}{\sin\left(\frac{\psi_y}{2}\right)}\right] \quad \text{(I.56)}$$

Where

$$\psi_x = kd_x \sin\theta\cos\phi + \beta_x \quad \text{(I.57)}$$

$$\psi_y = kd_y \sin\theta\sin\phi + \beta_y \quad \text{(I.58)}$$

Many maxima of the same magnitude can be formed when the spacing between the array elements is equal or superior than λ/2. The principal maximum is considered as the major lobe and the remaining as the grating lobes. To avoid appearance of the grating lobes in the x-z and y-z planes, the spacing between the elements must be less than λ/2 in the x and y directions [56].

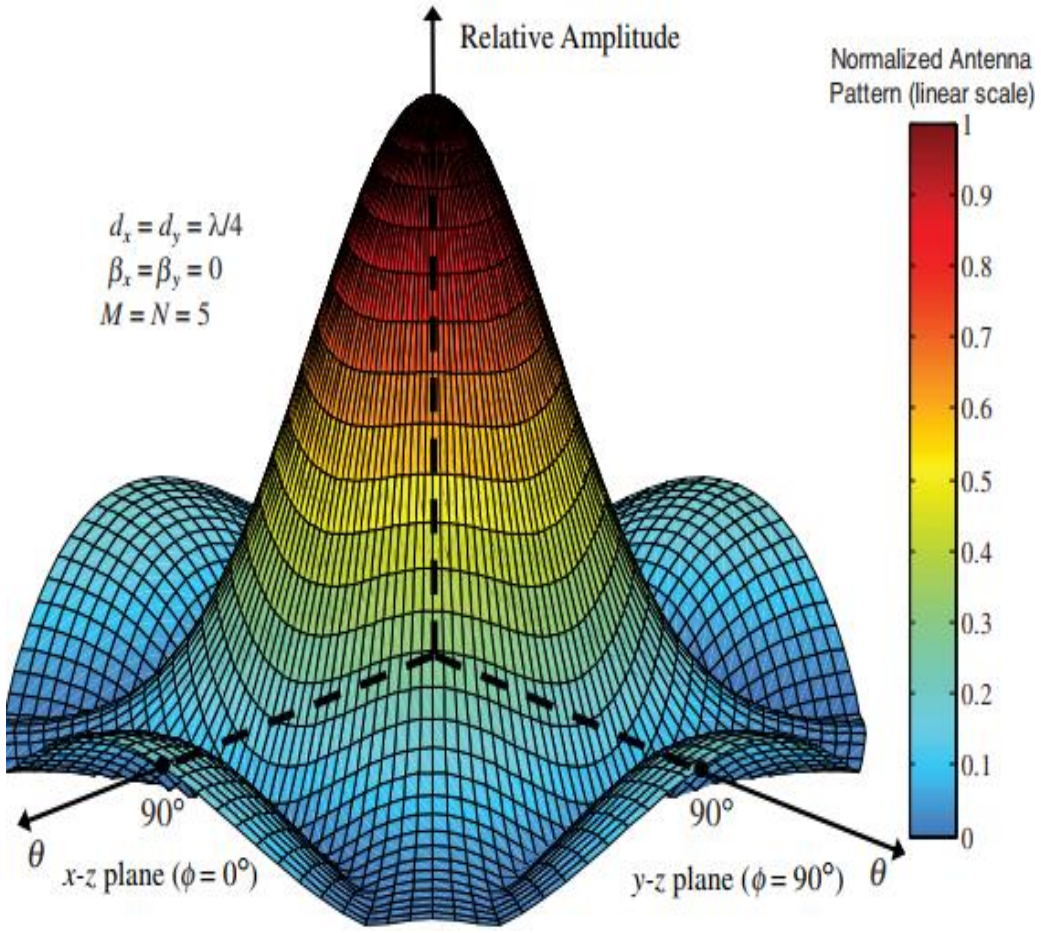

Figure I. 39. Three-dimensional planar array antenna pattern of isotropic elements with a spacing of dx= dy = λ/4, and equal amplitude and phase excitations [56].

I. 7. 2. Directivity

The directivity of the array factor AF (θ, ϕ) whose major beam is pointing in the $\theta = \theta_0$ and $\phi = \phi_0$ direction, is given by equation 59.

$$D_0 = \frac{4\pi\left[AF\left(\theta_0,\phi_0\right)\right]\left[AF\left(\theta_0,\phi_0\right)\right]^* \mathrm{I}_{max}}{\int_0^{2\pi}\int_0^{\pi}\left[AF\left(\theta,\phi\right)\right]\left[AF\left(\theta,\phi\right)\right]^* \sin\theta d\theta d\phi} \tag{I.59}$$

I. 8. Conclusion

In this chapter, we are interested in the different waveguide technologies such as volumetric technologies and planar technologies, which they allow to introduce a new very promising hybrid technology, which combines the advantages of the two technologies. The illustration of the design formulas for the SIW and its technique are shown in this chapter. In addition, the applications of DGS in microwave circuit were discuss. Several microwave components based on SIW and DGS have been characterized which allow us to design new configuration of this components.

References

[1] A. Noura, M. Benaissa, M.Abri, H. Badaoui, T. H Vuong and J. Tao, "Miniaturized half-mode SIW band-pass filter design integrating dumbbell DGS cells, "WILEY Microwave and Optical Technology Letters, Vol. 61, Iss. 6, pp. 1473-1477, Feb. 2019.

[2] B. Fellah, N. Cherif, M. Abri, and H. Badaoui, "CSRR-DGS Bandpass Filter Based on Half Mode Substrate Integrated Waveguide for X-Band Applications", AEM, vol. 10, no. 3, pp. 39–42, Nov. 2021.

[3] B. Fellah and M. Abri, "Design of antipodal linearly tapered slot antennas (ALTSA) arrays in SIW technology for UWB imaging", Springer: Recent Advances in Electrical Engineering and Control Applications, pp. 381-389, Dec. 2016.

[4] S. Doucha, M. Abri, H. Badaoui and B. Fellah, "A Leaky Wave Antenna Design Based on Half-mode Substrate Integrated Waveguide Technology for X Band Application," International Journal of Electrical and Computer Engineering (IJECE), Vol. 7, No. 6, pp. 3467-3474, Dec. 2016.

[5] M. Moulay, M. Abri and H. Badaoui, " Compact Quad-Band bandpass Filter Based on Complementary Split Ring Resonators as DGS", IEEE 6th International Conference on Image and Signal Processing and their Applications (ISPA,) Mostaganem, Algeria, Nov 24-25, 2019.

[6] B. Fellah, M. Abri and H. Badaoui," Optimized Bends, Corporate 1 × 4 and 1 × 8 SIW Power Dividers Junctions Analysis for V-Band Applications Using a Rigorous Finite Element Method, "Arabian Journal for Science and Engineering, Vol. 41, No. 9, pp. 3335–3343, Sept. 2015.

[7] L. Qinghua, F. Christophe, H. Wei, and R. Vahldieck, Characterization of the propagation properties of the half-mode substrate integrated waveguide, IEEE Trans Microwave Theory and Technique, vol. 57, iss. 8, pp. 1996 2004, (2009).

[8] Fellah Benzerga, " Étude et conception des réseaux d'antennes à ouverture progressive pour imagerie passive en technologie SIW: Modélisation par la méthode des éléments finis 2D " doctoral thesis, Tlemcen university, 2016.

[9] Doucha Souad, " Contribution à la Conception des Réseaux d'Antennes à Ondes de Fuites à Dépointage de Faisceau Alimentés par des Guides d'Ondes Intégrés aux Substrats " doctoral thesis, Tlemcen university, 2017.

[10] RABAH Mohammed Amin, " jet Contribution à la Conception et à la Réalisation des Composants Micro-ondes Compacts en Technologie Guides d'Ondes Intégrés aux Substrats : Modélisation par la Méthode des Eléments Finis 2D

[11] Jonathan Garreau, " Étude de filtres hyperfréquence SIW et hybride-planaire SIW en technologie LTCC " doctoral thesis, Bretagne occidental university of Brest, 2012.

[12] Wu K , "Integration and interconnect techniques of planar and nonplanar structures for microwave and millimeter-wave circuits-current status and future trend" In: Asia–pacific microwave conference 2001, Taipei, Taiwan, pp 411–416.

[13] Tarek Djerafi, Ali Doghri, and Ke Wu "Substrate Integrated Waveguide Antennas" Springer Science+Business Media Singapore , Z.N. Chen et al. (eds.), Handbook of Antenna Technologies, pp 1585-1655, 2016.

[14] Wu K, Deslandes D, Cassivi Y (2003) The substrate integrated circuits-a new concept for highfrequency electronics and optoelectronics. In: Telecommunications in modern satellite, cable and broadcasting service, TELSIKS 2003, 6th international conference, vol 1, pp P-III

[15] Wu K, Cheng YJ, Djerafi T, Hong W (2012) Substrate integrated millimeter-wave and terahertz antenna technology. Proc IEEE 100(7):2219–2232

[16] Bozzi M, Georgiadis A, Wu K (2011) Review of substrate-integrated waveguide circuits and antennas. IET Microwaves Antennas Propag 5:909–920

[17] Deslandes D, Wu K (2006) Accurate modeling, wave mechanisms, and design considerations of a substrate integrated waveguide. IEEE Trans Microwave Theory Tech 54(6):2516–2526

[18] K.C. Gupta, G. Ramesh, I.J Bahl, "Microstrip lines and slotlines" Artech House, May 2013, 594 pages.

[19] M. Rabah, M. Abri, H. Badaoui, J. Tao and T.H. Vuong, "Compact Miniaturized Half-Mode Waveguide/High Pass-Filter Design Based On SIW Technology Screens Transmit-IEEE C-Band Signals," WILEY Microwave and Optical Technology Letters, Vol. 58, No. 2 pp. 414-418, Dec 2016.

[20] S. Doucha, M. Abri, H. Badaoui and B. Fellah, "A Leaky Wave Antenna Design Based on Half-mode Substrate Integrated Waveguide Technology for X Band Application," International Journal of Electrical and Computer Engineering (IJECE), Vol. 7, No. 6, pp. 3467-3474, Dec. 2016.

[21] Deslandes D (2010) Design equations for tapered microstrip-to-substrate integrated waveguide transitions. In: International microwave symposium, Anaheim, 23–28 May 2010, pp 704–707.

[22] M. K. K. WAL, Binod Kumar Kanaujia, Sachin Kumar, Defected Ground Structure: Fundamentals, Analysis, and Applications in Modern Wireless Trends, hindawi International Journal of Antennas and Propagation , vol 2017, 1-22, January 2017.

[23] L. Yan and W. Hong, "Investigations on the Propagation Characteristics of the Substrate Integrated Waveguide Based on the Method of Lines," Proc. Inst. Elect. Eng. H, vol. 152, no.1, pp. 35–42, 2005

[24] Mukesh Kumar Khandelwal, Binod Kumar Kanaujia, Sachin Kumar, " Defected Ground Structure: Fundamentals, Analysis, and Applications in Modern Wireless Trends," hindawi International Journal of Antennas and Propagation , vol 2017, 1-22, January 2017.

[25] im, J.-S., C.-S. Kim, Y.-T. Lee, et al., "A spiral-shaped defected ground structure for coplanar waveguide," IEEE Microwave Compon. Lett., Vol. 12, No. 9, 330–332, 2002.

[26] Boutejdar, A., G. Nadim, S. Amari, et al., "Control of bandstop response of cascaded microstrip low-pass-bandstop filters using arrowhead slots in backside metallic ground plane," IEEE Antennas Propag. Soc. Int. Symp. , Vol. 1B, 574–577, 2005.

[27] Chen, H.-J., T.-H. Huang, C.-S. Chang, et al., "A novel cross- shape DGS applied to design ultra-wide stopband low-pass filters," IEEE Microwave Compon. Lett , Vol. 16, No. 5, 252–254, 2006.

[28] Li, J. L., J. X. Chen, Q. Xue, et al., "Compact microstrip lowpass filter based on defected ground structure and compensated microstrip line," IEEE MTT-S Int. Microwave Symp. Digest 1483–1486, 2005.

[29] L. H. Weng, Y. C. Guo, X. W. Shi, and X. Q. Chen, "AN OVERVIEW ON DEFECTED GROUND STRUCTURE" , Progress In Electromagnetics Research B, Vol. 7, 173–189, 2008

[30] Nanang I, Gunawan T.S, Santi K. S, Teguh P, and Eki A. Z. H. "Design of microstrip hairpin bandpass filter for 2.9 GHz–3.1 GHz S-band radar with defected ground structure", Malaysian Journal of Fundamental and Applied Sciences. 2020; 14 (4); 448-455.

[31] Hussein Shaman. "New S-Band Bandpass Filter (BPF) With Wideband Passband for Wireless Communication Systems", IEEE Microwave and Wireless Components Letters. 2012. 22; (5); .242-244.

[32] Weng M.H, Tsai C.Y, Chen D.L, Chung Y.C and Yang R.Y. "A Bandpass Filter Using Half Mode SIW Structure with Step Impedance Resonator", MDPI Electronics, 10; (1) pp. 1-8, 2020.

[33] Juan de Dios R, Félix L. M. V, Alejandro A.M, and Juan H. "Substrate Integrated Waveguide (SIW) With Koch Fractal Electromagnetic Bandgap Structures (KFEBG) for Bandpass Filter Design", IEEE Microwave and Wireless Components Letters. 25 (3); pp. 160 – 162. March 2015;

[34] J.P. Liu, Z.Q Lv and X. An, "Compact substrate integrated wave guide filter using dual-plane resonant cells," WILEY Microwave and Optical Technology Letters, Vol. 58, Iss. 1, pp. 111-114, Jan. 2016.

[35] M. Almalkawi, L. Zhu, and V. Devabhaktuni, "Dual-mode substrate integrated waveguide (SIW) bandpass filters with an improved upper stopband performance," IEEE International Conference on Infrared, Millimeter, and Terahertz Waves, Houston, TX, USA, Oct 2-7, 2011.

[36] S. Moitra, S. Nayak, R. Regar, S. Kumari, K. Kumari, F. Parween and F. Naseem, "Circular Complementary Split Ring Resonators (CSRR) based SIW BPF," IEEE Second International Conference on Advanced Computational and Communication Paradigms (ICACCP), Gangtok, India, Feb, 25-28, 2019.

[37] Y. L. Zhang, W. Hong, K. Wu, J. X. Chen, and H. J. Tang, "Novel substrate integrated waveguide cavity filter with defected ground structure," IEEE Transactions on Microwave Theory and Techniques, vol. 53, no. 4, pp. 1280–1287, 2005.

[38] W. Shen, W.-Y. Yin, and X.-W. Sun, "Compact substrate integrated waveguide (SIW) filter with defected ground structure," IEEE Microwave and Wireless Components Letters, vol. 21, no. 2, pp. 83–85, 2011.

[39] J.-S. Lim, C.-S. Kim, D. Ahn, Y.-C. Jeong, and S. Nam, " Design of low-pass filters using defected ground structure," IEEE Transactions on Microwave Theory and Techniques, vol. 53, no. 8, pp. 2539–2545, 2005.

[40] P. Ramanujam, Ramesh Venkatesan P. G., C. Arumugam and M. Ponusamy " Design of Compact Highpass Filter for 5G mm-wave Applications Using Complementary Split Ring Resonator" De Gruyter Frequenz 2020; 74 (5-6): 177–181

[41] D. Dealandes, and K. Wu, " Single-substrate integration techniques for planar circuits and waveguide filters" IEEE Trans. Microwave Theory Tech. 51(2), 593–596, 2003.

[42] J.S HONG " Microstrip Filter for RF/Microwave Applications Second Editioon " JOHN WILEY & SONS, INC., Hobooken, New Jersey, 2011.

[43] N. Marcuvitz " Waveguide Handbook" MIT Radiation Laboratory Series, McGraw-Hill, New York, vol. 10, 1951.

[44] R.. Matthaei, L. Young, and E. M. T. Jones, " Microwave filters, Impedance-Matching Networks and Coupling Structures", McGraw-Hill, New York, 1964.

[45] S. Alotaibi, and J.-S. Hong, Novel substrate integrated folded waveguide filter, Microwave Optical Technol. Lett. 50(4), 2008, 1111–1114.

[46] S. K. Alotaibi, and J.-S. Hong, Substrate integrated folded-waveguide filter with asymmetrical frequency response, In 38th European Microwave Conference, EuMC 2008. 27 31 Oct. 2008, 1002–1005.

[47] H.-Y. Chien, T.-M. Shen, T.-Y. Huang, W.-H. Wang, and R.-B. Wu, Miniaturized bandpass filters with double-folded substrate integrated waveguide resonators in LTCC, IEEE Trans. Microwave Theory Techn 57(7), 2009, 1774–1782

[48] R. J. Cameron, C. M. Kudsia, and R. R. Mansour, '' Microwave filters for communication systems,'' John Wiley Sons, INC., New Jersey, 2007

[49] European Space Agency, ''High Power Q/V-Band Diplexers for Ground Stations,'' ARTES 5.1 6B.025, October, 2015.

[50] Jiasheng Hong "Advances in Planar Filters Design "SciTech Publishing, an imprint of The Institution of Engineering and Technology, London, United Kingdom (March 27, 2019)

[51] Yu Jian Cheng "Substrate integrated antennas and arrays" CRC Press, Taylor and Francis Groupe, LLC, 2019.

[52] J. L. Volakis "Antenna engineering handbook", fourth editon. New York: McGraw-Hill, juin 2007.

[53] Z.Y. Zheng, K. Wu, and N. Yang “Broadband millimeter-wave quasi-Yagi antenna using substrate integrated waveguide technique”, IEEE Radio and Wireless Symposium, pp. 671–674, January 2008.

[54] G.H. Zhai, W. Hong, K. Wu, et al.” Printed quasi-Yagi antenna fed by half mode substrate integrated waveguide”, In 2008 Asia-Pacific Microwave Conference, December 2008.

[55] W. Hong, C. Yu, G.H. Zhai, et al “ Frequency notched wideband printed directional antennas”, In 2010 International Workshop on Antenna Technology, March 2010.

[56] Constantine A. Balanis “Antenna Theory: Analysis and Design”, 4th Edition, John Wiley & Sons, Inc., Hoboken, New Jersey, 2016.

[57] Benzerga Fellah, Mehadji Abri and Hadjira Badaoui "Analysis and Design of Vivaldi Antipodal (Antenna array AVA) for Passive Imaging Applications" The 1st Conference on Electrical Engineering, Algiers, Algeria, April 22-23, 2019.

[58] Yi Huang and Kevin Boyle " Antenna From Theory To Practice " Wiley–Blackwell, August 29, 2008.

CHAPTER II

SIW Filters Design, Fabrication and Measurement

II. 1. Introduction

The organization of this chapter is as follows: first, we present the design, simulation results and realization of a High Pass Filter based on SIW and its half mode. After that we present three band pass filter based on SIW and DGS -pass filter for S, X and Ku bands respectively then we present an SIW DGS diplexer. Finally, we end our chapter by the presentation of a Shuntinductive SIW filter for terahertz applications. We used CST and HFSS simulators to design and optimize our structures and PCB process for manufacturing.

II. 2. SIW High Pass Filter Design

The main problem in SIW circuit design is the losses. It is necessary to choose the right substrate also the value of diameter "d" of the metal vias and the distance "p" between the centers of two successive vias [1]. Using the CST we designed a SIW high pass filter to reject frequencies that are less than 6 GHz on Rogers 5880 based substrate having a loss tangent approximately 0.018, a relative permittivity of 2.2, a thickness h of 0.508 mm and the thickness of the conductor equal 0.05 mm. For the design rules, we used the equation that are presented in chapter I [2].

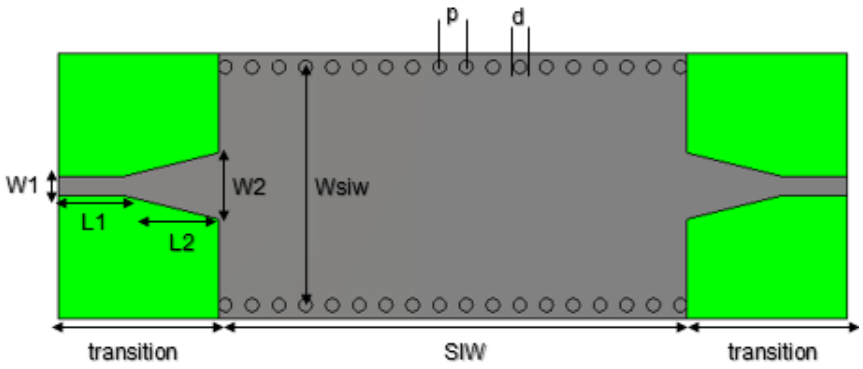

Figure II. 1. Geometry of the SIW highpass filter configuration.

Table II. 1. The optimized parameters value of the proposed filter.

Parameter	Value (mm)	Parameter	Value (mm)
W1	1.5	Wsiw	18
W2	5.0	p	1.8
L1	5.0	d	0.9
L2	7.5	h	0.508

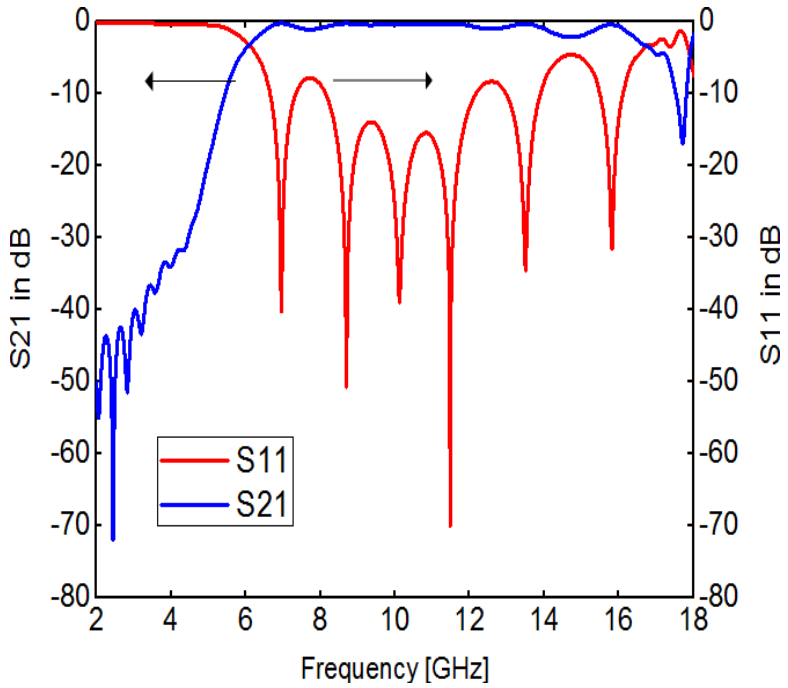

Figure II. 2. Transmission coefficient and return loss of SIW high pass filter.

The simulated S11 and S21 of the proposed filter show in the Figure II.2, we observe that the filtering band range from 6 to 18 GHz and the filter reject he frequency under 6 GHz with an transmission coefficient about of -0.5 dB with the appearance of many peaks the best reached -70 dB at the frequency of 11.8 GHz. The rejection is very good under 6 GHz and its level is below -10 dB in all rejection band with a maximum value of -72 dB around the frequency of 2.2 GHz. From this analysis, we can say that this SIW filter is functional to transmit cm waves that range from 6 to 18 GHz.

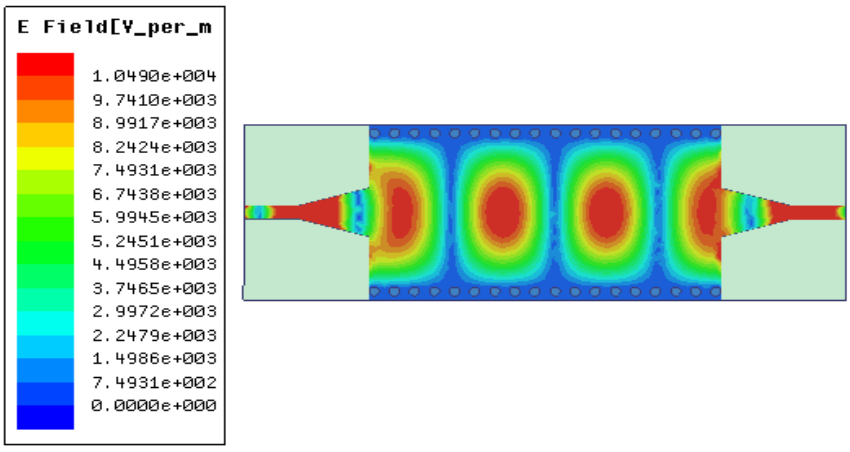

Figure II. 3. Distribution of the electric field at the frequency of 11.5 GHz.

As we show in the Figure II.3 we can notice that the electric field is well delimited and distributed in the all SIW high pass filter and its dominate mode is TE_{10}.

II. 3. Half Mode SIW High Pass Filter Design

For The half-mode SIW filter, simply modification of the previous structure by eliminate one-half and keep the other half. We use the parametric study by CST software for optimized the filter performance. The HMSIW high pass filter configuration is illustrated in the Figure II.4.

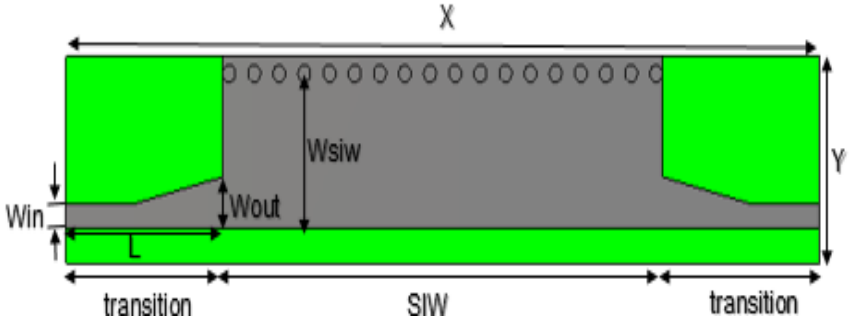

Figure II. 4. HMSIW high pass filter configuration.

TABLE II. 2 The optimized parameters of the HMSIW high pass filter.

Parameters	Value (mm)	Parameters	Value (mm)
Win	1.5	X	60
Wout	2.5	Y	12
L	12.5	Wsiw	9

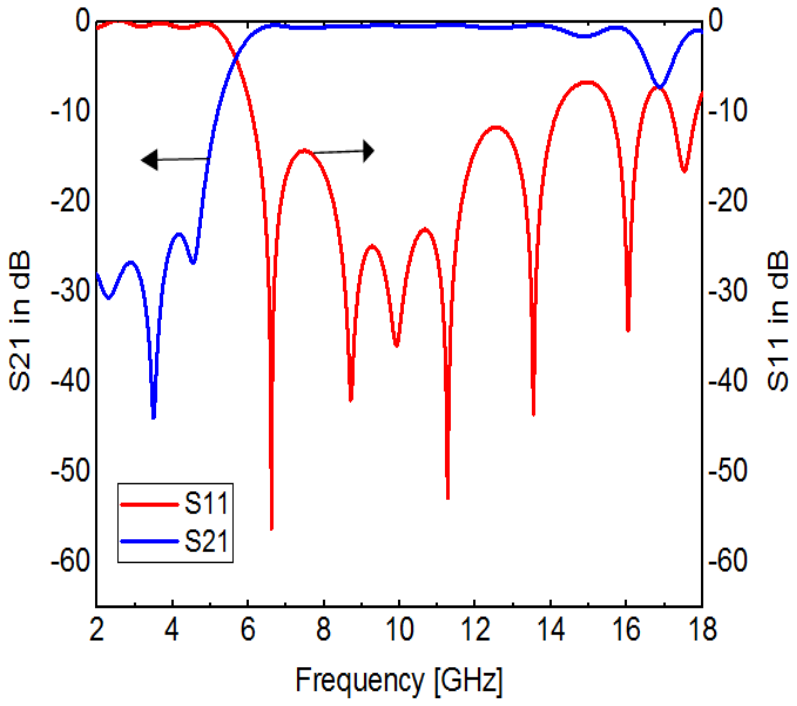

Figure II. 5. Transmission coefficient and return loss of HMSIW filter.

From Figure II.5 we observe that the filter less pass the frequency above 6 GHz and eliminate the frequency under 6 GHz with an transmission coefficient about of -0.5 dB, we also observe the appearance of many resonance frequency under -10 dB the best reached -55 dB at the frequency of 6.8 GHz. The rejection is good under 6 GHz and its level is below -10 dB in all rejection band with a maximum value of -44 dB around the frequency of 3.9 GHz. We notice that the filter did not lose its performance when we used the half-mode technique.

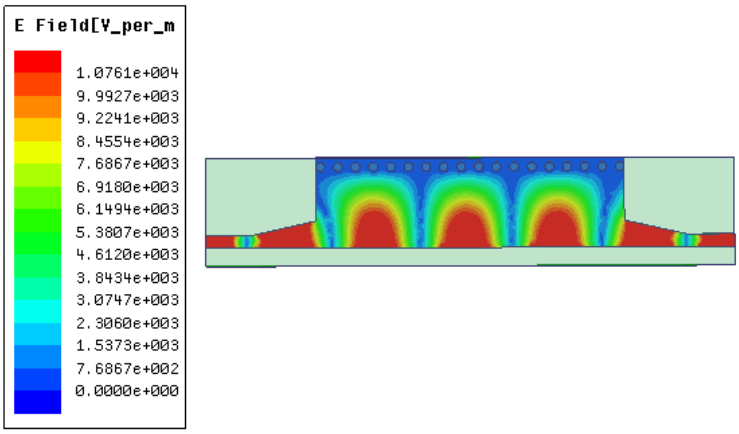

Figure II. 6. Distribution of the electric field at the frequency of 6.1 GHz.

We observe from distribution of the electric of the frequency of 6.1 GHz in the HMSIW that the its dominate mode is approximately half of the TE_{10} and it is well located in the HMSIW.

II. 4. Results Comparison

The Figures II.7 and II.8 represent the comparisons between CST Studio and Ansoft HFSS simulation results respectively transmission coefficient and return loss. HFSS simulator based on the finite element method and CST Microwave studio uses FIT (finite integration technique, a relative of FDTD) for its transient solver. From the Figure II.7 it is show that excellent results are obtained. The simulation results show a good agreement of the cut-off frequency. We observe a good agreement in the functional band that ranging from 6 to 18 GHz also we obtained a good agreement in resonances frequencies. It can also be noted that we have an agreement in the rejection under 6 GHz.

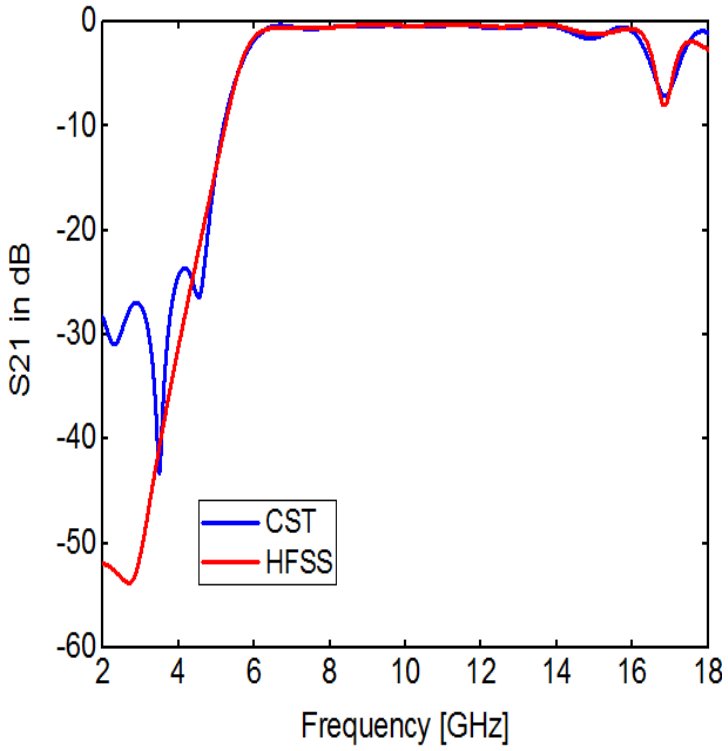

Figure II. 7. Transmission coefficient of HMSIW filter.

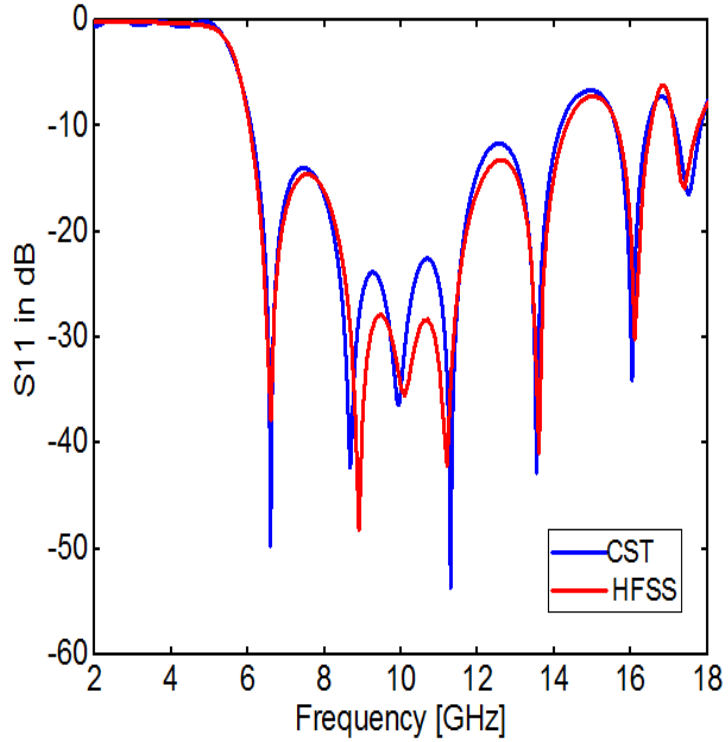

Figure II. 8. Return loss of HMSIW filter.

II. 5. Experimental Results

To validate the simulation results, the proposed half-mode SIW high pass-filter is fabricated and measured using PCB process by ProtoMat S103 and R&S ZVA 40 Vector Network Analyzer respectively. The Figure II.10 shows a picture of the fabricated half-mode SIW high pass-filter. The measured return loss and insertion loss are shown in Figure II.11 and Figure II.12 compared with the simulation results obtained by CST simulator.

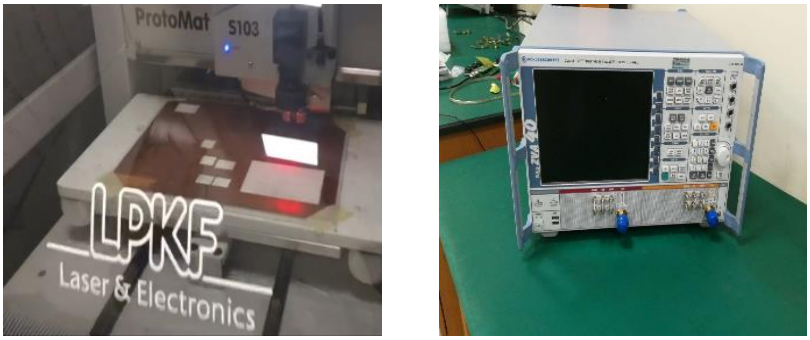

(a) (b)

Figure II. 9. (a) ProtoMat S103 (b) NAV ZVA 40.

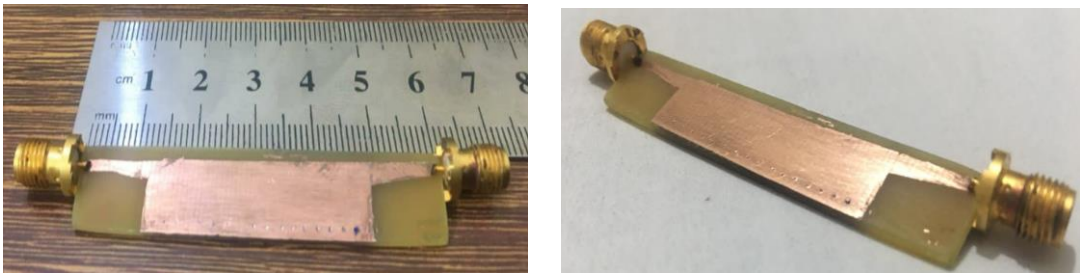

(a)

(b)

Figure II. 10. The photograph of the fabricated HMSIW high pass filter.

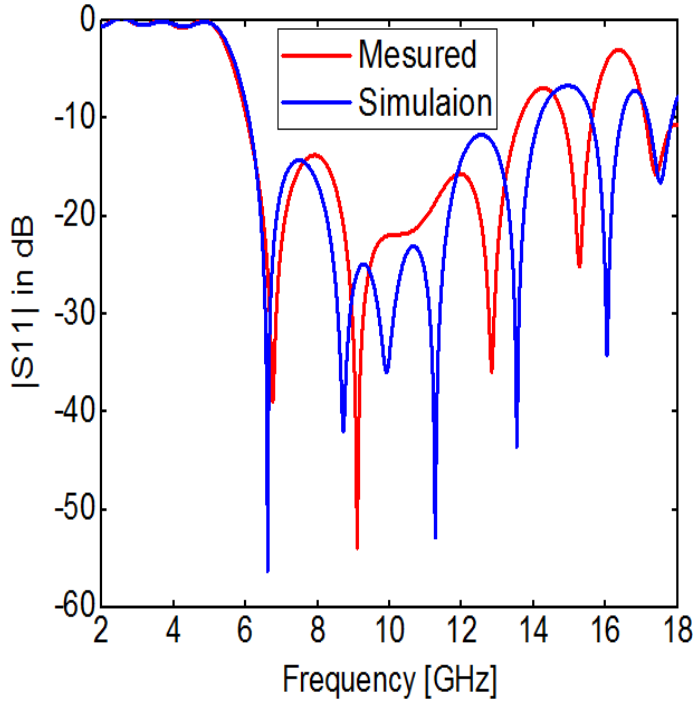

Figure II. 11. The comparison of Return loss.

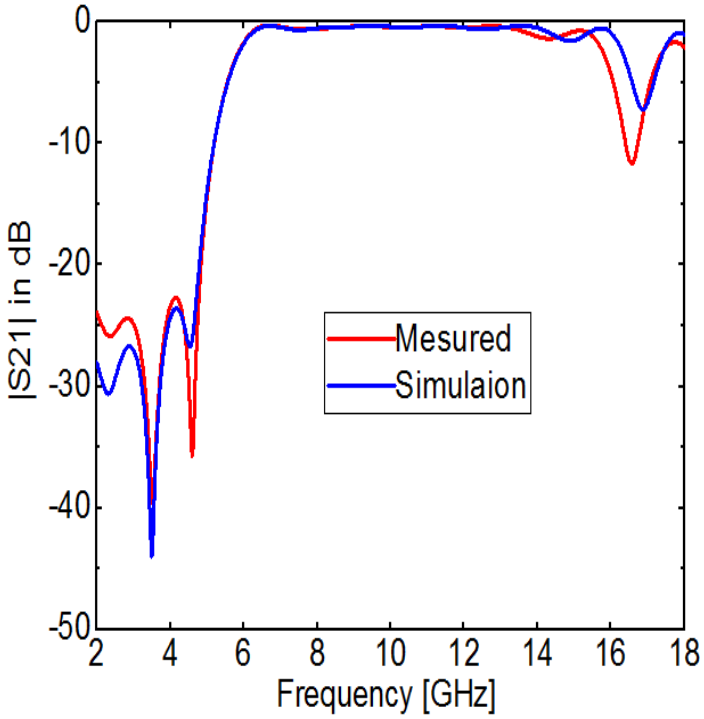

Figure II. 12. The comparison of Transmission coefficient.

From the Figures II.11 and II.12, we notice a good agreement between simulation results and experimental results of the operational frequency range from 6 GHz to 18 GHz. From the measured curve plotted in Figure II.11, we notice a reflection coefficient S11 below -10 dB in all band which range from 6 to 18 GHz with the appearance of several

resonance frequencies the best reached -51 dB at the frequency of 9 GHz. The measured insertion loss is shown in Figure II.12 and it is approximately −1.1 dB. Good rejection is observed under 6 GHz with a level below -10 dB from 2 to 6 GHz.

II. 6. Wideband SIW Bandpass Filter Based on Circle CSRR and Dumbbell DGS

In this section we proposed a novel configuration of bandpass filter with two vertically periodic double circle CSRR as DGS cells etch in the top plane with a distance between them equal to 1.0 mm and three cascading dumbbell DGS cells etched in the ground plane with a distance between them equal to 0.5 mm. the parameters of CSRR and dumbbell are optimized using the parametric study with CST simulator [3].

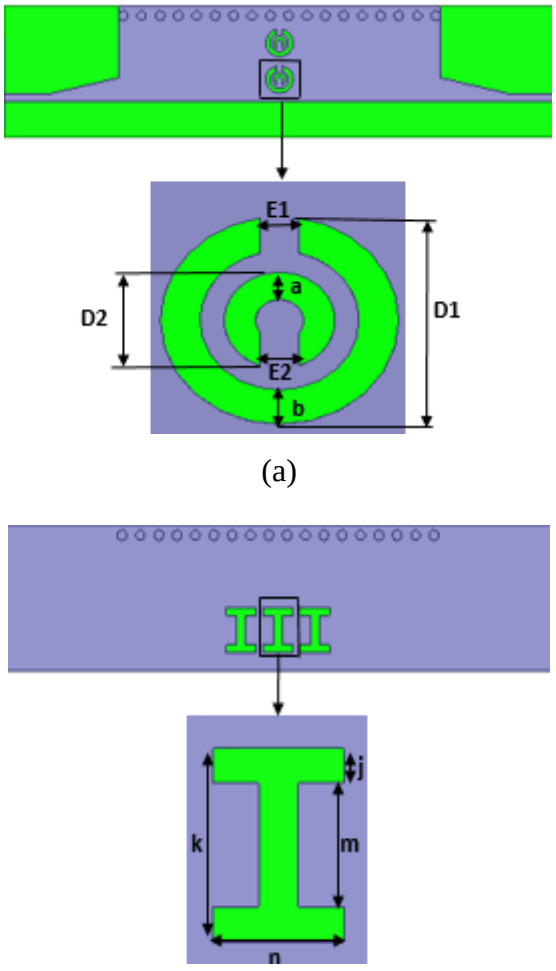

Figure II. 13. Configuration of the proposed DGS bandpass filter, (a) top view (b) bottom view.

The simulation results of the HMSIW shown in the Figures II.14 and II.15 respectively transmission coefficient and reflection coefficient.

Table II. 3. The optimized parameters value of the proposed bandpass filter.

Parameters	Value (mm)	Parameters	Value (mm)
E1	0.5	b	0.5
E2	0.5	j	0.8
D1	3.0	k	4.5
D2	1.4	m	2.9
a	0.4	n	2.7

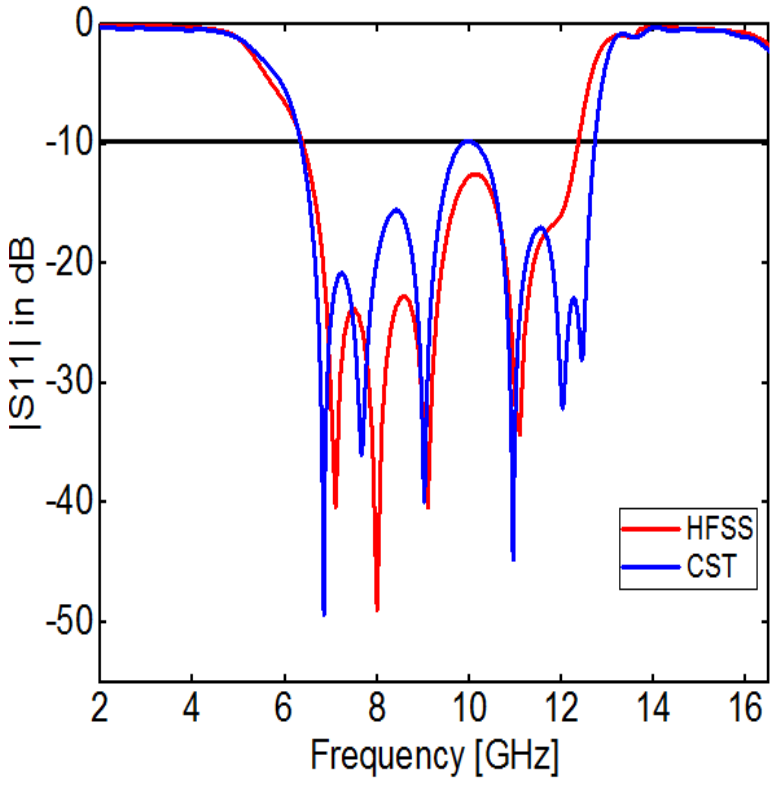

Figure II. 14. Return loss of the proposed HMSIW DGS bandpass filter.

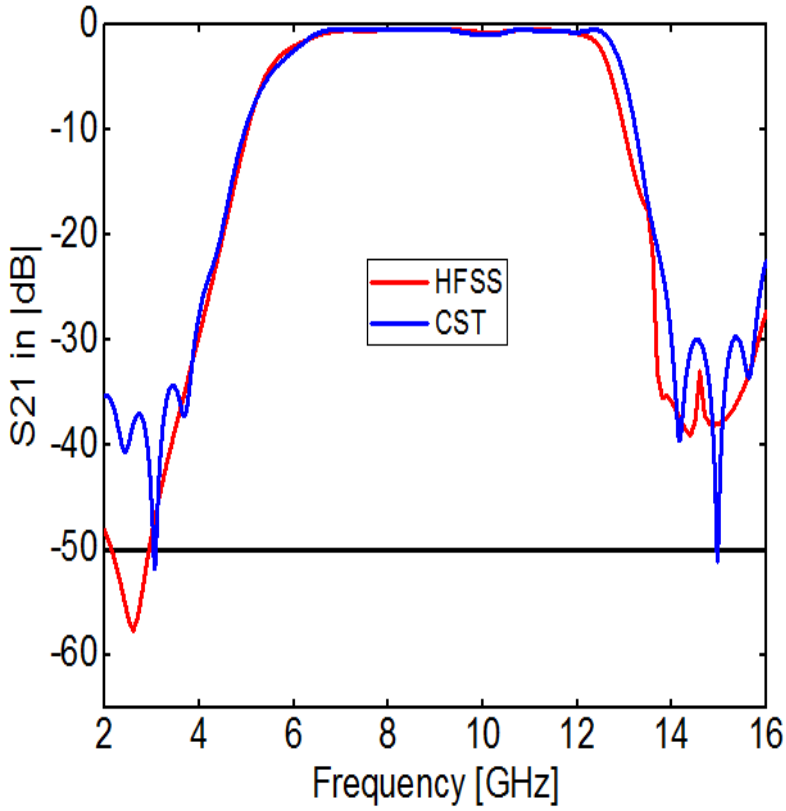

Figure II. 15. Transmission coefficient of the proposed HMSIW DGS filter.

From the previous figures, we observe that the filtering band range from 6.2 to 12.7 GHz, with an insertion loss around of −0.5 dB and about the return loss, we notice the appearance of many peaks, the best reached -48 dB at the frequency of 6.8 GHz. The rejection is very good and it range from 2 to 6 GHz and from 13 to 16 GHz with the attenuation below −20 dB, and the maximum rejection even reaches −50 dB at the frequencies of 3.1 GHz and 15.1 GHz.

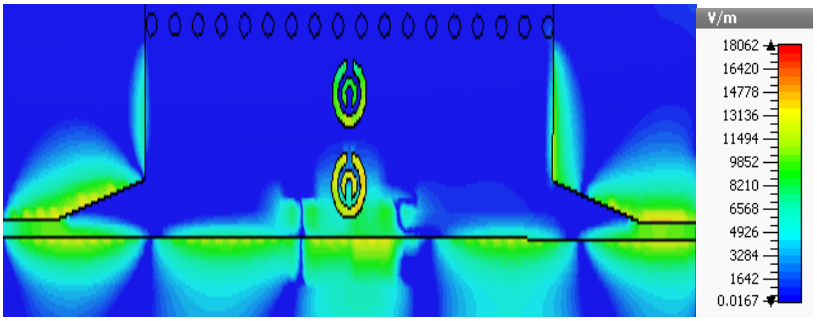

(a)

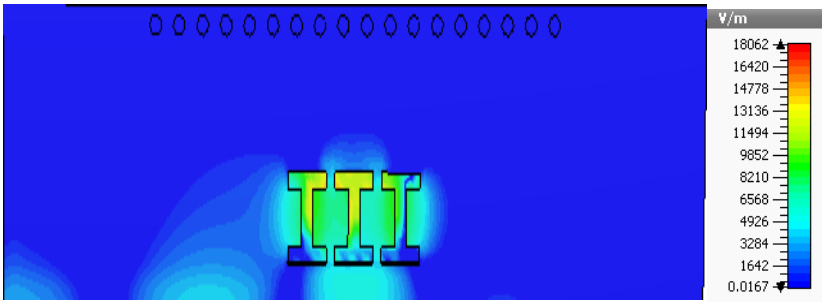

(b)

Figure II. 16. Distribution of the electric field at the frequency of 9 GHz, (a) top view (b) bottom view.

II. 7. Wideband SIW And HMSIW Bandpass Filter Based On Periodic Square CSRR As DGS

Using the CST simulator, we designed a new SIW-DGS band-pass filter for ku-band on Arlon Cu Clad 217 base a thickness h of 0.508 mm. For miniaturized the filter size we used the half mode technique. The DGS CSRR inserted at the top plane are shown in the Figure II.17. We designed the filter based on two cascading square CSRR in the top plane separated by a distance of 5.5 mm and for impedance matching we used tapered transition [4].

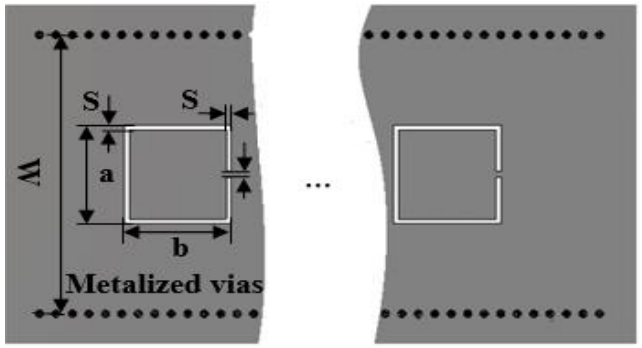

(a)

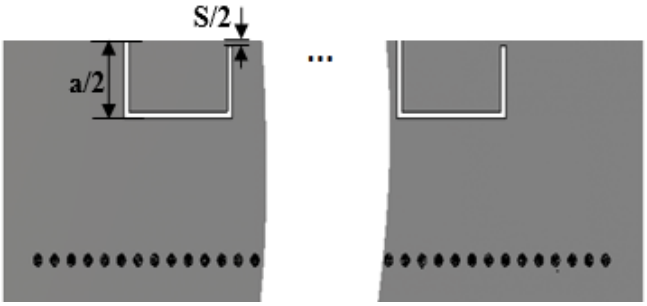

(b)

Figure II. 17. The proposed CSRR Configuration (a) front view (b) bottom view.

Table II. 4. The optimal parameter values of the proposed DGS filter

Parameters	Value (mm)	Parameters	Value (mm)
S	0.3	b	6.5
L	0.3	W	18
a	6.5	h	0.508
M	5.5	d	0.8

From Figure II.18 we observe that the insertion loss is about of 1.6 dB in band ranging from 13.1 GHz to 14.3 GHz also we observe the appearance of two peaks, the best reached -47 dB at the frequency of 14.1 GHz. The rejection is fair under 13 GHz and above 14.5. From this analysis, it can be said that this SIW filter is functional in the ku band with good performance. By using the half-mode technique, we reduced the filter size and kept the same performance of the SIW filter. The half mode SIW band pass filter configuration and simulation are shown in the Figure II.19.

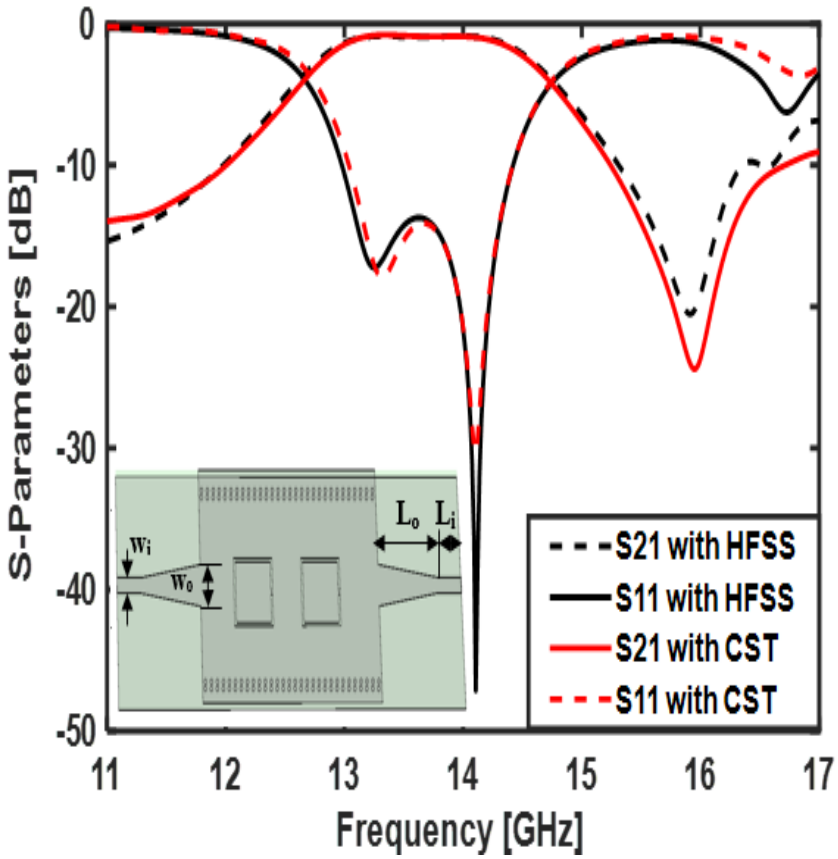

Figure II. 18. Return loss and transmission coefficient of the proposed DGS filter with Wi=1.55 mm, Wo=3 mm, Lo=4 mm, Li=2.4mm.

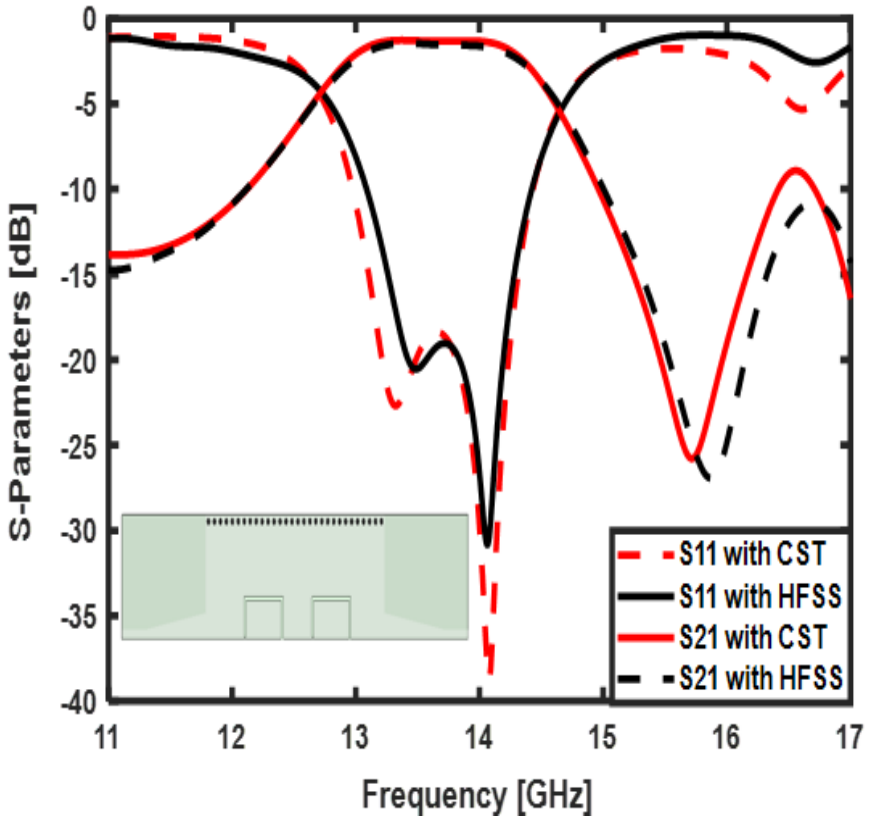

Figure II. 19. Transmission coefficient and return loss of DGS HMSIW filter.

From the previous figure, we observe that: the transmission energy level is under -7 dB in the band ranging from 11 to 12.7 GHz and the reflection is maximum. the transmission is increased In the band ranging from 13.1GHz to 14.2 GHz and it reaches -1.8 dB and the reflection decreased also several resonance frequency has been appeared the best reaches –37 dB around the frequency of 14.1 GHz. and the rejection level is good above 14.3 GHz and it reached -27 dB at the frequency of 15.7 GHz. In the next step, we have cascaded three DGS cells in the top plane with a separated distance of 4.86 mm.

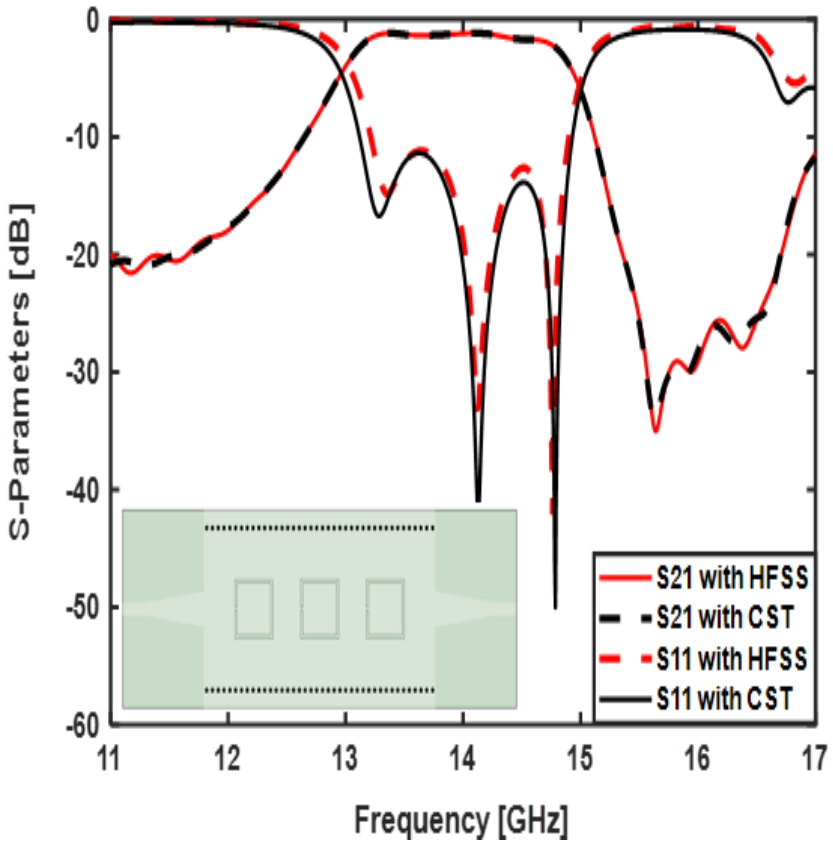

Figure II. 20. Transmission coefficient and return loss of the DGS SIW filter.

From the Figure II.20 it is show that good results are obtained. The simulation results show a good agreement of the cut-off frequency that is of 13 GHz. We observe a good agreement in the filtered band ranging from 13.1 GHz to 15.1 GHz with an insertion loss of about −1.5 dB in the transmitted bandwidth and the recorded return loss reached −50 dB at the frequency of 14.8 GHz and the rejection stretching from 15.2 GHz until 17 GHz. By using the half-mode technique, we reduced the filter size and kept the same performance of the SIW filter. The half mode SIW band pass filter configuration and simulation are shown in the Figure II.21.

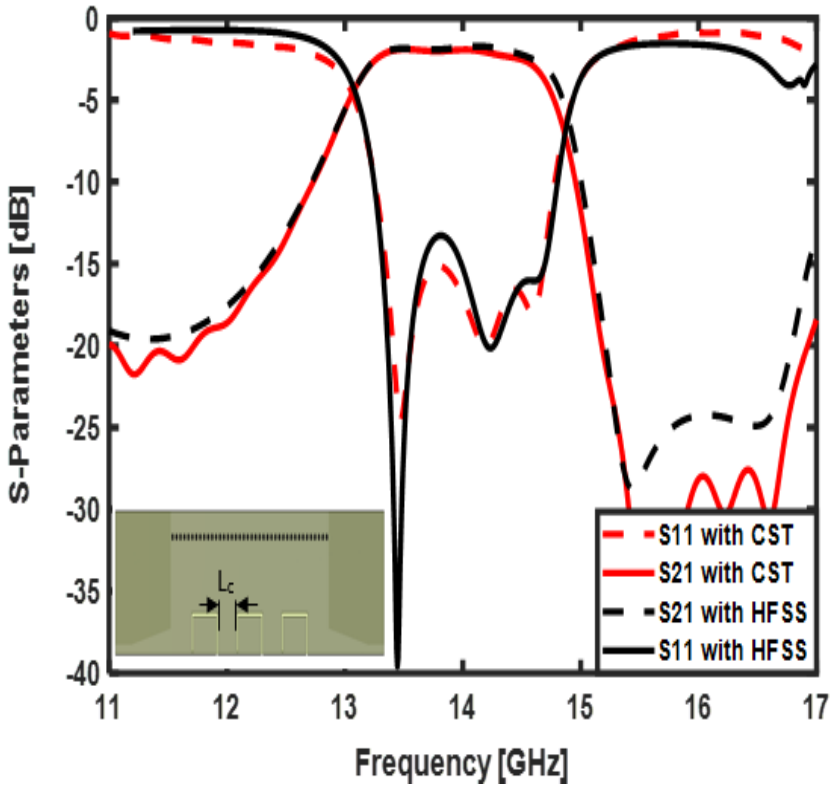

Figure II. 21. S parameters of HMSIW filter with: Lc = 4.86 mm.

It can also be noted that we have an improvement in the rejection bands that ranging from 11 GHz to 13.2 GHz and from 14.8 GHz to 17 GHz also the return loss is under -14 dB in all filtering band about insertion loss is about of -2.6 dB in the transmitted band. We obtained a good agreement between CST Studio and Ansoft HFSS results, which demonstrates our proposed filter.

II. 8. Narrowband SIW Bandpass Filter Based on Cross Shape and Couple C Shape as DGS Cells

In this work, a DGS SIW bandpass filter is designed, simulated, fabricated and measured. We used the design method discussed in chapter I. The proposed filter has a transmitted bandwidth extends from 6.2 GHz to 12.7 GHz and it features by compact size and high rejection. The HMSIW filter has a size reduction of 50 % compared to a similar SIW filter. The advantage of this type of filter is easy for integration with other planar circuit. The proposed SIW DGS bandpass filter has high-rejection so it is suitable for practical applications. Using the CST, we proposed a new SIW-DGS band-pass filter structure for sub-mm 5G using FR-4 substrate, which is characterized by a loss tangent of about 0.025,

a dielectric constant of 4.3 and a thickness of 1.54 mm and the height of the conducting material is equal to 0.05 mm. The first design comprises of six cross-shaped slots are inserted as DGS cells in the upper plane with a horizontal distance equal to 5.5 mm between two consecutive DGS cells and a vertical distance equal to 6.5 mm between two opposite DGS cells and three coupled of C shape DGS cells in the middle of the bottom plane with a distance between each couple equal to 2.61 mm as can be seen in Figure II.22. For impedance matching, we insert four L-shaped slots in the upper plane [5]. Figure II.23 illustrates the simulated results of the proposed filter by CST Microwave based on finite integration technique, a relative of FDTD for its transient solver.

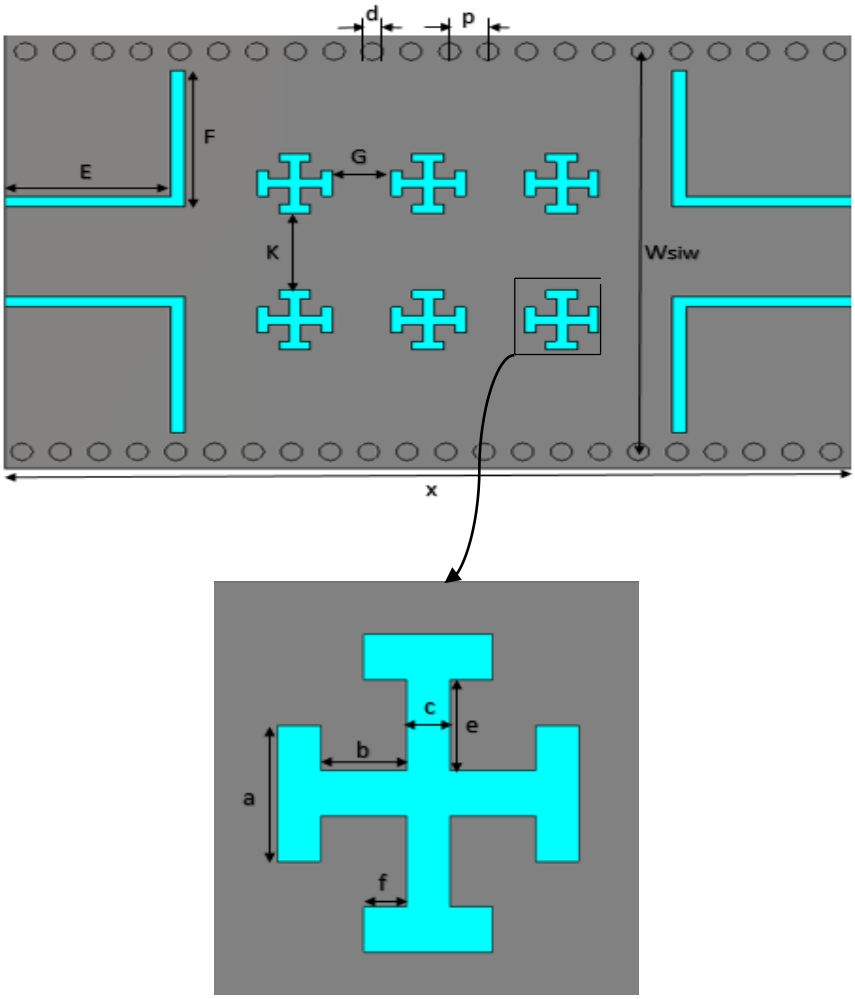

(a)

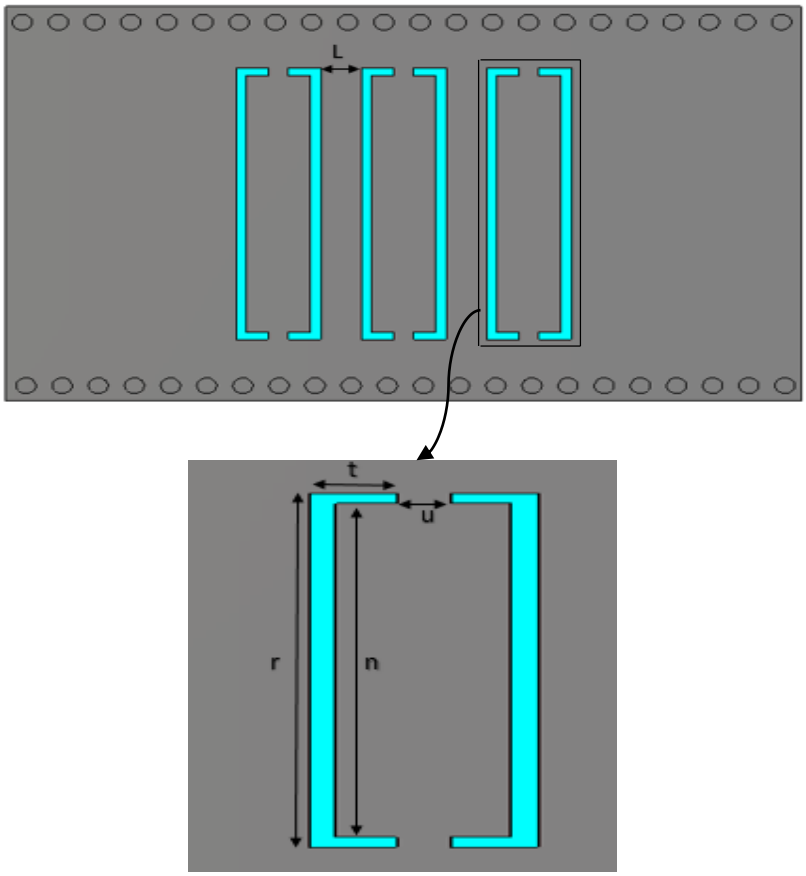

Figure II. 22. DGS-SIW band-pass filter Configuration, (a) front view (b) bottom view.

Table II. 5. The optimal values of the proposed DGS SIW bandpass filter

Parameters	Value(mm)	Parameters	Value (mm)
E	7.2	L	2
F	8	p	2
k	3.9	d	1
G	2.8	x	38.8
Wsiw	23.5	a	1.5
b	1	c	0.5
e	1	f	0.5
r	12	n	11
t	1.63	u	1

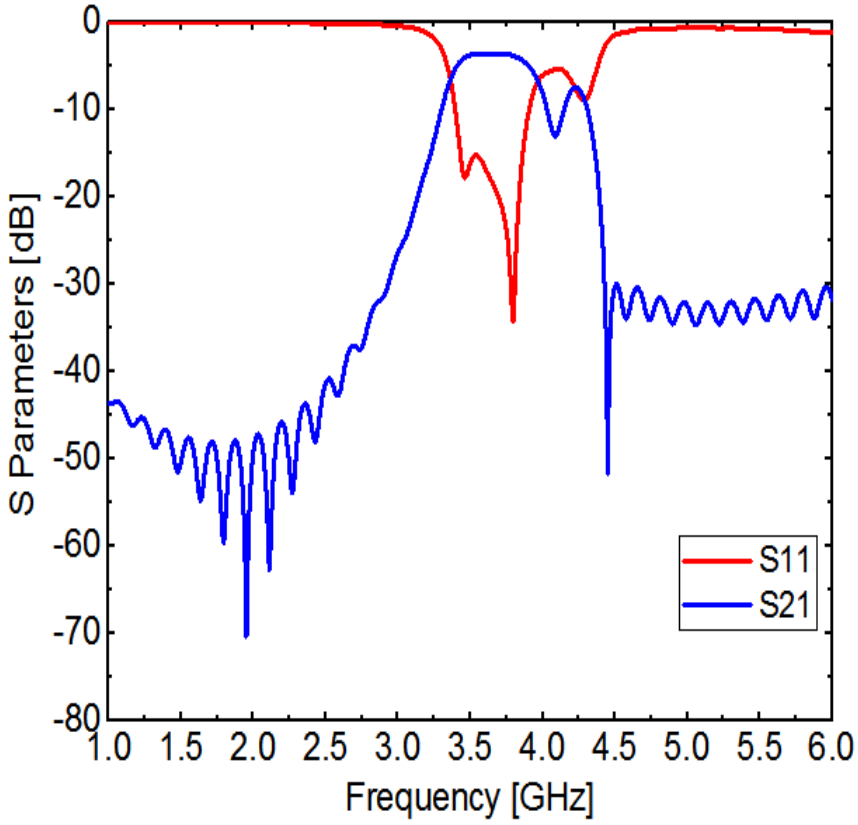

Figure II. 23. S-Parameters of SIW DGS filter.

From Figure II.23 we observe that the filtered band ranging from 3.4 GHz to 3.8 GHz with a long rejection and good return loss. The insertion loss is about of −3.5 dB and the reflection coefficient reached −36 dB at the frequency of 3.7 GHz. It is observed that the stop band rejection exceeds from 1 GHz to 3.4 GHz and from 3.8 GHz to 6 GHz with an amplitude below –30 dB at all rejection band with many transmission zeros, the maximum at 2 GHz and 4.5 GHz.

II. 8. Design of a Narrowband DGS HMSIW Bandpass Filter

The design of the novel miniaturized HMSIW band-pass filter is simulated in this section. The filter is covering the band ranging from 3.4 GHz to 3.8 GHz and it keeps the same SIW filter characteristic with size reduction of 50%. The DGS cells positions are optimized by CST simulator. The HMSIW bandpass filter configuration is depicted in the Figure II.24.

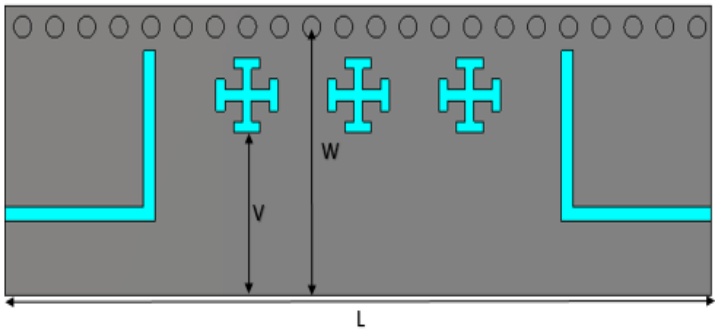

(a)

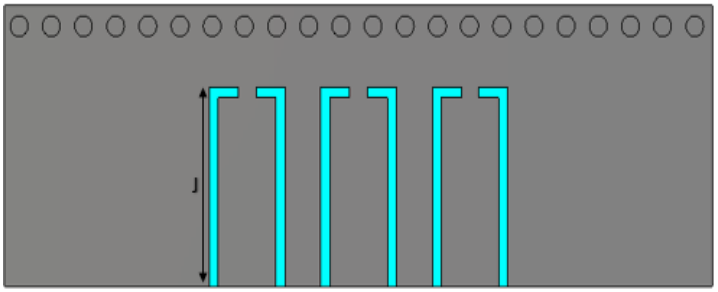

(b)

Figure II. 24. DGS-HMSIW band-pass filter Structure, (a) front view (b) bottom view with W=11.75 mm, V=7.65 mm, J=9.6 mm, L=38.6.

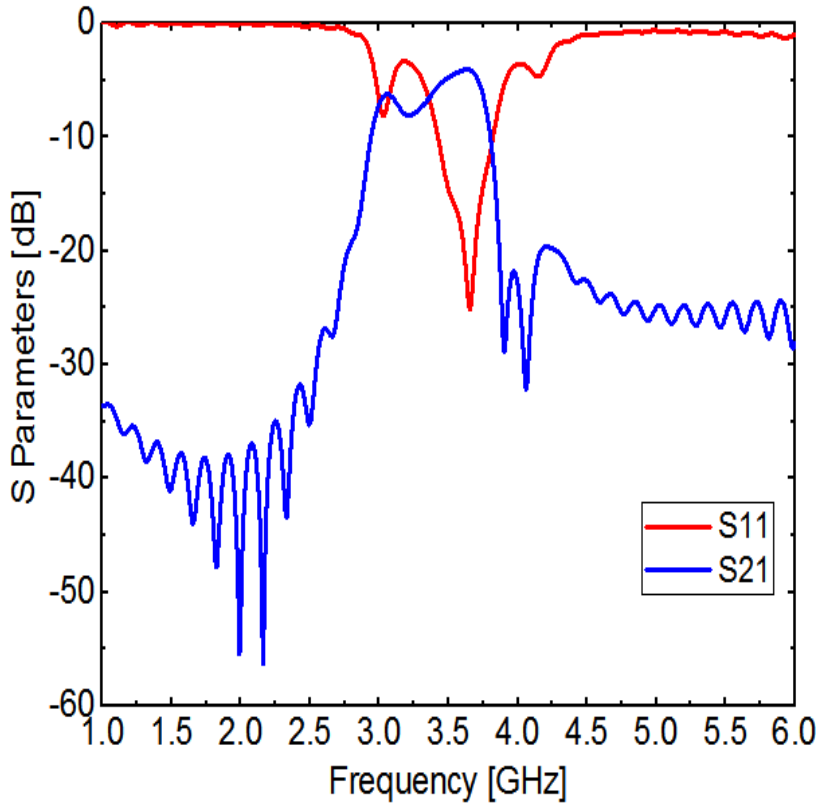

Figure II. 25. Transmission coefficient and Return loss of SIW DGS filter.

Obviously, the filtering band extend from 3.4 GHz to 3.8 GHz with a resonant frequency at 3.7 GHz with a return loss level about of -26 dB. The higher simulated insertion loss is −4.4 dB in transmitted bandwidth. A good rejection is obtained under 3.4 GHz and upper 3.8 GHz with a level less -20 dB in all rejection bands and the maximum rejection reached −55 dB and − 32 dB at the frequencies 2.2 GHz and 4.1 GHz, respectively.

II. 9. Experimental Results

The proposed DGS half-mode SIW bandpass filter is manufactured and measured for proposal validation. Figure II.26 shows the front and back views of the prototype SIW-based bandpass filter. The measurement results of the return loss and the insertion loss of the proposed filter are displayed in Figure II.27.

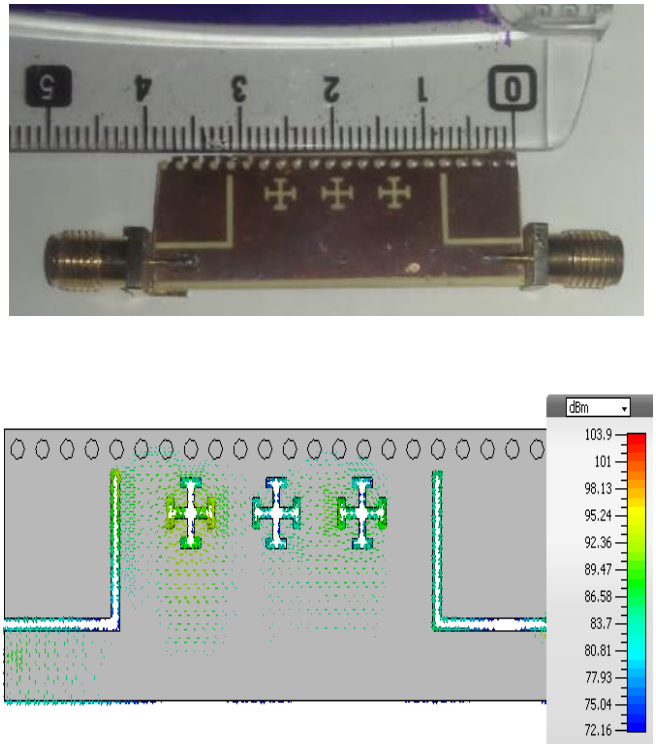

(a)

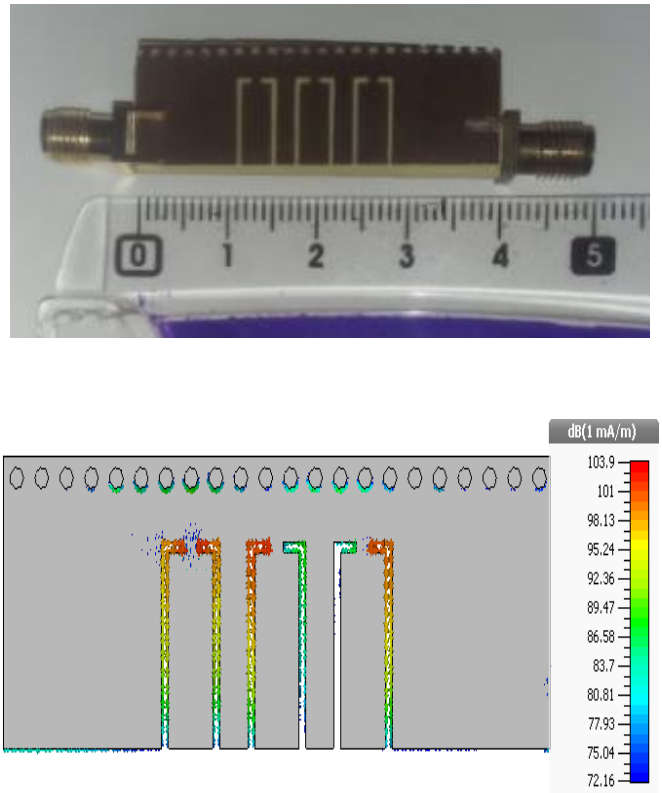

(b)

Figure II. 26. The fabricated filter prototype and Surface Current Distribution, (a) front view, (b) bottom view.

The current distribution indicates that the current mainly flows around the L-shape slots and DGS cells while in the rest of the surface not much current flows as shown in Figure II.26. The coupling distance has an important effect on the filter. The coupling between DGS cells increases when decreasing the distance between them; this is leads to shifting of the transmitted bandwidth. The design is optimized so that the DGS cells work collectively with coupling effect and not separately.

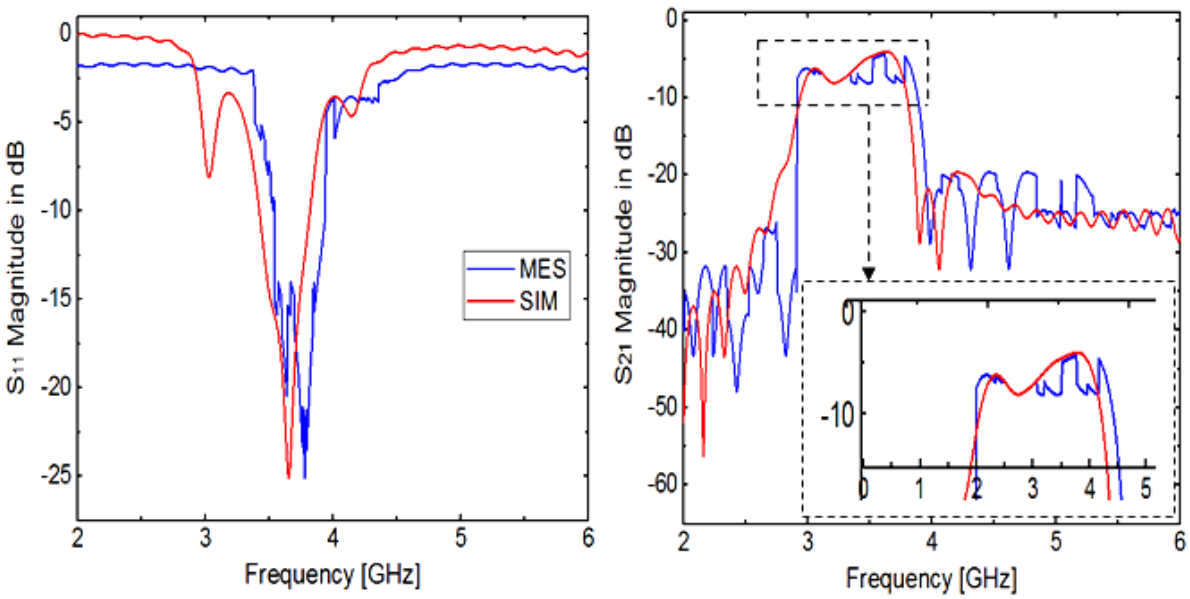

Figure II. 27. Measured transmission coefficient and return loss of SIW DGS filter.

From Figure II.27, we notice that the filter operates in the band ranging from 3.4 to 3.8 GHz with two-resonance frequency at 3.6 and 3.7 GHz, respectively. The measurement result of the lower return loss is less than −34 dB at 6.2 GHz and the measurement result of the higher insertion loss is about −4.6 dB. In addition, good rejection is obtained less than 3.4 GHz and greater than 3.8 GHz. We observed some degradations caused by some factors such as network Analyzer calibration and soldering problem.

II. 10. Half Mode SIW DGS Based Diplexer

The proposed half mode SIW loaded CSRRs diplexer is depicts in Figure II.28 it is implemented with two band pass filters based on HMSIW and CSRR, which are connected to a 50 Ω input microstrip line at port 1 [6]. The first filter is discussed in the previous section and in the second filter we inserted five half CSRR in the bottom plane. The two band-pass filters are combined with a T-junction. The proposed diplexer size is 88 mm × 20 mm. The simulation and optimization of the proposed diplexer were made by CST simulator. The response of the diplexer is illustrated in the Figure II.29.

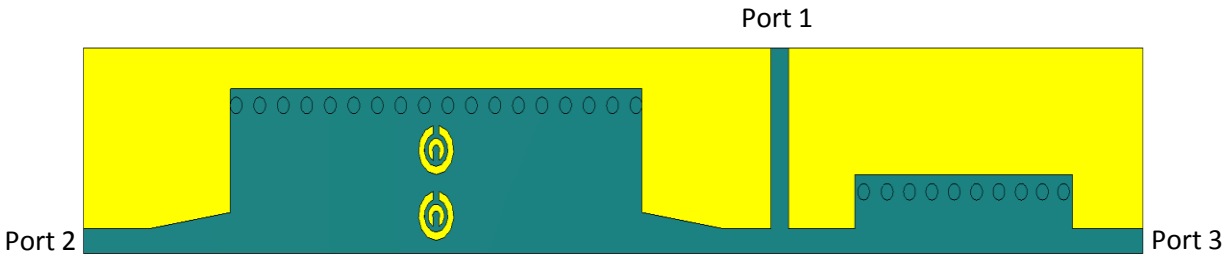

(a) Top plan

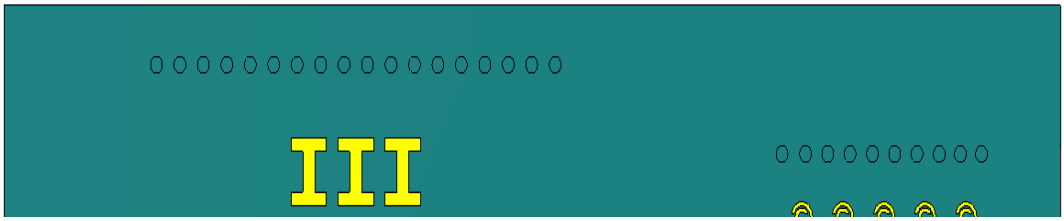

(b) Bottom plan

Figure II. 28. The proposed SIW Diplexer.(a) Top plan (b) Bottom plan.

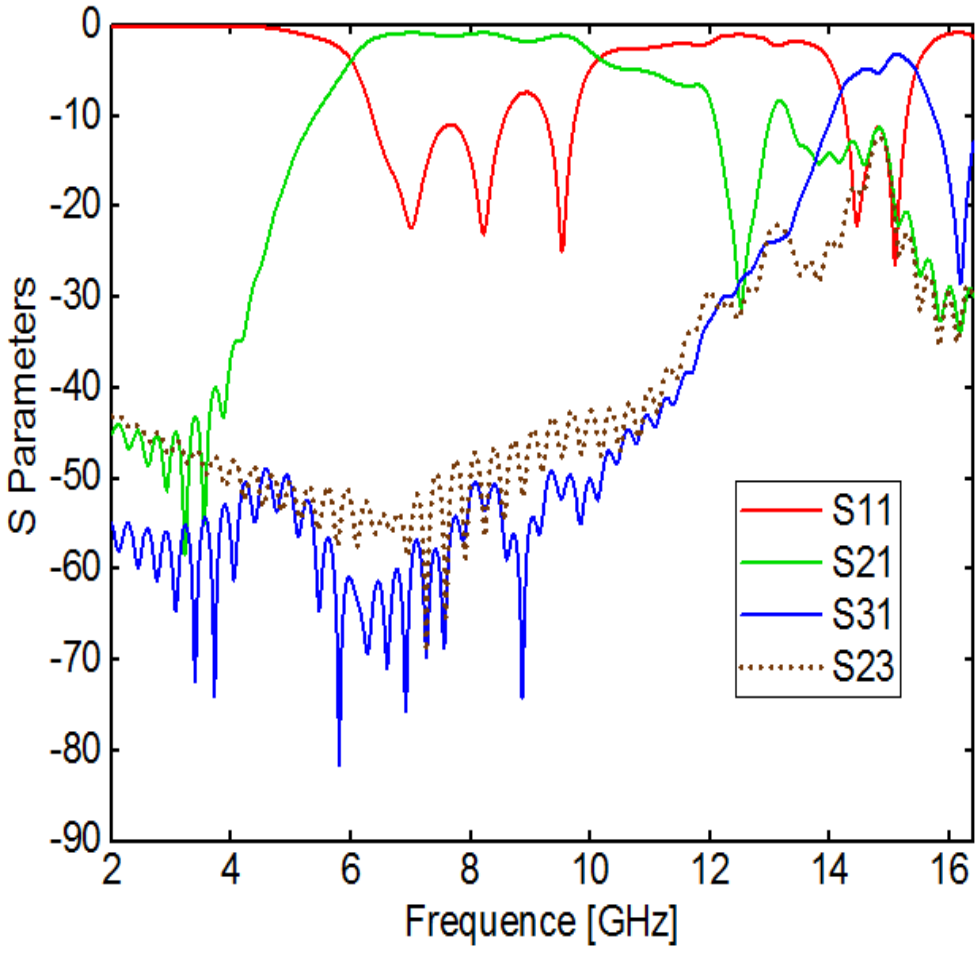

Figure II. 29. S Parameters of the proposed Diplexer.

The simulated Passband of the first bandpass channel is ranging from 6 GHz to 10 GHz, whereas the simulated Passband of the second bandpass channel is ranging from 14 GHz to 15.4 GHz, with insertion loss 1.7 dB and 4.5 dB respectively. In addition, we notice that a good isolation between outputs ports are achieved (less than -15 dB).

II. 11. Symmetrical Shuntinductive Post SIW Bandpass Filter for Terahertz Applications

In the previous section we designed SIW band pass filters based on DGS cells, in this section we will used the shuntinductive post technic which is explain in chapter I. The Figure II.30 illustrate the configuration of the proposed SIW filter with taper transition and symmetric shuntinductive post

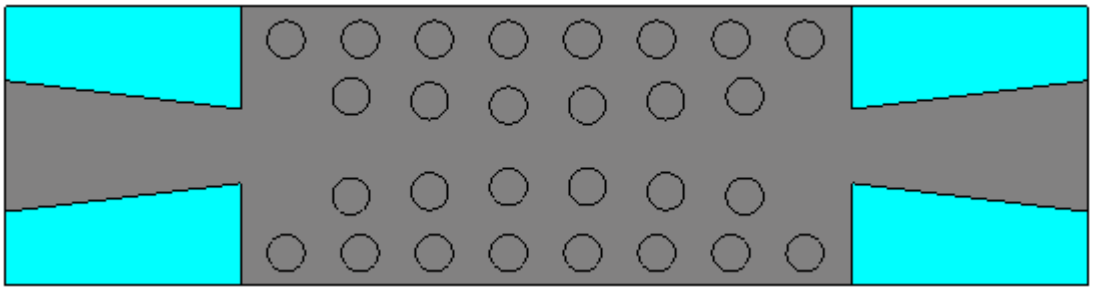

Figure II. 30. The proposed shuntinductive SIW bandpass filter.

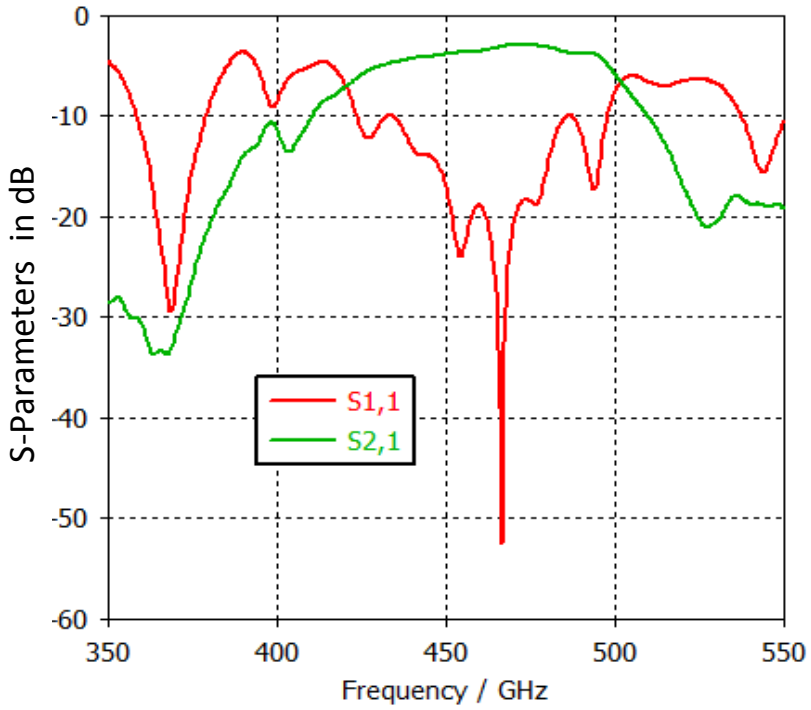

Figure II. 31. S-Parameters of Shuntinductive SIW Bandpass filter.

We notice that band pass effect is successful applied after integrated the symmetrical posts. The transmitted bandwidth is from 420 GHz to 500 GHz with an insertion loss about of -4 dB and the rejection band extend from 350 GHz to 420 GHz and from 500 GHz to 550 GHz with a level below -18 dB.

II. 12. Conclusion

In this chapter we have designed and realized many SIW filter, the design method discussed in chapter I and the studied in chapter I allow us to proposed high performance filters. Good agreement between simulations results and measurements. The HMSIW filter has a size reduction of 50% compared to a similar SIW filter. The proposed filter has small size and high stop-band rejection. This type of filters is easy for integration with other planar circuit compared by using conventional waveguide and it is suitable for practical applications.

References

[1] Mohammed El Amine Chaib, Mehadji Abri, Hadjira Badaoui and Nabil Cherif," Bandpass Filters Based on Hybrid Structure of Substrate IntegratedWaveguide (SIW) and Hilbert Defected Ground Structure (HDGS)," Progress In Electromagnetics Research Letters, Vol. 104, PP. 27–35, May 11 2022.

[2] Cherif Nabil, Hichem Chaker, Mehadji Abri, Fellah Benzerga, Hadjira Badaoui, Junwu Tao, Tan-Hoa Vuong and Sarosh Ahmad, " A High Pass Filter Based on Half Mode Substrate IntegratedWaveguide Technology for cm Waves" Progress In Electromagnetics Research Letters, Vol. 104, PP. 149–154, June 15 2022

[3] Nabil Cherif, Mehadji Abri, Benzerga Fellah, Hadjira Badaoui and Junwu Tao "A Compact Wideband DGS Bandpass Filter Based on Half Mode Substrate Integrated Waveguide Technology," International Journal of Microwave and Optical Technology, Vol. 16, No. 2, PP. 142-146, March 2022.

[4] Benzerga Fellah, Nabil Cherif, Mehadji Abri and Hadjira Badaoui," CSRR-DGS Bandpass Filter Based on HalfMode Substrate Integrated Waveguide for X-Band Applications," Advanced Electromagnetic, Vol. 10, No. 3, PP. 39-42, November 2021.

[5] Nabil Cherif, Mehadji Abri, Sarosh Ahmad, Adnan Ghaffar, Chahira Khial, Fellah Benzerga, Mohammed El Amine Chaib, Hadjira Badaoui and Bouabdallah Roumeica," Miniaturizing Bandpass Filter Based on Half-Mode SIW for Sub-mm 5G Applications " Progress In Electromagnetics Research Letters, Vol. 104, PP. 155-160, June 20 2022.

[6] Pejman Mohammadi and Rana Gheibi " A new design of substrate integrated waveguide diplexer using complementary split ring resonators," Wiley RF And Microwave Computer-Aided Engineering " Vol. 29, Iss. 8, PP. 1-5, August 2019.

CHAPTER III

SIW Traveling Wave Antennas Array Design

III. 1. Introduction

Millimeter wave circuit for satellite communication [1] automotive radars [2] and imaging [3] and Terahertz antennas [4] have great importance in industrial and academic research [5]. Previously the circuits were heavy and their design was impressive but in recent years, the research was dedicated to use the Substrate Integrated Waveguide (SIW) [6-7]. High gain antennas are essential for radar imaging and detection devices and wireless communication due to the high propagation loss of the mm-wave and THz wave transmission. Wideband Array antennas have developed for serving several applications in communications systems and by using SIW, it is possible to miniaturizing its size [8]. Several literature presented on SIW antenna array among them a broadband 1×4 Vivaldi antenna array using SIW was presented in [9] for ka-band With a gain over 12 dBi. In [10] a 1×8 Vivaldi antenna array was presented for ka band with the gain up to 16 dBi. In [1] a continuation of the work in [10] with an optimization of the results, the gain was enhanced and up to 18 dBi. The main problem in mm wave band is to reach a high gain due to high loss of array feeding using PCB fabrication process [9]. Our research effort in this chapter is divided in two section first we focused on the design of a broadband Eight-Way 1×8 antenna array based on SIW technology operate in V-band using novel configuration. Initially, a single element antipodal antenna, which has comb shape profile, was proposed and designed covering the V band. Next, a 1×8 antenna array fed by SIW power divider is designed and we analysed return loss, radiation pattern and gain using CST simulator. Second, a broadband two-way 1×2 linear antenna array based on SIW technology operating from 0.135 THz to 0.205 THz was proposed. Initially, a single element antipodal antenna was proposed and designed ranging from 0.133 THz to 0.243 THz. Next, a 1×2 SIW power divider having Y junction was proposed, designed and optimized. Finally, the proposed antenna is integrated with the optimized 1×2 SIW power divider for realizing the antenna array.

III. 2. The Proposed Step Constant LTSA SIW Antenna

In this section, we are interested in study of a SIW travelling wave antenna (TWA) with single element used in arrays in order to achieve high gain, maximum directivity and wide band. Using the CST and HFSS Simulators, we designed a new SIW TWA structure for V-band on Rogers RT5880 substrate having a loss tangent (tg∂) approximately 0.0009, a relative

permittivity of 2.2, a thickness h of 0,508 mm . We used a perfect conductor with a thickness of 0.05 mm.

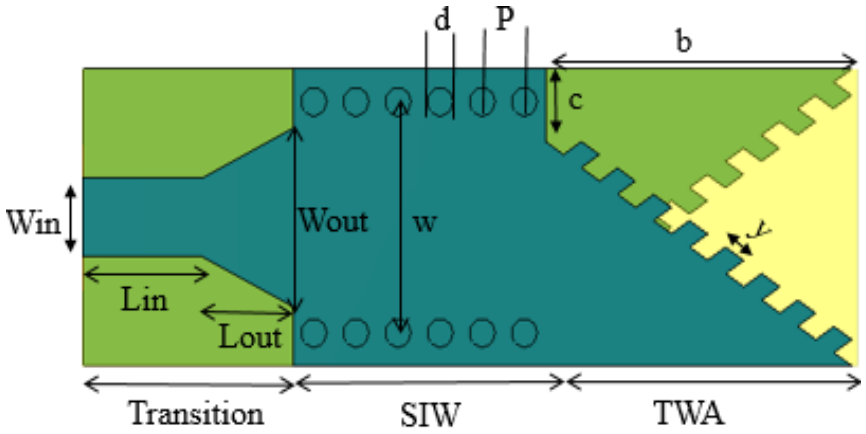

Figure III. 1. The proposed antenna configuration.

Table III. 1. The optimized values of the parameters of the proposed antenna.

Parameters	Value (mm)	Parameters	Value (mm)
Win	1.5	w	3.4
Wout	2.7	p	0.7
Lin	2.0	d	0.4
Lout	1.5	y	0.36
c	0.9	b	5.5

The proposed antenna is composed of three structures: The first part is the taper transition for impedance matching between microstrip and SIW. The second part is the SIW that features by the diameter “d” of the metal vias, the distance “p” between centers of two successive via and the transverse spacing “w” between the centers of opposite vias which is given by the same propagation characteristics with the equivalent waveguide. To minimize the radiation and return loss two conditions are required: $p < 0.2\times\lambda g$ and $p \leq 2\times d$. The third part consists of the antipodal radiating arms, which have comb-shaped profile configuration. The parameter y represents the step constant of the antenna and it is optimized using the parametric study with CST simulator. The parameter y represent the antenna length and it is optimized using the parametric study with CST simulator.

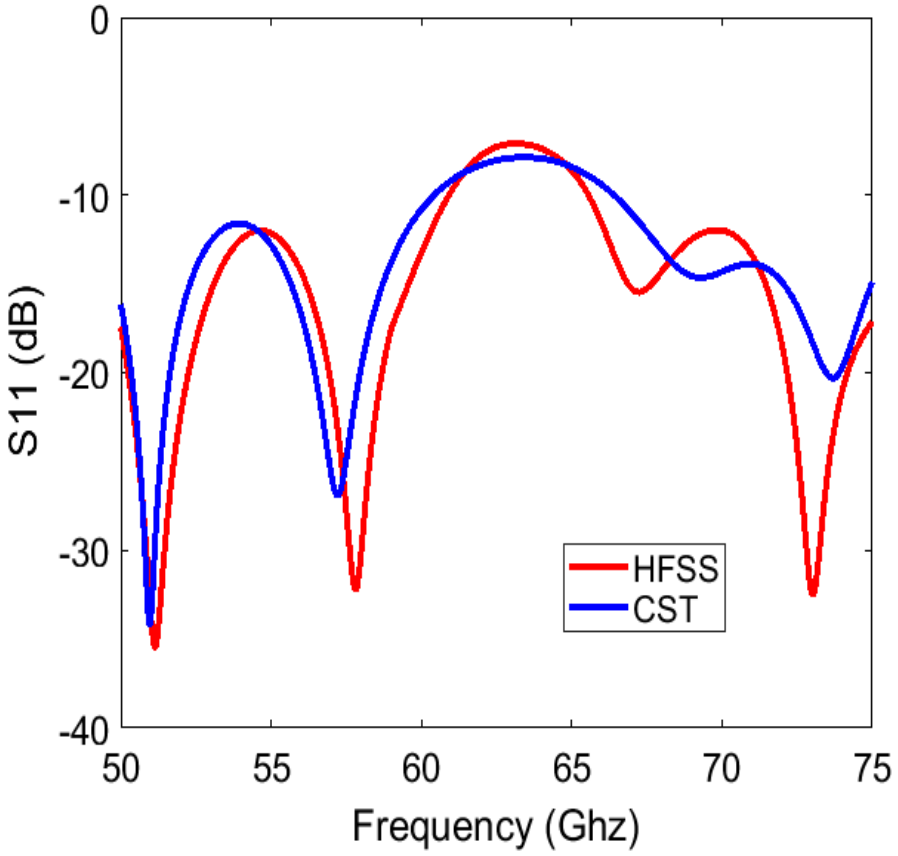

Figure III. 2. Simulated S_{11} of the SIW single antenna element.

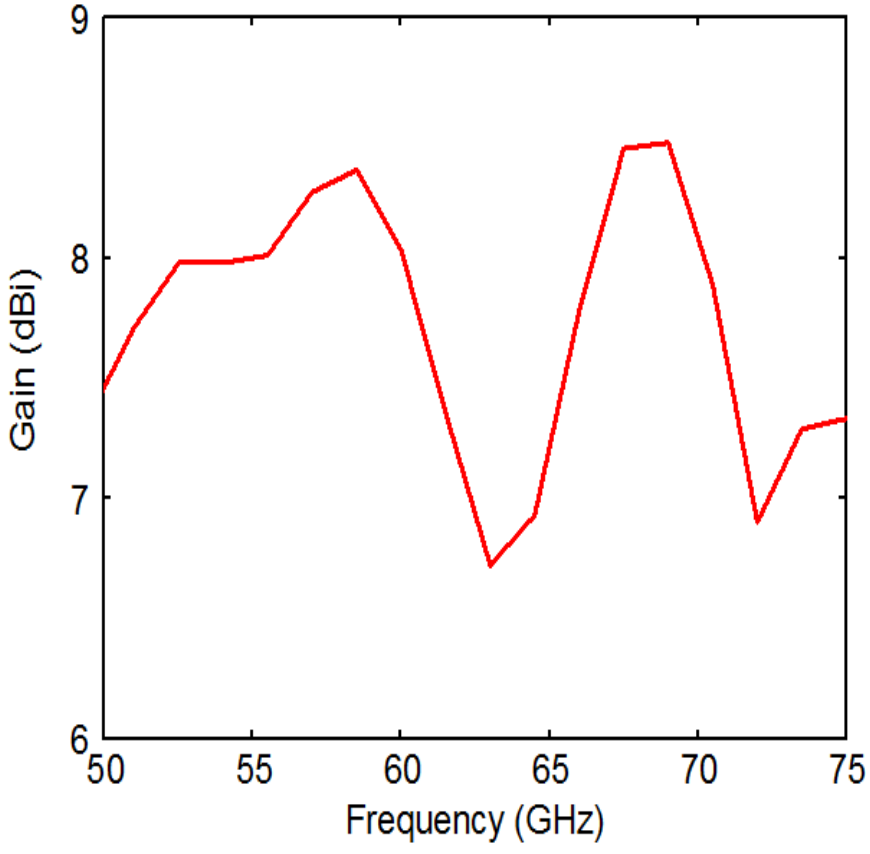

Figure III. 3. Simulated gain of the SIW single antenna element.

The simulated S11 of the proposed antenna is shown in the Figure III.2, it can be notice that the antenna is well adapted, the value of return loss below -10 dB range over 50-61 GHz and over 66-75 GHz and its lower value is about -35 dB at the frequency of 52 GHz. There is a good agreement between simulation results of CST and HFSS. About the simulated gain shown in Figure III.3, we notice that the gain value is acceptable, it varies from 6.5 to 8.4 dBi over all band and it reaches a maximum value of 8.4 dBi at the frequency of 58 GHz and 69 GHz.

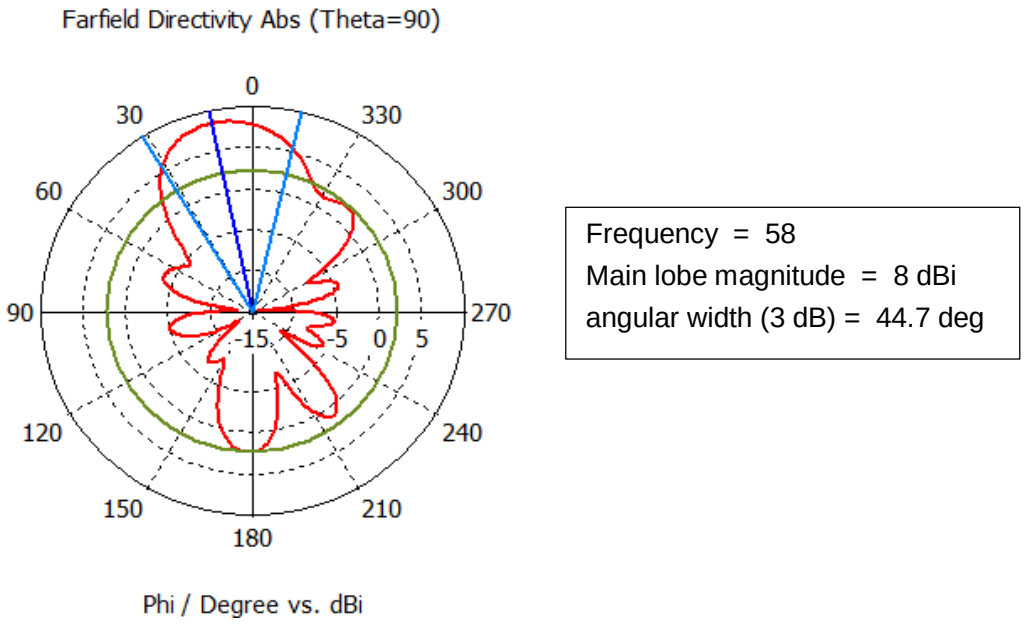

Figure III. 4. The radiation pattern in polar coordinates of the proposed antenna.

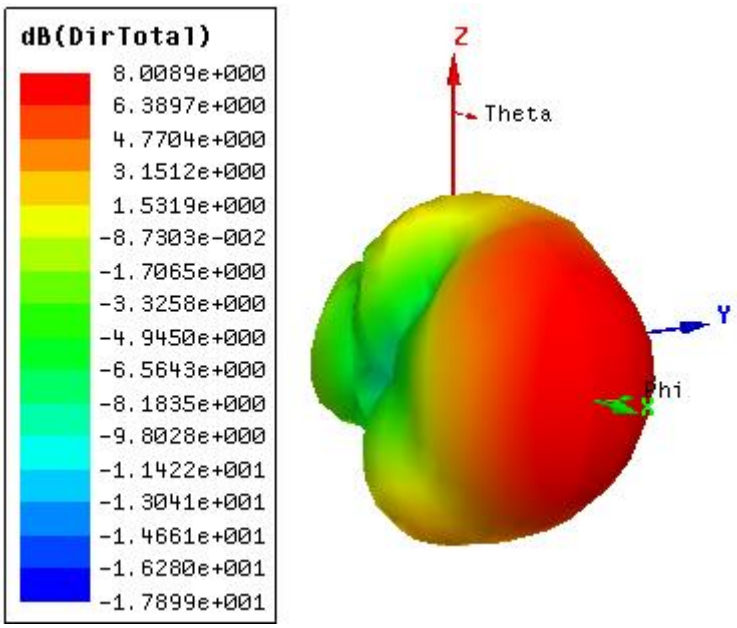

Figure III. 5. The radiation pattern in 3D of the proposed antenna.

The Figures III.4 and III.5 represent the radiation pattern of the single antenna element for the frequency of 58 GHz. We can see that the radiation is maximum in the plane (Theta= 90 °), the most of the radiation radiate into the direction of the Ox axis and the maximum directivity is around the 8 dB with an aperture angle of 3 dB of 44.7°. It is then pointed out that the antenna has a longitudinal directional radiation. According to these results, we can use this antenna to construct the antenna array.

III. 3. Eight-Way 1×8 SIW Antenna Array Design

In this part, we design a SIW antenna array fed by SIW eight-way power divider having T-junction configuration. The following structure shown in the Figure III. 6 is composed of a distribution of uniform antennas elements along de Y axis printed in Rogers RT5880 dielectric substrate with an optimal distance of 5.3 mm between elements, powered by optimized SIW 1×8 power divider [11]. The overall size of the proposed antenna array is 25 mm × 42.4 mm which make it more compact compared with conventional antenna array.

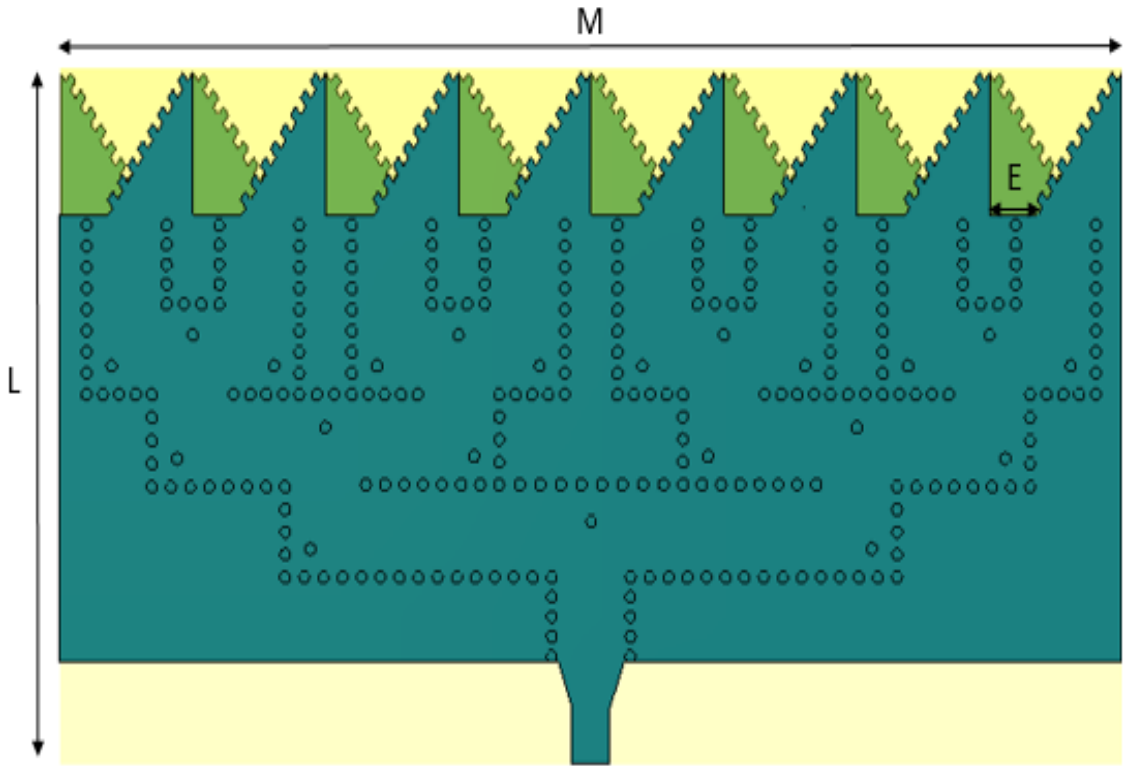

Figure III. 6. Geometry of antenna array with M=42.4mm, L=25mm, E=5.3mm.

From the Figure III.7 which represent the simulated S_{11} of the eight way antenna array, we notice that antenna array coverers the bandwidth from 55 GHz to 70 GHz except some degradations around de 57 GHz and 60 GHz caused by the discontinuity the current on the radiating arms, we notice also the appearance of several resonance frequencies the best reached -38 dBi for the frequency of 66 GHz. A good agreement between the simulation results of CST and HFSS. As observed in Figure III.8 the simulated gain of the proposed antenna array exceed 15.3 dBi and reaches 17.5 dBi from 55 GHz to 66 GHz and it droop to 8.5 dBi from 66 GHz.

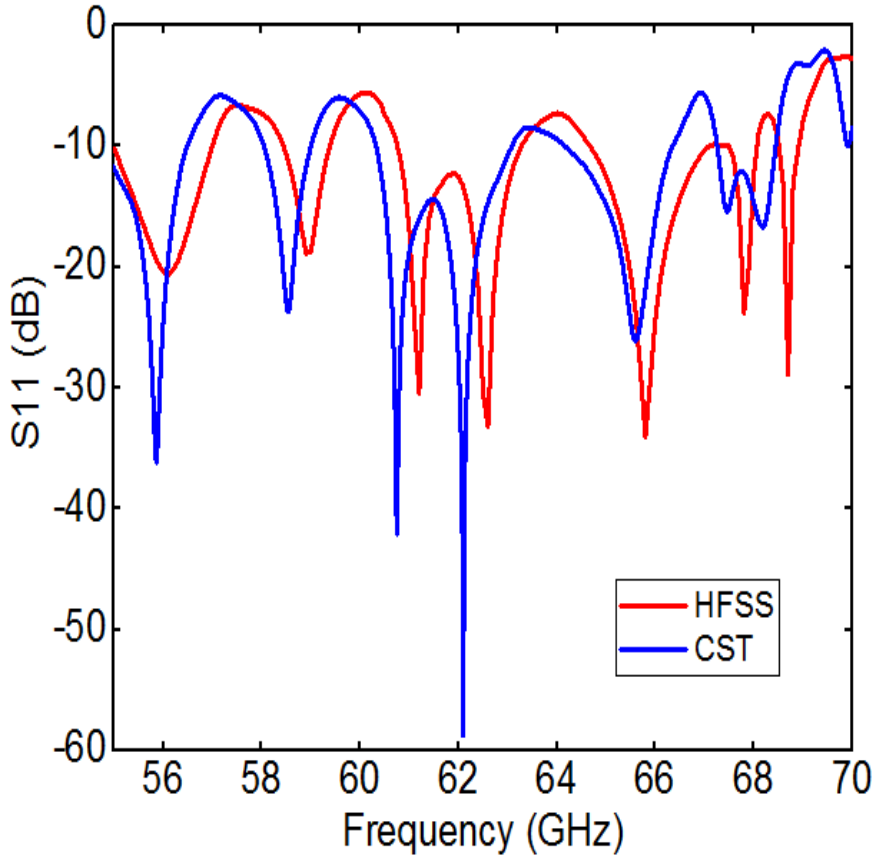

Figure III. 7. Simulated S11 of the SIW 1×8 antenna array.

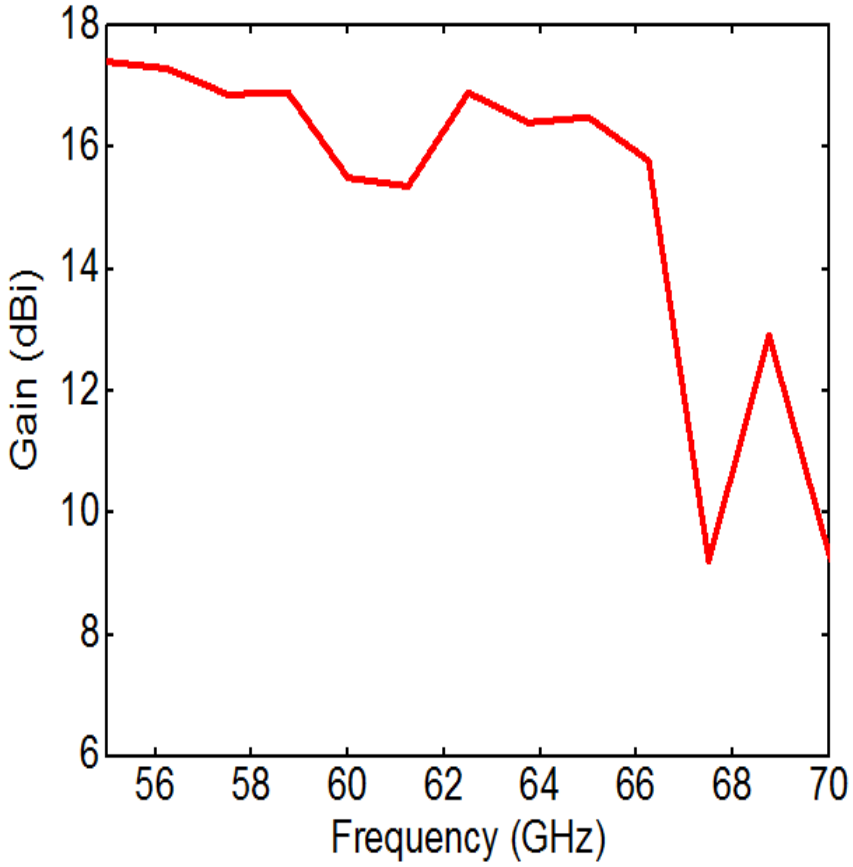

Figure III. 8. Simulated gain of the SIW 1×8 antenna array.

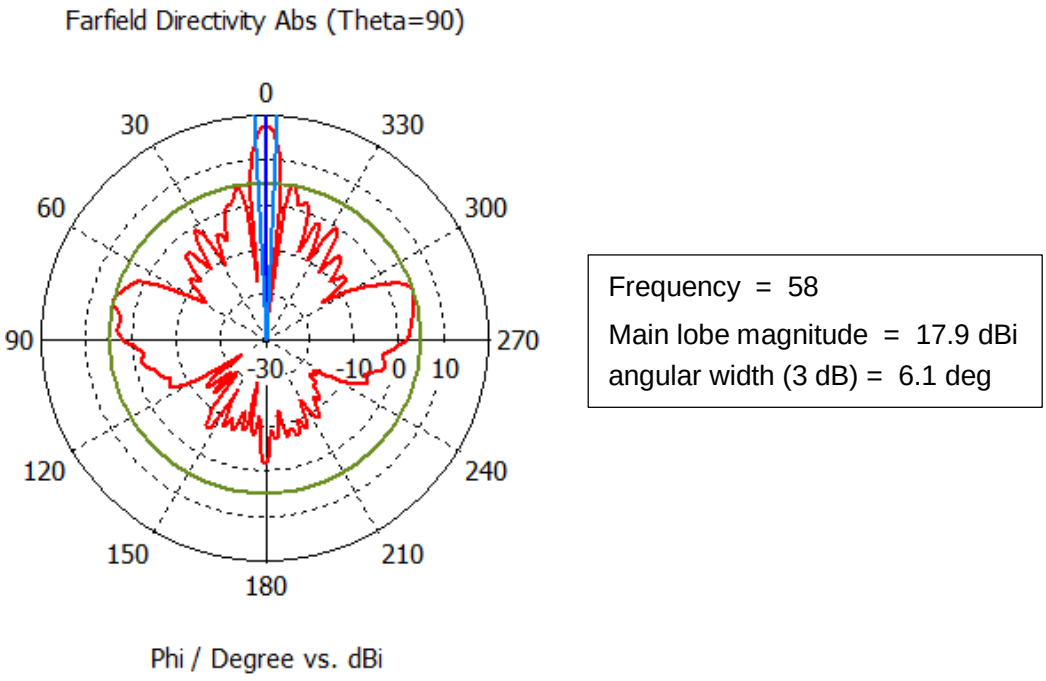

Figure III. 9. The radiation pattern in polar coordinates of the antenna array.

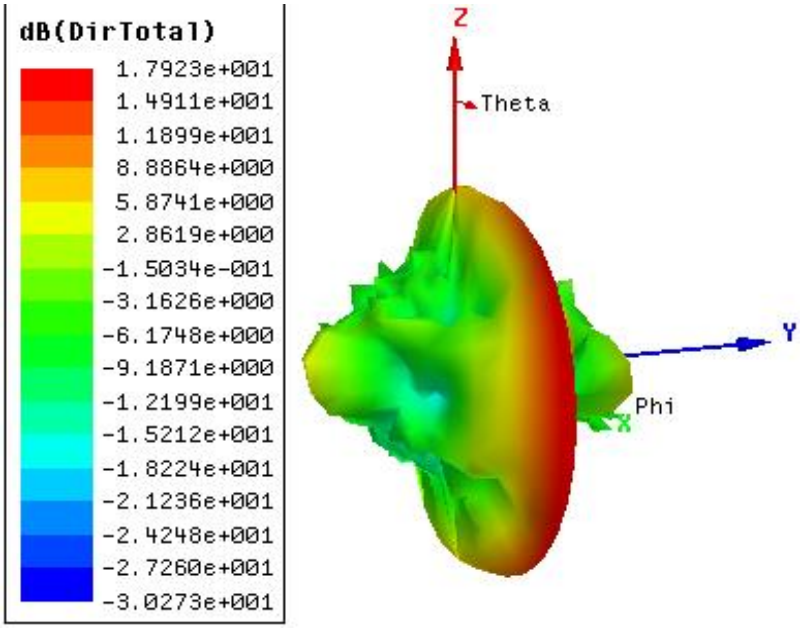

Figure III. 10. The radiation pattern in 3D of the antenna array.

The Figures III.9 and III.10 represent the radiation pattern in 3D and 2D patterns of the SIW 1×8 antenna array for the frequency of 58 GHz. We can see that the radiation is maximum in the plane (Theta= 90°), the maximum directivity is around the 17.9 dB with an aperture angle of 3 dB of 6.1°. We notice that the directivity is increased and the aperture angle is decreased. We can also see that the antenna array radiate in the longitudinal direction.

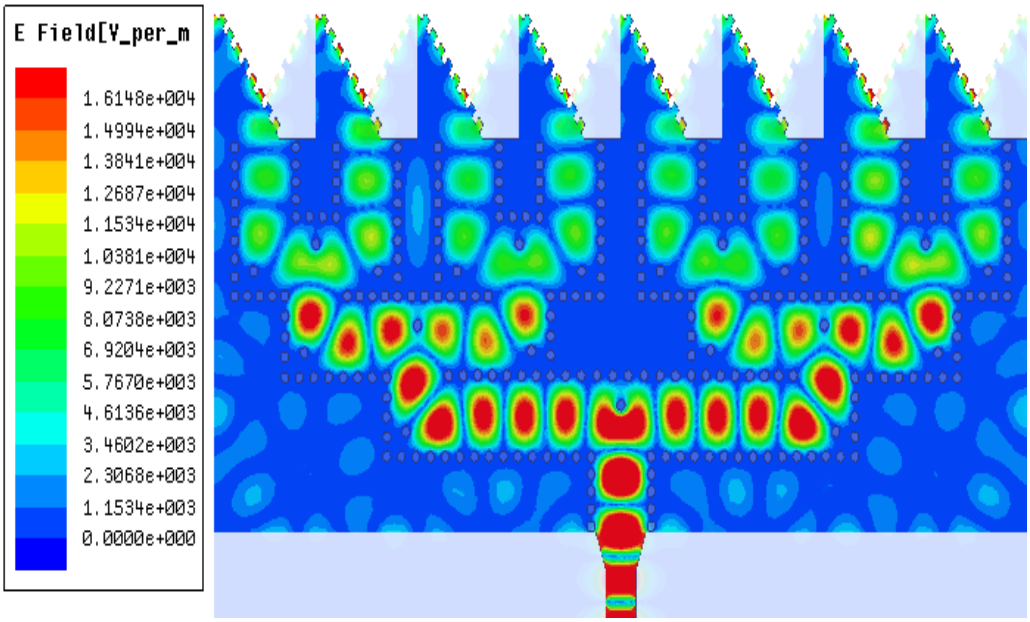

Figure III. 11. Electric field distribution for the frequency of 58 GHz.

The phenomenon of the electric field distribution of the frequency of 58 GHz for the TE_{10} guided mode in the antenna array shown in the Figure III.11. We notice that the field is well located in the all power divider and it is well distributed in all radiating arms, which mean that the antenna array radiates perfectly with equiamplitude excitation.

III. 4. The Proposed Log Periodic Dipole SIW Antenna Design

In this part, we are going to design of a new SIW travelling wave antenna (TWA) with single element used to construct the antenna arrays. Using the CST, we designed a SIW TWA structure with modified comb shaped profile configuration. The geometry of the proposed SIW antenna element is shown in Figure III.12. The used substrate is Rogers 5880 characterized by a loss tangent (tg∂) about of 0.0009, a dielectric constant of 2.2, and a thickness h of 0,508 mm [5]. As shown in Figure III.12 the modified antipodal comb-shaped antenna is comprised of three parts: the taper transition, the SIW feed and the antipodal radiating arms. The optimized value of the taper and the required vias conditions are determined by using the equations presented in chapter I. The input impedance is characterized by 50 Ohm. The optimized parameters value of the antenna are presented in the Table III.2.

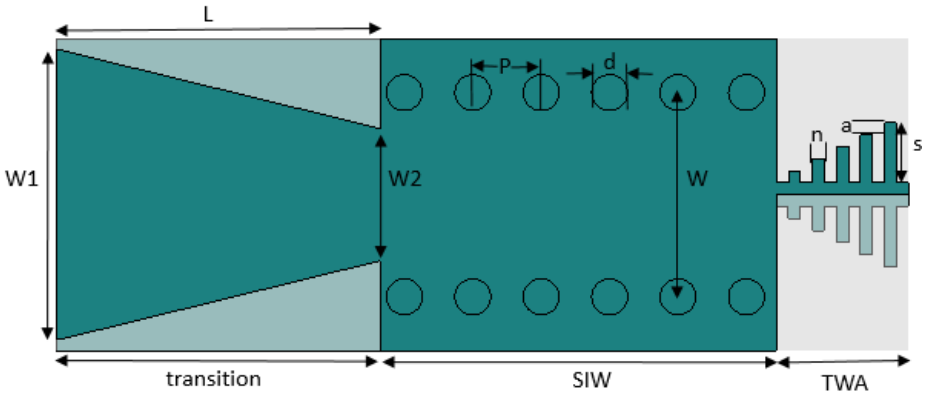

Figure III. 12. The proposed antenna element configuration.

Table III. 2. The optimized parameters of the proposed antenna.

Parameters	Value (mm)	Parameters	Value (mm)
W1	2.4	d	0.3
W2	1.1	n	0.1
L	2.7	a	0.1
W	1.7	s	0.5
p	0.6	h	0.508

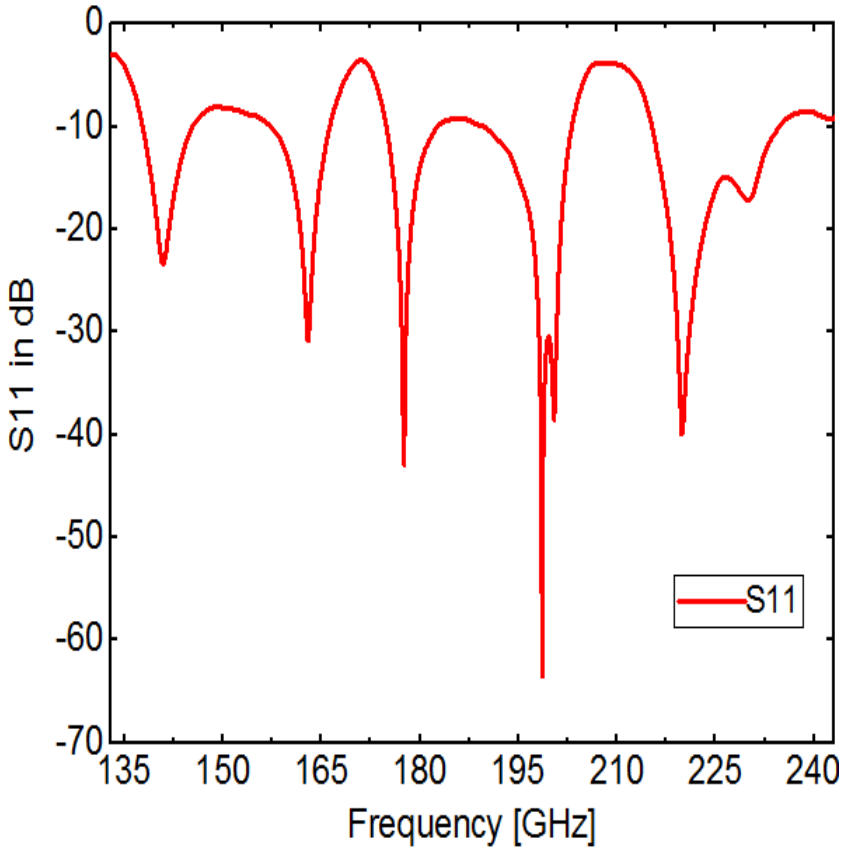

Figure III. 13. Reflection coefficient of the proposed antenna.

From the Figure III.13 it can be notice that the proposed SIW antenna is well adapted, it operates in the band ranging from 0.133 THz to 0.243 THz, and its lower return loss value is exceeded -60 dB at the frequency of 0.198 THz, with the appearance of the several resonance frequencies.

III. 5. The Proposed Two Way Power Divider

In this section, we designed a 1×2 SIW power divider having Y-junction used to feeding the array antenna and for dividing the power by the same amount. The post P1 and P2 are positioned at the right angle to improve the input reflection coefficient [12]. We used Rogers RT5880 substrate for construct the power divider and we used the parametric study with CST for optimized the simulation results.

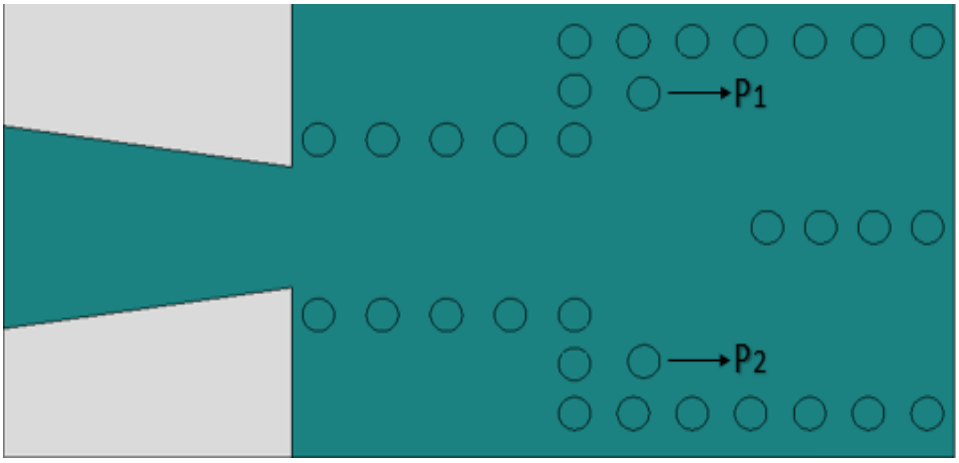

Figure III. 14. Two-Way SIW power divider.

Figure III.14 shows the simulation results of the S-parameters of the proposed SIW power divider. The simulation results of S11, S21 and S31 point out that the power divider is operational over 0.135 THz to 0.205 THz with a reflection coefficient below -10 dB. The lower return loss value is about of -33 dB at the frequency of 143 GHz. It is also noted that the transmission coefficient S21is above than -10 dB in the operating band.

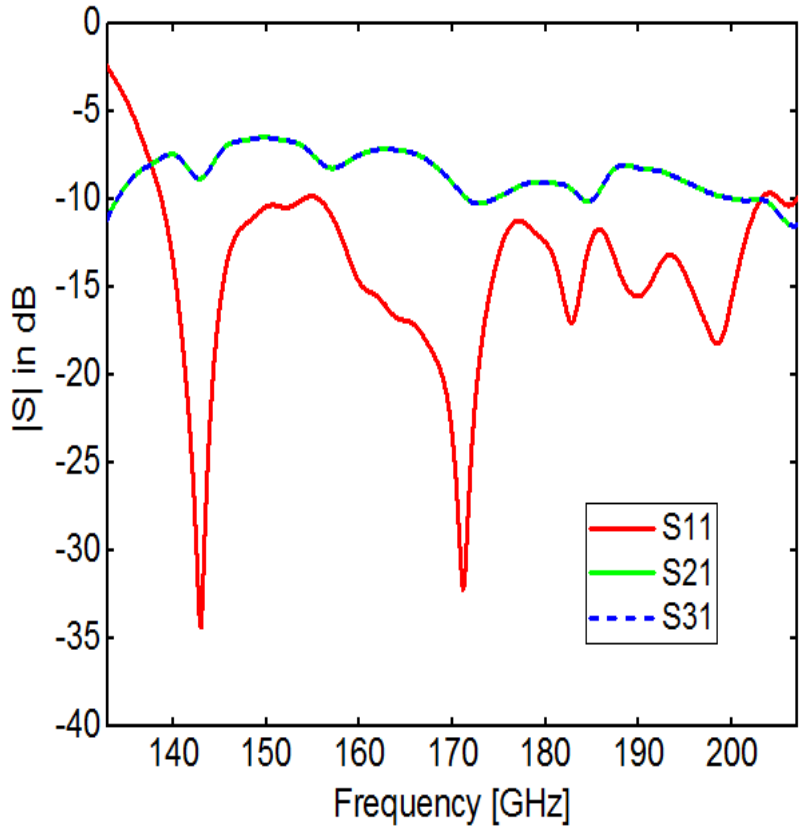

Figure III. 15. The Simulated S-Parameters of the 1×2 SIW power divider.

III. 6. The Proposed Two Way Linear SIW Antenna Array

The proposed antenna element is integrated with the optimized SIW power divider to construct a 1 × 2 linear antenna array. The overall size of the proposed SIW array antenna is 10 mm × 4.3 mm × 0.6 mm that make it a compact component.

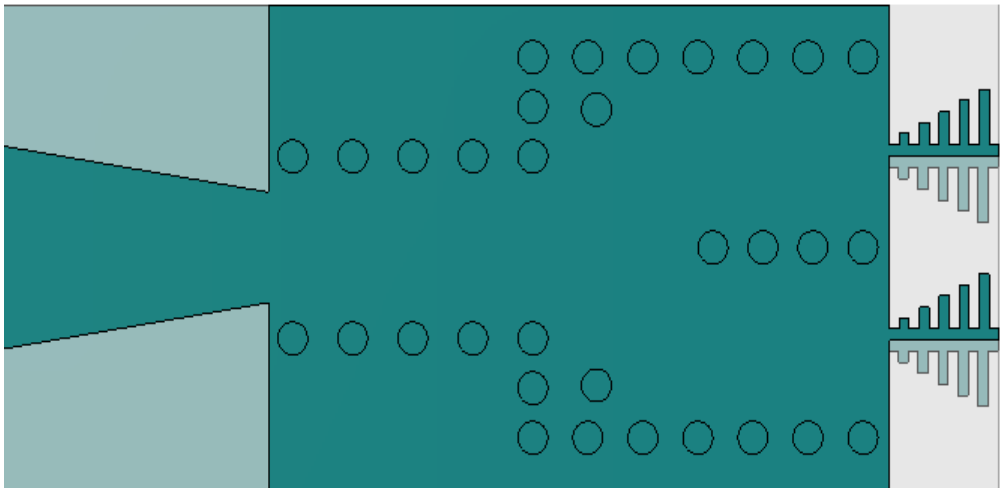

Figure III. 16. 1×2 SIW antenna array.

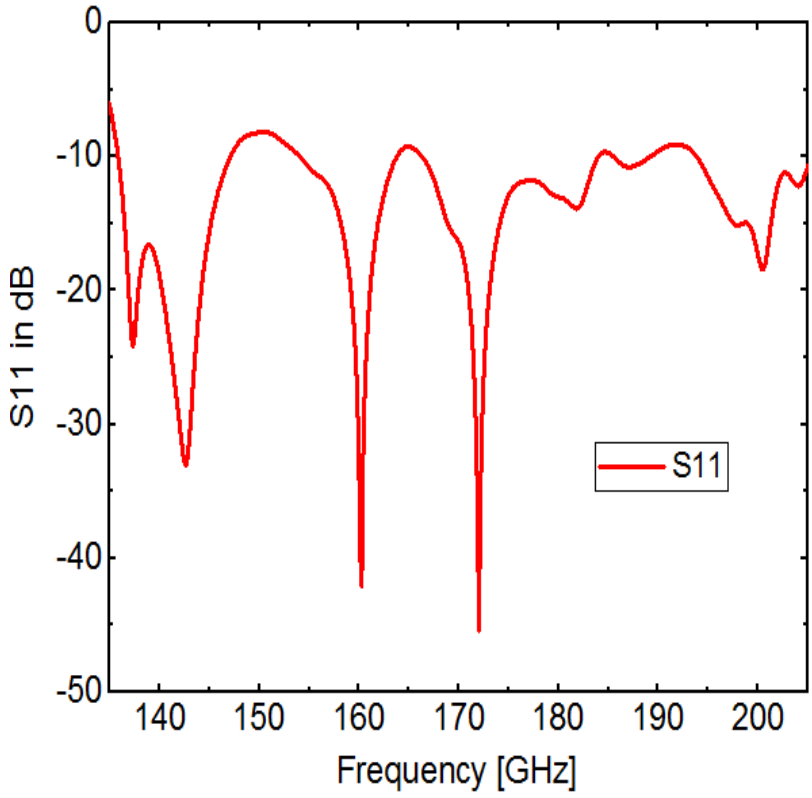

Figure III. 17. The 1×2 SIW array antenna return loss.

From Figure III.17 we notice that the value of S11 lower than -10 dB ranging from 0.135 THz to 0.205 THz and it reached -45 dB at 172 GHz. Some deteriorations appeared around the 0.150 THz caused by the resonance between the two elements of the antenna array.

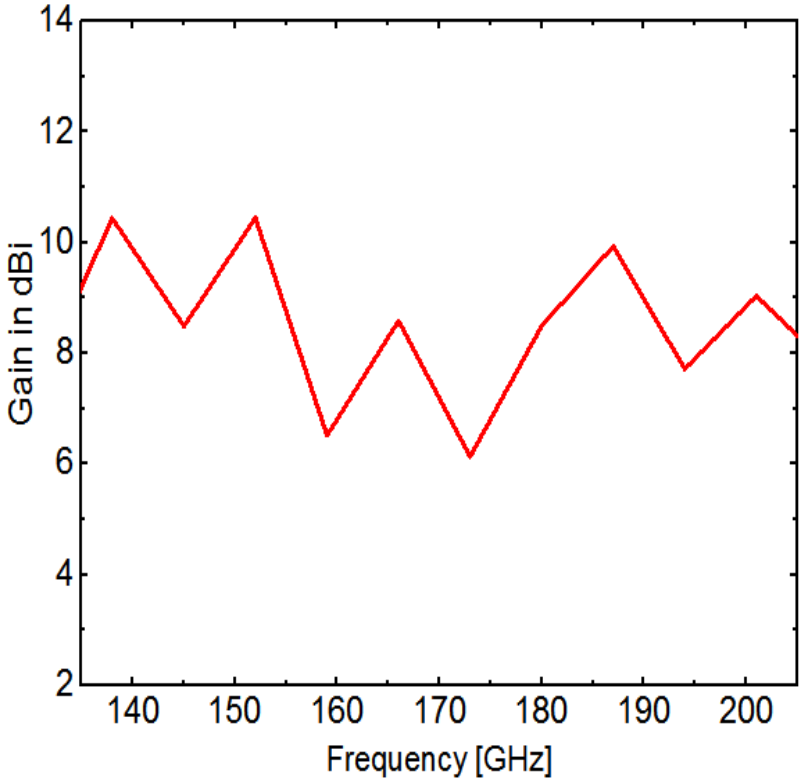

Figure III. 18. The 1×2 SIW array antenna simulated gain.

Regarding to the simulated gain shown in Figure III.18 we notice that the gain values is acceptable with fair flatness, it exceeds 7.5 dBi from 0.135 THz to 0.155 THz and from 0.177 THz to 0.205 THz and its highest value is 10.3 dBi at the both frequency of 0.137 THz and 0.152 THz.

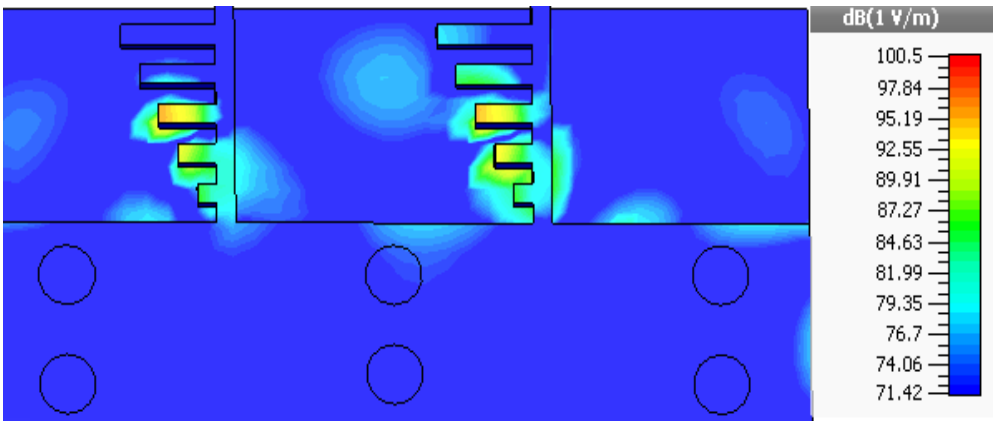

Figure III. 19. Electric field distribution for the frequency of 0.172 THz.

The Figure III.19 show the electric distribution in the radiating arms for the frequency of 0.172 THz. We notice that the field is well distributed in the radiating arms, which mean that the antenna array radiates perfectly with equiamplitude excitation.

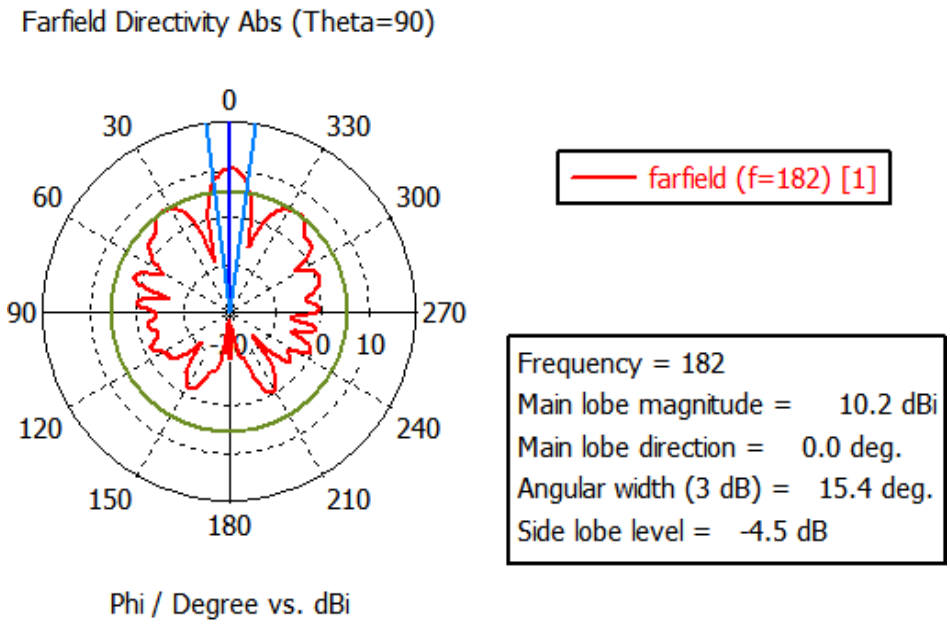

(a)

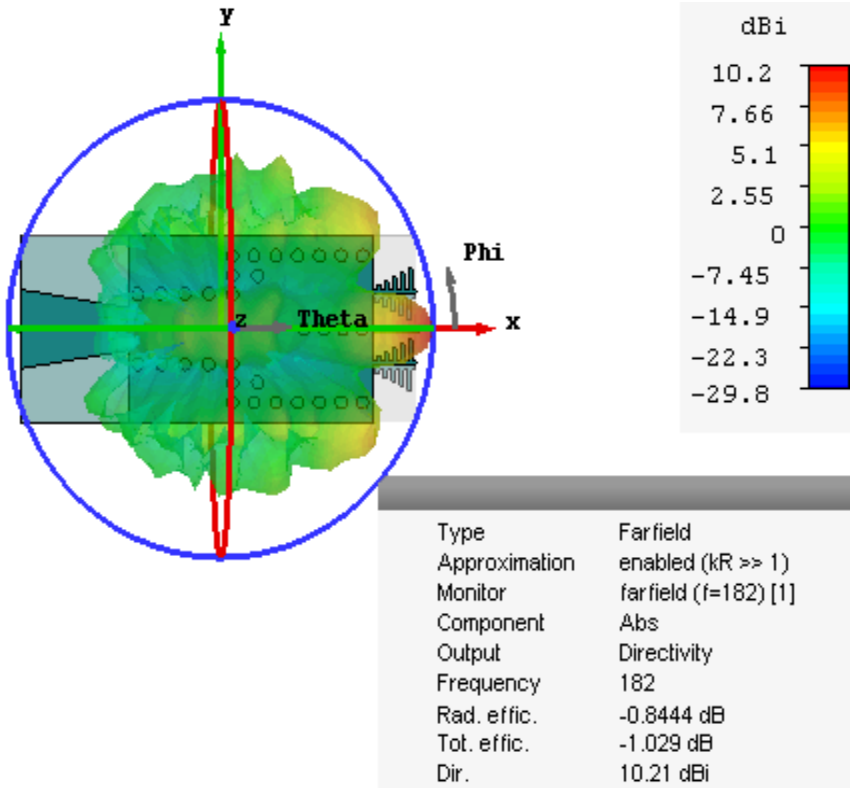

(b)

Figure III. 20. The 1×2 SIW array antenna pattern in (a) polar coordinates (b) 3D.

The Figure III.20 represent the 1×2 SIW array antenna pattern for the frequency of 0.182 THz. We can see that the radiation is maximum in the plane (Theta= 90°) in the longitudinal direction, and the maximum directivity is around the 10.2 dB with an aperture angle of 3 dB of 15.4°. According to these results, we can use this SIW antenna array for terahertz applications and we can consider it as a novel contribution for scientific research.

III. 7. Conclusion

This chapter is dedicated to the design and simulate two antenna array; the first is a 1×8 SIW TWA array for V-Band. First, we designed a TWA with a single element, which has comb shape profile than we used this antenna for construct 1×8 TWA array fed by SIW power divider. The simulated result show that the 1×8 antenna array range from 55 GHz to 70 GHz with a peak gain of 17.3 dBi and narrow beam width of 6.1°. This antenna array can use for electronic detection devices and mm wave radars. The second is a 1×2 SIW TWA array for terahertz applications. First, we designed a TWA with a single element than we used this antenna for construct 1×2 TWA array fed by SIW power divider. The simulated result show that the 1×2 antenna array range from 0.135 THz to 0.205 THz with an average gain is about of 8 dBi and narrow beam width of 15.4°. This antenna array can be used for biomedical sensors and radars imaging. As a perspective, we will work to increase the gain and directivity by adding more antenna elements and proposing solutions for enhancing the return loss.

References

1. X. Li, Y. Li, Z. Li, Q. Kong , H. Wang and G. Lv, Wideband high gain SIW fed antenna array for mm-Wave applications, Microwave and Optical Technology Letters 62 (2019), 1341-1351, DOI: 10.1002/mop.32149.
2. W. J. Fleming, New automotive sensors—a review, IEEE Sensors Journal 8 (2008), 1900 – 1921, DOI: 10.1109/JSEN.2008.2006452.
3. B. Fellah and M. Abri, Design of antipodal linearly tapered slot antennas (ALTSA) arrays in SIW technology for UWB imaging, Springer: Recent Adv Electr Eng Control Appl 411 (2016), 381-389, DOI: 10.1007/978-3-319-48929-2_30.
4. Wu, K., Cheng, Y.J., Djerafi T. and Hong, W. : Substrate-Integrated Millimeter Wave and Terahertz Antenna Technology. Proceedings of The IEEE, Vol. 100 pp. 2219 – 2232, (2012)
5. Li, X., Xiao, J., Qi , Z. and Zhu, H. : Broadband and High-gain Millimeter-wave and Terahertz Antenna Arrays. 2019 International Conference on Microwave and Millimeter Wave Technology (ICMMT) Guangzhou China, (2019) 19-22.
6. D. Deslandes and K. Wu, Integrated microstrip and rectangular waveguide in planar form, IEEE Microwave and Wireless Component Letters 11 (2001), 68-70, DOI: 10.1109/7260.914305.
7. S. Doucha, M. Abri, H. Badaoui and B. Fellah, A leaky wave antenna design based on half-mode substrate integrated waveguide technology for X band application, International Journal of Electrical and Computer Engineering 7 (2017), 3467-3474, DOI: 10.11591/ijece.v7i6.pp3467-3474.
8. R.Kazemi, A.E. Fathy, and R.A.Sadeghzadeh, Dielectric rod antenna array with substrate integrated waveguide planar feed network for wideband applications, IEEE Transactions on Antennas and Propagation 60 (2012), 1312–1319, DOI: 10.1109/TAP.2011.2182489.
9. L. Bin, D. Liang and Z. Jiao-cheng, The research of broadband millimeter-Wave vivaldi array antenna using SIW technique, IEEE 2010 International Conference on Microwave and Millimeter Wave Technology Chengdu, China (2010), 997-1000, DOI: 10.1109/ICMMT.2010.5525122.
10. X. Li, K. Xu, Y. Li, S. Ye, J. Tao and C. Wang, SIW-fed Vivaldi array for mm-Wave applications, 2019 IEEE International Conference on Computational Electromagnetics (ICCEM), Shanghai, China, (2019), DOI: 10.1109/COMPEM.2019.8779095.
11. Benzerga, F., Abri, M. and Badaoui, H " Optimized bends, corporate 1 × 4 and 1 × 8 SIW power dividers junctions analysis for V-Band applications using a rigorous finite element method," Arabian Journal for Science and Engineering, Vol. 41, PP. 3335–3343, 2016.
12. Li, X., Xu, K., Li,Y., Ye, S., Tao, J. and Wang, C. : SIW-fed Vivaldi array for mm- Wave applications. 2019 IEEE International Conference on Computational Electromagnetics (ICCEM), Shanghai China (2019).

General Conclusion And Perspectives

In this thesis, we have interested in the design and analysis of microwave components based on substrate integrated waveguide technology for different frequency bands. We based on our work on the microwave filters and antennas. The proposed filters feature by high rejection and compact size and the proposed antennas feature by high gain and wideband.

In the first chapter, we studied the characteristics and fundamental principles of SIW and DGS technologies. We also studied the design of the filters and the antenna based on SIW. These studies allow us to design new configurations of microwave components and to improve the performance of these components.

The first chapter is dedicated to the design of novel configurations of the high and bandpass filter based on SIW. We have used different DGS cell (CSRR, Cross shape and dumbbell) and we used CST and HFSS simulators for design and optimize our structures. The proposed filters have a compact size and high rejection, which demonstrate the advantage of SIW and DGS over the classical techniques.

The third chapter is reserved to the design of original configuration of the traveling wave antennas based on SIW. This antenna is dedicated to millimeter wave and sub-terahertz applications. To improve the gain of antennas, we have integrated these antennas with optimal SIW power dividers to build the antenna arrays. We demonstrated the effectiveness of SIW in designing a high gain antennas

These very encouraging results open up many perspectives. We quote in particular:

- ✓ Design and realization of a reconfigurable filters and antennas based on SIW.
- ✓ Design and Realization of the filters and antennas based on Air-filled SIW technology.
- ✓ Design and realization of the RF filters based on quad mode SIW and novel DGS cells.
- ✓ Applied the SIW for the design of other microwave components such us circulators, amplifiers and couplers.
- ✓ Realizations of SIW components on the same substrate (SICs).

The Scientific Researches

Cherif, N., Abri, M., Benzerga, F., Badaoui, H. and Tao., J. "A Compact Wideband DGS Bandpass Filter Based on Half Mode Substrate Integrated Waveguide Technology" *International Journal of Microwave and Optical Technology*, vol 16, pp.142-147, March 2021.

Cherif Nabil, Hichem Chaker, Mehadji Abri, Fellah Benzerga, Hadjira Badaoui, Junwu Tao, Tan-Hoa Vuong and Sarosh Ahmad, " A High Pass Filter Based on Half Mode Substrate IntegratedWaveguide Technology for cm Waves" *Progress In Electromagnetics Research Letters*, Vol. 104, PP. 149–154, June 15 2022

Nabil Cherif, Mehadji Abri, Sarosh Ahmad, Adnan Ghaffar, Chahira Khial, Fellah Benzerga, Mohammed El Amine Chaib, Hadjira Badaoui and Bouabdallah Roumeica," Miniaturizing Bandpass Filter Based on Half-Mode SIW for Sub-mm 5G Applications " *Progress In Electromagnetics Research Letters*, Vol. 104, PP. 155-160, June 20 2022.

B. Fellah, **N. Cherif**, M. Abri, and H. Badaoui, "CSRR-DGS Bandpass Filter Based on Half Mode Substrate Integrated Waveguide for X-Band Applications", *Advanced Electromagnetics (AEM)*, vol. 10, no. 3, pp. 39–42, Nov. 2021.

Nabil Cherif, Mehadji Abri, Fellah Benzerga, Hadjira Badaoui, Junwu Tao,Tan-Hoa Vuong, and Sarosh Ahmad " Broadband SIW Travelling Wave Antenna Array for Terahertzes Applications " *in book Advances in Terahertz Technology and Its Applications, Springer*, pp. 211-219, October 2021.

Nabil CHERIF, Mehadji ABRI, Benzerga FELLAH, Hadjira BADAOUI and Sarosh AHMAD "Novel Form for High Gain Millimeter Wave Antenna Array Based on Substrate Integrated Waveguide Technology "*International Conference on Advances in Communication Technology, Computing and Engineering (ICACTCE)* At: Morocco, Mars 2021.

CHERIF Nabil, ABRI Mehadji, FELLAH Benzerga, KHIAL Chahira, BOUABDALLAH Roumeiça " Design of a New SIW-DGS band-pass Filter Configuration for C-band " *The Electrical Engineering International Conference EEIC'19* , Bejaia, Algeria. September 2019.

Nabil Cherif, Mehadji Abri, Benzerga Fellah, Hadjira Badaoui and Hadjira Hamadouche "4G LTE Radio Network analysis, Design and Simulation " *Conférence Nationale sur les Télécommunications et ses Applications (CNTA'21)* At: Ain-Témouchent, Algeria, December 2021.

Sarosh Ahmad, Adnan Ghaffar, Xue Jun Li, **Nabil Cherif** "A Millimetre-Wave Tri-Band Antenna Embedded on Smart Watch for Wearable Applications " *IEEE 2021 International Symposium on Antennas and Propagation (ISAP)*, Taipei Taiwan , 19-22 Oct. 2021

Nabil Cherif "Wideband Antenna Array for mm-wave applications Based on SIW Technology" *Doctoral day*, Mascara university, 30 November 2021.